N-acyl Dopamines – renoprotective therapeutics, acting on TRPV1 signaling

Biological properties and molecular mechanisms

Prama Pallavi

2020

Studies presented in this thesis were supported by
Research Training Group GRK 880, German Research Foundation (DFG)
Albert und Anneliese Konanz-Stiftung, University of Applied Science Mannheim.
Printing of the thesis was supported by:
University Medical Center Groningen, University of Groningen, The Netherlands.

Cover Design and Layout: Michał Sławiński, thesisprint.eu
Printed: FVG-Zentrum, Mediziniche Fakultät Mannheim,
University of Heidelberg, Germany

university of groningen

N-acyl Dopamines - renoprotective therapeutics, acting on TRPV1 signaling

Biological properties and molecular mechanisms

PhD thesis

to obtain the degree of PhD at the
University of Groningen
on the authority of the
Rector Magnificus Prof. C. Wijmenga
and in accordance with
the decision by the College of Deans.

This thesis will be defended in public on

Tuesday 24 November 2020 at 11.00 hours

by

Prama Pallavi

born on 20 February 1987
in Bettiah, India

Supervisors
Prof. M.C. Harmsen
Prof. B. A. Yard
Prof. M. Hafner

Assessment Committee
Prof. R.H. Henning
Prof. M. Keese
Prof. K. Bieback

Paranimfen
Annette Breedijk
Ramkumar Ramani Mohan

Table of Contents

To my family

Introduction

Chapter 1

General Introduction

N-Acyl Dopamines

The concept of lipids as signaling molecules facilitating communication within and between cells has emerged and developed over the past fifty years, significantly contributing to state-of-the art research in a multitude of scientific disciplines. Much attention has been paid to *N*-acyl conjugates of amino acids and neurotransmitters (NAANs) as their potential roles in the nervous system, vasculature, and immune system have emerged. NAANs are compounds such as glycine, gamma-aminobutyric acid, or dopamine conjugated with long-chain fatty acids. *N*-acyl dopamines (NADs), initially thought to be a means of dopamine inactivation [1, 2], have evolved as a family of compounds with important biological activities and will be the main topic of this thesis.

Fueled by the discovery of the cannabinoid receptor in 1988 [3] and its endogenous ligand-anandamide [4], further interest in fatty acid conjugates arose, and several NADs were synthesized. Many of these synthetic NADs interacted with proteins of the endogenous cannabinoid system [5–7] and were potent inhibitors of 5-lipoxygenase [8]. In 2002, the first endogenous fatty acid amide of dopamine *N*-arachidonoyl dopamine (NADA) was discovered in rat and bovine brain tissue and reported as an endogenous ligand of the transient receptor potential channel of the vanilloid receptor subfamily, subtype 1 (TRPV1) [9]. A year later Chu et al. identified other endogenous NADs—*N*-oleoyl dopamine (OLDA), *N*-palmitoyl dopamine, and *N*-stearoyl dopamine—in lipid extracts of the bovine brain [10]. The presence of endogenous NADs has so far only been assessed in the central nervous system, and their concentration or body distribution remains unknown [9, 10].

NADs consist of an aromatic head group and a hydrocarbon tail. The hydrocarbon tail with polar groups provides some of these compounds' ability, to a limited extent, to dissolve in water. In an analogy with capsaicin (the classical TRPV1 agonist), these molecules can be structurally divided into three regions: the aromatic moiety (A region), the linker (B region), and the hydrocarbon side chain (C region) [11–13] (Figure 1). Because all NADs are conjugates of dopamine, they carry the same A and B regions, while the C region may vary from an unsaturated to completely saturated hydrocarbon tail of varying length.

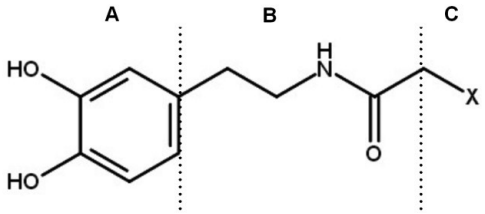

Figure 1. Generalized structure of the NADs. The structures can be divided into three regions: the aromatic moiety (A region), the amide bond (B region), and the hydrophobic side chain (C region). X is the hydrocarbon chain, which can be of varying length and degree of saturation.

Although the biosynthesis of the NADs is yet to be fully elucidated, two major biosynthetic routes have been proposed: The first is the conjugation of the amino acid/neurotransmitter with arachidonic acid or arachidonoyl coenzyme A, and the second involves sequential modification of a precursor fatty acid conjugate to form the final NAD [9, 14].

In vitro, NADs appear to be subject to degradation involving hydrolysis of the ester bond and modification of the dopamine moiety and fatty acid residue. In mammals, the NADs are mainly metabolized through low-efficiency hydrolysis with a possible involvement of hydrolase of fatty acid amides [9, 10] and methylation of the catechol group by the cytoplasmic Catechol-O-Methyltransferase [9, 15], as well as through oxidation of the dopamine moiety by NADH oxidoreductases in the plasma membrane and mitochondria [15]. In rat tissues, sulfation of the dopamine entity of NADs has been reported by aryl sulfotransferase [16].

Biological Properties of *N*-acyl Dopamines

NADs display diverse biological activities from information transformation within the nervous system, modulation of signal transduction, and antioxidative properties to immune modulatory effects. Some of the important biological properties of NADs are described in the following paragraphs:

Agonist at the Cannabinoid Receptors

Although all NADs exhibit modest affinity toward the cannabinoid receptor type 1 (CB1) and cannabinoid receptor type 2 (CB2) receptor *in vitro*, not all NADs activate the cannabinoid receptors. For instance, NADA is shown to activate CB1 [7, 17], while OLDA is a weak ligand for the CB1 receptor [10].

Agonist at TRPV1

NADs are the endogenous agonist at TRPV1—a multimodal (pH-, temperature-, and mechano-sensitive) nonselective ion channel. TRPV1 activation leads to influx of Na^{+} and Ca^{+2} ions. NADA and OLDA are agonists at the TRPV1 channel. NADA and OLDA have both induced calcium transients in TRPV1-transfected Human Embryonic Kidney cells, with EC_{50} potencies of ≈ 50 nm and ≈ 36 nm, respectively [9, 10].

It is noteworthy to mention that the activation pattern of TRPV1 by NADs is rather complex; for instance, the receptor sensitivity and maximal response for NADA is reported to increase dramatically after phosphorylation of the receptor by protein kinase C by approximately fifteen fold [18]. Similarly, capsaicin responses in sensory neurons have exhibited robust potentiation by cAMP-dependent protein kinase A [19].

In vivo NADs exhibit a complex pattern of effects based on the duality of their targets—anti-nociceptive CB1 receptors and pro-nociceptive TRPV1 [20, 21].

Anti-Inflammatory Properties

Almost all NADs exhibit anti-inflammatory properties. The endogenous NADs—NADA and OLDA—inhibit human T cell activation by blocking Nuclear Factor of Activated T-cells (NFAT), nuclear factor κB (NF-κB), and activator protein 1 (AP-1) pathways [22]. Another NAD, *N*-acetyl dopamine, was shown to decrease lipopolysaccharide stimulated Tumor Necrosis Factor (TNF) production in monocytes and phorbol ester-stimulated superoxide production in neutrophils [23].

NADs may elicit anti-inflammatory properties independent of CB1 and TRPV1. For example, NADA is reported to activate redox-sensitive mitogen-activated protein kinase p38, resulting in stabilization of cyclooxygenase-2 (COX-2) mRNA, which in turn increases COX-2 protein expression. At the same time NADA inhibits the expression of Prostaglandin E synthase-1 while upregulating Lipocalin-type prostaglandin D synthase expression. The net effect of this action is a shift from eicosanoid prostaglandin E_2 to prostaglandin D_2, resulting in the onset of the resolution phase of the inflammatory response. This ability of NADA is solely dependent on its dopamine moiety [24].

NADA stimulates transcriptional activity of peroxisome proliferator-activated receptors (PPAR), a family of nuclear receptors/transcription factors that regulate cell differentiation, metabolism, and immune function [25]. The interaction of NADA with PPAR-γ has been shown to cause endothelium-, nitrogen oxide (NO)-, and superoxide dismutase-dependent vasorelaxation in rat-isolated aorta [25].

Antioxidative Properties

The presence of the catechol moiety in NADs makes these compounds eligible to participate in redox cycling. Hence, depending on their environment, they can either donate or accept $2H^{+}$ and $2e^{-}$, thereby changing from an enol to an enone configuration or vice

versa; for example, NADA protects cultured granular neurons of rat cerebellum against H_2O_2 with the reduction of intracellular peroxide concentration [26]. Oxenkrug et al. showed that *N*-acetyl dopamine inhibits rat brain lipid peroxidation induced by lipopolysaccharide [23], and Perianayagam et al. reported lipopolysaccharide-induced oxidative stress suppression by the same substance [23]. Saturated NADs (derivatives of octanoic, decanoic, dodecanoic, and tetradecanoic acids) efficiently protected human umbilical vein endothelial cells [27] and cardiomyocytes [28] against cold-inflicted oxidative stress.

As a result of their ability to easily undergo oxidation, these NADs under normal conditions produce mild oxidative stress. Several studies suggest that mild triggers keep the system alert; for example, it has been shown that mild oxidative stress strongly activates antioxidant response element (ARE)-dependent gene expression and contributes to neuroprotective ischemic preconditioning [29].

Biological Stability

Although a number of NADs have been found in brain tissue [9, 10, 30] and in human plasma [31], the half-life and biological stability of NADs *in vivo* are not yet known. Their physiological role and production site are unknown. Synthesized NADs show temperature sensitivity and degrade faster at room temperature, indicating that NADs in general might have a rapid response system similar to neurotransmitters.

NOD – A synthetic *N*-Acyl dopamine

In vitro experimental studies [32–34], *in vivo* animal studies [35, 36], and clinical prospective and retrospective studies [37–40] all unequivocally point to the protective effects of low-dose donor dopamine treatment on allograft quality. The downside of donor dopamine treatment, however, is that in approximately fifteen percent of the brain-dead donors, tachycardia or hypertension may occur, requiring cessation of dopamine infusion [41]. Because dopamine is rapidly degraded in the circulation by monoamine oxidase, sufficient tissue dopamine levels can only be obtained if dopamine treatment is continued until cross-clamping. Renal allografts obtained from donors in whom treatment was terminated earlier no longer profit from dopamine. It should also be emphasized that even though renal allografts retrieved from non-heart-beating donors may have an increased risk of delayed graft function, dopamine treatment of such donors is not an option. With the aim of overcoming the hemodynamic adverse effects of dopamine and of finding compounds more efficacious than dopamine, Loesel et al. synthesized NADs with short saturated fatty acids. *N*-octanoyl dopamine (NOD) was forty times more effective than dopamine in terms of protection against cold-inflicted injury. NOD does not affect mean arterial blood pressure *in vivo*; its effect is neither adrenergic nor dopaminergic receptor mediated, nor does it function as a competitive inhibitor of these receptors [27].

NOD protects cultured cardiomyocytes, as well as endothelial and renal epithelial cells, against cold-inflicted injury much more effectively than dopamine can [27, 28]. In addition, NOD strongly inhibits TNFα-mediated Vascular cell adhesion protein 1 (VCAM-1) expression along with a variety of inflammatory chemo-and cytokines [42]. Moreover, like other catechol-containing structures, NOD induces the expression of heme oxygenase-1 (HO-1) as a consequence of Nuclear factor erythroid 2-related factor 2 (Nrf-2) activation [42, 43]. In the setting of warm ischemia-induced acute kidney injury (AKI) in rats, bolus application of NOD shortly before and after the induction of AKI displayed renoprotective properties [44].

In vitro NOD transiently inhibits T cell proliferation in a dose-dependent fashion and, displays a synergistic effect with calcineurin inhibitor to suppress T cell proliferation [45]. Furthermore, NOD inhibited platelet function [46], improved renal function in allograft recipients when applied to brain-dead donors [47], improved donor cardiac and graft function after transplantation [48], attenuated transplant vasculopathy in rat aortic allografts [49], induced the unfolded protein response (UPR) in endothelial cells, and appeared to shift cells toward hypometabolism [50].

All these properties of NOD tempt one to think of NOD as an attractive drug candidate to ameliorate tissue damage caused either by inflammation or other inciting events [51]. Yet those who conduct pharmacokinetic, toxicological, or structure-activity studies are required to think of NOD as a potential drug.

Beneficial Effects of NADs in Ischemia-Induced AKI

Before discussing the beneficial effect of NADs in ischemia-induced AKI, the pathophysiology of the latter is briefly summarized in the following paragraphs.

Pathophysiology of AKI

Although AKI has a multifactorial aetiology, ischemia is a common denominator in many of these aetiologies—vascular injury, tubular injury, loss of tubuloglomerular feedback, and finally the involvement of the immune system—which are important events in ischemia-induced AKI.

Ischemia-mediated AKI results from a generalized or localized impairment of oxygen and nutrient delivery to, and waste product removal from, the cells of the kidney [52]. There is a mismatch of local tissue oxygen supply and demand and accumulation of waste products of metabolism. Ischemia damages the renal vasculature, causing increased tissue levels of vasoconstrictor (e.g., endothelin-1, angiotensin II) [53, 54], while the production of vasodilators by the endothelium, such as NO, is reduced [55]. The blood vessels constrict in response to out-of-balance vasoconstrictors. The scenario is further worsened by the sympathetic nerve stimulation, resulting in loss of autoregulation of

renal blood flow. Because ischemia is accompanied by inflammation, the inflammatory cytokines exert direct or indirect vasoactive properties, further perpetuating the dysfunction in local vascular tone [56].

Renal microvascular permeability increases as a result of disruption of the endothelial monolayer and actin cytoskeleton and a severely compromised integrity of adherence junctions. Consequently, tissue edema is formed, resulting in an increased interstitial pressure, which in turn may occlude small vessels, further impairing perfusion and oxygenation of the affected tissue [57]. Endothelial cell dysfunction is aggravated by activation of the coagulation system, leading to thrombus formation and facilitation of tissue inflammation [58]. As such, continued activation of inflammation, vascular leakage, and activation of the coagulation pathway may lead to secondary ischemia, causing a vicious circle of ischemia and endothelial dysfunction.

Oxygen deprivation, together with a high energy demand in tubular epithelial cells, leads to rapid degradation of Adenosine triphosphate (ATP) to Adenosine diphosphate (ADP) and Adenosine monophosphate (AMP). Prolongation of ischemia results in breakdown of AMP to adenine nucleotides, which are subsequently converted to hypoxanthine. Accumulation of hypoxanthine, in turn, contributes to the generation of reactive oxygen species, which then perpetuate renal tubule cell injury by peroxidation of lipids, oxidation of proteins, damage to DNA, and induction of apoptosis [59].

Because ATP is required for calcium homeostasis within cells, ATP depletion leads to increase in free intracellular calcium, causing activation of the proteases and the phospholipases and cytoskeletal degradation [60]. This rapid disruption of the apical actin cytoskeleton and rearrangement of the actin from the apical domain and microvilli into the cytoplasm gives rise to the formation of blebs—membrane-bound, free-floating extracellular vesicles that are either lost or internalized in the tubular lumen. These blebs contribute to cast formation and obstruction in the lumen and have been detected in the urine of animals and humans suffering from AKI [61].

Disruption of the actin cytoskeleton is followed by redistribution of basolateral Na^+/K^+- ATPase pumps to the apical membrane [62], resulting in the back transport of sodium into the tubular lumen. When filtrates with a high sodium concentration reach the distal tubules, this is sensed by the macula densa and translated into vasoconstriction of the afferent arteriole, a physiological process to regulate glomerular filtration, also known as tubuloglomerular feedback [63]. Disruption of the apical cytoskeleton further potentiates loss of tight junctions and adherent junctions, resulting in loss of tubular barrier function and, consequently, a back leak of the glomerular filtrate [64, 65]. Thus, proximal tubular cell injury and dysfunction during ischemia lead to afferent arteriolar vasoconstriction mediated by the tubuloglomerular feedback, luminal obstruction as a consequence of cast formation, and back leak of the filtrate across the injured proximal tubular cell [66, 67].

NOD, a TRPV1 Agonist and an Attractive Drug Candidate in Ameliorating AKI

In the past decade, several studies have demonstrated the protective effect of the TRPV1 agonists in ischemia-reperfusion-induced renal dysfunction [68–70]. This can be attributed to the fact that the renal pelvis, pelviureteric junction, and ureter are innervated with TRPV1-positive sensory nerves [71, 72]. These sensory nerve endings contain vasoactive neuropeptides, such as calcitonin gene-related peptide (CGRP) and substance P (SP), which are released upon TRPV1 activation [73–75]. Release of these vasoactive neuropeptides from TRPV1-positive sensory nerve fibers may regulate local blood flow.

Although *in vitro* experiments have indicated that NOD is an agonist of TRPV1 [44], and NOD treatment yields renoprotective effects in ischemia-induced AKI, it is currently not clear if the reno-protective properties of NOD are mediated via TRPV1. Nonetheless, other TRPV1 agonists have shown a beneficial effect on ischemia reperfusion injury (IRI) in different organs [69, 76, 77]. Activation of TRPV1 may result in the release of CGRP and SP [78–80] from sensory nerves, possibly causing local vasodilation in end organs [76, 81–84]. Its TRPV1-activating property and anti-inflammatory property, along with other tissue-protective properties, make NOD an attractive drug candidate to ameliorate tissue damage caused either by inflammation or other inciting events [51].

Aim of This Thesis

The main aim of this thesis was to determine the signaling pathway by which NOD conveys protection in the setting of ischaemia-induced AKI. Furthermore, secondary aims were to delineate the molecular entities within NOD that are required for biological properties—TRPV1 activation and anti-inflammatory property; to study *in vivo* tissue distribution and elimination kinetics of NOD; and finally, to demonstrate that the redox activity of NOD significantly affects cell behaviour. The following paragraphs describe the scope of this thesis.

NADs have been reported to be tissue protective in a variety of models, albeit the underlying mode of action has not clearly been demonstrated. The potential use of NADs in transplantation medicine has been reviewed in **Chapter 2**.

TRPV1 agonists are capable of rendering a renoprotective effect in settings of ischaemia-induced AKI. Because NOD is a TRPV1 agonist and exhibits a renoprotective effect in ischaemia-induced AKI, **Chapter 3** addresses the question of whether the renoprotective properties of NOD are mediated via TRPV1 and whether renal transplant recipients can also benefit from the NOD treatment.

In **Chapter 4**, we subsequently tried to delineate the structural entities of the NADs required for TRPV1 agonistic and anti-inflammatory properties. This was achieved via systematic modification of the aromatic, linker, and side chain regions of NOD. In this chapter, the interaction between NOD and the TRPV1-binding pocket that leads to TRPV1 activation is also studied.

Pharmacokinetics and tissue distribution are important prerequisites for further development of NADs toward clinical application. In **Chapter 5**, we sought to address this by developing a NOD-based radiotracer F-NOD. After assessing that the *in vitro* biological properties of a nonradioactive reference compound F-NOD are similar to those of NOD, tissue distribution and elimination kinetics of [^{18}F] F-NOD were determined by means of Positron-emission tomography (PET) imaging.

Based on the facts that the NADs are able to donate reduction equivalents, the catechol structure of NADs can chelate iron [24], and the amphiphilic nature of NADs provides them with access to various cellular compartments, in **Chapter 6** we investigated if NADs would influence the redox homeostasis in the Endoplasmic Reticulum (ER) and, in turn, oxidative protein folding [25, 26]. In addition, we made use of synthetic NADs that were either changed at the aromatic ring or in the aliphatic chain to identify the structural entities within NOD that might be important for UPR activation. Furthermore, we addressed whether activation of the UPR by NOD compromises cell viability or whether it represents a protective response, allowing cells to adapt to more aggravating conditions such as hypothermic preservation.

Finally, in **Chapter 7**, the outcomes of the studies are discussed and their perspective provided.

References

1. Goldstein, M. and J.M. Musacchio, *The formation in vivo of N-acetyldopamine and N-acetyl-3-methoxydopamine.* Biochim Biophys Acta, 1962. **58**: p. 607–8.
2. Elchisak, M.A. and E.A. Hausner, *Demonstration of N-acetyldopamine in human kidney and urine.* Life Sci, 1984. **35**(25): p. 2561–9.
3. Devane, W.A., et al., *Determination and characterization of a cannabinoid receptor in rat brain.* Mol Pharmacol, 1988. **34**(5): p. 605–13.
4. Devane, W.A., et al., *Isolation and structure of a brain constituent that binds to the cannabinoid receptor.* Science, 1992. **258**(5090): p. 1946–9.
5. Kolocouris, N., et al., *[Dopamine amides with essential or fundamental fatty acids. Synthesis and pharmacological study].* Ann Pharm Fr, 1991. **49**(2): p. 99–110.
6. Bezuglov, V.V., et al., *[Artificially functionalized polyenoic fatty acids— a new lipid bioregulators].* Bioorg Khim, 1997. **23**(3): p. 211–20.
7. Bisogno, T., et al., *N-acyl-dopamines: novel synthetic CB(1) cannabinoid-receptor ligands and inhibitors of anandamide inactivation with cannabimimetic activity in vitro and in vivo.* Biochem J, 2000. **351 Pt 3**: p. 817–24.
8. Tseng, C.F., et al., *Inhibition of in vitro prostaglandin and leukotriene biosyntheses by cinnamoyl-beta-phenethylamine and N-acyldopamine derivatives.* Chem Pharm Bull (Tokyo), 1992. **40**(2): p. 396–400.
9. Huang, S.M., et al., *An endogenous capsaicin-like substance with high potency at recombinant and native vanilloid VR1 receptors.* Proc Natl Acad Sci U S A, 2002. **99**(12): p. 8400–5.
10. Chu, C.J., et al., *N-oleoyldopamine, a novel endogenous capsaicin-like lipid that produces hyperalgesia.* J Biol Chem, 2003. **278**(16): p. 13633–9.
11. Walpole, C.S., et al., *Analogues of capsaicin with agonist activity as novel analgesic agents; structure-activity studies. 1. The aromatic "A-region".* J Med Chem, 1993. **36**(16): p. 2362–72.
12. Walpole, C.S., et al., *Analogues of capsaicin with agonist activity as novel analgesic agents; structure-activity studies. 3. The hydrophobic side-chain "C-region".* J Med Chem, 1993. **36**(16): p. 2381–9.
13. Walpole, C.S., et al., *Analogues of capsaicin with agonist activity as novel analgesic agents; structure-activity studies. 2. The amide bond "B-region".* J Med Chem, 1993. **36**(16): p. 2373–80.
14. Pokorski, M. and Z. Matysiak, *Fatty acid acylation of dopamine in the carotid body.* Med Hypotheses, 1998. **50**(2): p. 131–3.
15. Akimov, M.G., et al., *[New aspects of biosynthesis and metabolism of N-acyldopamines in rat tissues].* Bioorg Khim, 2007. **33**(6): p. 648–52.
16. Akimov, M.G., et al., *Sulfation of N-acyl dopamines in rat tissues.* Biochemistry (Mosc), 2009. **74**(6): p. 681–5.
17. Bezuglov, V., et al., *Synthesis and biological evaluation of novel amides of polyunsaturated fatty acids with dopamine.* Bioorg Med Chem Lett, 2001. **11**(4): p. 447–9.
18. Premkumar, L.S., et al., *Enhancement of potency and efficacy of NADA by PKC-mediated phosphorylation of vanilloid receptor.* J Neurophysiol, 2004. **91**(3): p. 1442–9.
19. Bhave, G., et al., *cAMP-dependent protein kinase regulates desensitization of the capsaicin receptor (VR1) by direct phosphorylation.* Neuron, 2002. **35**(4): p. 721–31.

20. Sagar, D.R., et al., *TRPV1 and CB(1) receptor-mediated effects of the endovanilloid/endocannabinoid N-arachidonoyl-dopamine on primary afferent fibre and spinal cord neuronal responses in the rat.* Eur J Neurosci, 2004. **20**(1): p. 175–84.
21. O'Sullivan, S.E., D.A. Kendall, and M.D. Randall, *Characterisation of the vasorelaxant properties of the novel endocannabinoid N-arachidonoyl-dopamine (NADA).* Br J Pharmacol, 2004. **141**(5): p. 803–12.
22. Sancho, R., et al., *Immunosuppressive activity of endovanilloids: N-arachidonoyl-dopamine inhibits activation of the NF-kappa B, NFAT, and activator protein 1 signaling pathways.* J Immunol, 2004. **172**(4): p. 2341–51.
23. Perianayagam, M.C., G.F. Oxenkrug, and B.L. Jaber, *Immune-modulating effects of melatonin, N-acetylserotonin, and N-acetyldopamine.* Ann N Y Acad Sci, 2005. **1053**: p. 386–93.
24. Navarrete, C.M., et al., *Endogenous N-acyl-dopamines induce COX-2 expression in brain endothelial cells by stabilizing mRNA through a p38 dependent pathway.* Biochem Pharmacol, 2010. **79**(12): p. 1805–14.
25. O'Sullivan, S.E. and D.A. Kendall, *Cannabinoid activation of peroxisome proliferator-activated receptors: potential for modulation of inflammatory disease.* Immunobiology, 2010. **215**(8): p. 611–6.
26. Bobrov, M.Y., et al., *Antioxidant and neuroprotective properties of N-arachidonoyldopamine.* Neurosci Lett, 2008. **431**(1): p. 6–11.
27. Losel, R.M., et al., *N-octanoyl dopamine, a non-hemodyanic dopamine derivative, for cell protection during hypothermic organ preservation.* PLoS One, 2010. **5**(3): p. e9713.
28. Vettel, C., et al., *Dopamine and lipophilic derivates protect cardiomyocytes against cold preservation injury.* J Pharmacol Exp Ther, 2014. **348**(1): p. 77–85.
29. Bell, K.F., et al., *Mild oxidative stress activates Nrf2 in astrocytes, which contributes to neuroprotective ischemic preconditioning.* Proc Natl Acad Sci U S A, 2011. **108**(1): p. E1–2; author reply E3–4.
30. Liu, X., et al., *Formation of dopamine adducts derived from brain polyunsaturated fatty acids: mechanism for Parkinson disease.* J Biol Chem, 2008. **283**(50): p. 34887–95.
31. Hauer, D., et al., *Plasma concentrations of endocannabinoids and related primary fatty acid amides in patients with post-traumatic stress disorder.* PLoS One, 2013. **8**(5): p. e62741.
32. Yard, B., et al., *Prevention of cold-preservation injury of cultured endothelial cells by catecholamines and related compounds.* Am J Transplant, 2004. **4**(1): p. 22–30.
33. Brinkkoetter, P.T., et al., *Hypothermic injury: the mitochondrial calcium, ATP and ROS love-hate triangle out of balance.* Cell Physiol Biochem, 2008. **22**(1–4): p. 195–204.
34. Brinkkoetter, P.T., et al., *Hypothermia-induced loss of endothelial barrier function is restored after dopamine pretreatment: role of p42/p44 activation.* Transplantation, 2006. **82**(4): p. 534–42.
35. Gottmann, U., et al., *Effect of pre-treatment with catecholamines on cold preservation and ischemia/reperfusion-injury in rats.* Kidney Int, 2006. **70**(2): p. 321–8.
36. Gottmann, U., et al., *Influence of donor pretreatment with dopamine on allogeneic kidney transplantation after prolonged cold storage in rats.* Transplantation, 2005. **79**(10): p. 1344–50.
37. Benck, U., et al., *Effects of donor pre-treatment with dopamine on survival after heart transplantation: a cohort study of heart transplant recipients nested in a randomized controlled multicenter trial.* J Am Coll Cardiol, 2011. **58**(17): p. 1768–77.

38. Schnuelle, P., et al., *Effects of catecholamine application to brain-dead donors on graft survival in solid organ transplantation.* Transplantation, 2001. **72**(3): p. 455–63.
39. Schnuelle, P., et al., *Donor catecholamine use reduces acute allograft rejection and improves graft survival after cadaveric renal transplantation.* Kidney Int, 1999. **56**(2): p. 738–46.
40. Schnuelle, P., et al., *Impact of donor dopamine on immediate graft function after kidney transplantation.* Am J Transplant, 2004. **4**(3): p. 419–26.
41. Juste, R.N., et al., *Dopamine clearance in critically ill patients.* Intensive Care Med, 1998. **24**(11): p. 1217–20.
42. Hottenrott, M.C., et al., *N-octanoyl dopamine inhibits the expression of a subset of kappaB regulated genes: potential role of p65 Ser276 phosphorylation.* PLoS One, 2013. **8**(9): p. e73122.
43. Kim, H., et al., *Caffeic acid phenethyl ester activation of Nrf2 pathway is enhanced under oxidative state: structural analysis and potential as a pathologically targeted therapeutic agent in treatment of colonic inflammation.* Free Radic Biol Med, 2013. **65**: p. 552–62.
44. Tsagogiorgas, C., et al., *N-octanoyl-dopamine is an agonist at the capsaicin receptor TRPV1 and mitigates ischemia-induced acute kidney injury in rat.* PLoS One, 2012. **7**(8): p. e43525.
45. Wedel, J., et al., *N-Octanoyl dopamine transiently inhibits T cell proliferation via G1 cell-cycle arrest and inhibition of redox-dependent transcription factors.* J Leukoc Biol, 2014. **96**(3): p. 453–62.
46. Ait-Hsiko, L., et al., *N-octanoyl-dopamine is a potent inhibitor of platelet function.* Platelets, 2013. **24**(6): p. 428–34.
47. Spindler, R.S., et al., *N-Octanoyl Dopamine for Donor Treatment in a Brain-death Model of Kidney and Heart Transplantation.* Transplantation, 2015. **99**(5): p. 935–41.
48. Li, S., et al., *Donor preconditioning after the onset of brain death with dopamine derivate n-octanoyl dopamine improves early posttransplant graft function in the rat.* Am J Transplant, 2017.
49. Wedel, J., et al., *N-octanoyl Dopamine Attenuates the Development of Transplant Vasculopathy in Rat Aortic Allografts Via Smooth Muscle Cell Protective Mechanisms.* Transplantation, 2016. **100**(1): p. 80–90.
50. Stamellou, E., et al., *N-octanoyl dopamine treatment of endothelial cells induces the unfolded protein response and results in hypometabolism and tolerance to hypothermia.* PLoS One, 2014. **9**(6): p. e99298.
51. Hottenrott, M.C., et al., *N-Octanoyl Dopamine Inhibits the Expression of a Subset of kappa B Regulated Genes: Potential Role of p65 Ser276 Phosphorylation.* PLoS One, 2013. **8**(9).
52. Bonventre, J.V. and L. Yang, *Cellular pathophysiology of ischemic acute kidney injury.* J Clin Invest, 2011. **121**(11): p. 4210–21.
53. Conger, J., *Hemodynamic factors in acute renal failure.* Adv Ren Replace Ther, 1997. **4**(2 Suppl 1): p. 25–37.
54. Brooks, D.P., *Role of endothelin in renal function and dysfunction.* Clin Exp Pharmacol Physiol, 1996. **23**(4): p. 345–48.
55. Kurata, H., et al., *Protective effect of nitric oxide on ischemia/reperfusion-induced renal injury and endothelin-1 overproduction.* Eur J Pharmacol, 2005. **517**(3): p. 232–9.
56. Bonventre, J.V. and A. Zuk, *Ischemic acute renal failure: an inflammatory disease?* Kidney Int, 2004. **66**(2): p. 480–5.
57. Molitoris, B.A. and T.A. Sutton, *Endothelial injury and dysfunction: role in the extension phase of acute renal failure.* Kidney Int, 2004. **66**(2): p. 496–9.

58. Gupta, A., et al., *Activated protein C and acute kidney injury: Selective targeting of PAR-1.* Curr Drug Targets, 2009. **10**(12): p. 1212–26.
59. Himmelfarb, J., et al., *Oxidative stress is increased in critically ill patients with acute renal failure.* J Am Soc Nephrol, 2004. **15**(9): p. 2449–56.
60. Devarajan, P., *Cellular and molecular derangements in acute tubular necrosis.* Curr Opin Pediatr, 2005. **17**(2): p. 193–9.
61. Molitoris, B.A., *Actin cytoskeleton in ischemic acute renal failure.* Kidney Int, 2004. **66**(2): p. 871–83.
62. Molitoris, B.A., A. Geerdes, and J.R. McIntosh, *Dissociation and redistribution of Na + ,K(+)-ATPase from its surface membrane actin cytoskeletal complex during cellular ATP depletion.* J Clin Invest, 1991. **88**(2): p. 462–9.
63. Molitoris, B.A., *Na(+)-K(+)-ATPase that redistributes to apical membrane during ATP depletion remains functional.* Am J Physiol, 1993. **265**(5 Pt 2): p. F693–7.
64. Kwon, O., et al., *Backleak, tight junctions, and cell-cell adhesion in postischemic injury to the renal allograft.* J Clin Invest, 1998. **101**(10): p. 2054–64.
65. Lee, D.B., E. Huang, and H.J. Ward, *Tight junction biology and kidney dysfunction.* Am J Physiol Renal Physiol, 2006. **290**(1): p. F20–34.
66. Alejandro, V., et al., *Mechanisms of filtration failure during postischemic injury of the human kidney. A study of the reperfused renal allograft.* J Clin Invest, 1995. **95**(2): p. 820–31.
67. Ramaswamy, D., et al., *Maintenance and recovery stages of postischemic acute renal failure in humans.* Am J Physiol Renal Physiol, 2002. **282**(2): p. F271–80.
68. Ueda, K., et al., *Preventive effect of SA13353 [1-[2-(1-adamantyl)ethyl]-1-pentyl-3-[3-(4-pyridyl)propyl]urea], a novel transient receptor potential vanilloid 1 agonist, on ischemia/reperfusion-induced renal injury in rats.* J Pharmacol Exp Ther, 2009. **329**(1): p. 202–9.
69. Ueda, K., et al., *Preventive effect of TRPV1 agonists capsaicin and resiniferatoxin on ischemia/reperfusion-induced renal injury in rats.* J Cardiovasc Pharmacol, 2008. **51**(5): p. 513–20.
70. Tsagogiorgas, C., et al., *N-octanoyl-dopamine is an agonist at the capsaicin receptor TRPV1 and mitigates ischemia-induced [corrected] acute kidney injury in rat.* PLoS One, 2012. **7**(8): p. e43525.
71. Guo, A., et al., *Immunocytochemical localization of the vanilloid receptor 1 (VR1): relationship to neuropeptides, the P2X3 purinoceptor and IB4 binding sites.* Eur J Neurosci, 1999. **11**(3): p. 946–58.
72. Rolle, U., E. Brylla, and B. Tillig, *Immunohistochemical detection of neuronal plexuses and nerve cells within the upper urinary tract of pigs.* BJU Int, 1999. **83**(9): p. 1045–9.
73. Inoue, R., et al., *Transient receptor potential channels in cardiovascular function and disease.* Circ Res, 2006. **99**(2): p. 119–31.
74. Szolcsanyi, J., *Forty years in capsaicin research for sensory pharmacology and physiology.* Neuropeptides, 2004. **38**(6): p. 377–84.
75. Huang, S.M. and J.M. Walker, *Enhancement of spontaneous and heat-evoked activity in spinal nociceptive neurons by the endovanilloid/endocannabinoid N-arachidonoyldopamine (NADA).* J Neurophysiol, 2006. **95**(2): p. 1207–12.
76. Zhong, B. and D.H. Wang, *N-oleoyldopamine, a novel endogenous capsaicin-like lipid, protects the heart against ischemia-reperfusion injury via activation of TRPV1.* Am J Physiol Heart Circ Physiol, 2008. **295**(2): p. H728–35.

77. Wang, M., et al., *TRPV1 Agonist Capsaicin Attenuates Lung Ischemia-Reperfusion Injury in Rabbits.* J Surg Res, 2010.
78. Li, J. and D.H. Wang, *Increased GFR and renal excretory function by activation of TRPV1 in the isolated perfused kidney.* Pharmacol Res, 2008. **57**(3): p. 239–46.
79. Alawi, K. and J. Keeble, *The paradoxical role of the transient receptor potential vanilloid 1 receptor in inflammation.* Pharmacol Ther, 2010. **125**(2): p. 181–95.
80. Benarroch, E.E., *CGRP Sensory neuropeptide with multiple neurologic implications.* Neurology, 2011. **77**(3): p. 281–287.
81. Harrison, S. and P. Geppetti, *Substance p.* Int J Biochem Cell Biol, 2001. **33**(6): p. 555–76.
82. Mizutani, A., et al., *Activation of sensory neurons reduces ischemia/reperfusion-induced acute renal injury in rats.* Anesthesiology, 2009. **110**(2): p. 361–9.
83. Jin, H., et al., *Involvement of perivascular nerves and transient receptor potential vanilloid 1 (TRPV1) in vascular responses to histamine in rat mesenteric resistance arteries.* Eur J Pharmacol, 2012. **680**(1–3): p. 73–80.
84. Tsuji, F. and H. Aono, *Role of Transient Receptor Potential Vanilloid 1 in Inflammation and Autoimmune Diseases.* Pharmaceuticals, 2012. **5**(8): p. 837–852.

Chapter 2

N-acyl dopamine derivatives as lead compound for implementation in transplantation medicine

Published in Transplantation reviews (Orlando, Fla.) 2015 Jul;29(3):109–13.

Prama Pallavi*, Johannes Wedel*, Eleni Stamellou, Benito A.Yard

*Equally contributing authors

Modified

Abstract

Conjugates of fatty acids with ethanolamine, amino acids or monoamine neurotransmitters occur widely in nature giving rise to so-called endocannabinoids. Anandamide and 2-arachidonoyl glycerol are the best characterized endocannabinoids activating both cannabinoid receptors (CB1 and CB2) and transient receptor potential vanilloid type 1 (TRPV1) channels (anandamide) or activating cannabinoid receptors only (2-arachidonoyl glycerol). TRPV1 is also activated by vanilloids, such as capsaicin, and endogenous neurolipins, e.g. *N*-arachidonoyl dopamine (NADA) and *N*-oleoyl dopamine (OLDA). Because donor dopamine treatment has shown to improve transplantation outcome in renal and heart recipients, this review will mainly focus on the biological activities of *N*-acyl dopamines (NADs) as potential non-hemodynamic alternative for implementation in transplantation medicine. Hence the influence of NADs on transplantation relevant entities, i.e. cold inflicted injury, cytoprotection, I/R-injury, immune-modulation and inflammation will be summarized. The cytoprotective properties of endogenous endocannabinoids in this context will be briefly touched upon.

Brain death

Donor organ shortage is the major bottle neck in contemporary organ transplantation and warrants new strategies to increase the donor pool, to diminish the number of organ allografts that are not suitable for transplantation, to improve post-transplant survival and thus to reduce the need for re-transplantation. While it is generally considered that the quality of organ allografts obtained from living donors is superior to that of allografts procured from post-mortem donors [1], the latter constitutes the largest part of the donor organ pool. The inferior quality of post-mortem donor allografts is a consequence of various deleterious events which occur after the onset of brain death. Brain death is characterized by a massive catecholamine release, initially leading to an increased blood pressure and subsequently to a sharp decline, frequently followed by a hemodynamic collapse [2]. In addition, brain death is accompanied by reduced levels of cortisol, insulin, thyroid and pituitary hormones [3], which may have both a hemodynamic and metabolic impact on donor organs. Moreover, brain death is considered to be an inflammatory condition [4], albeit that the precise mechanism that leads to inflammation in end-organs is still being discussed. Early and adequate donor management is of utmost importance not only for maintaining donor organ quality but also for increasing the number of retrievable organs from potential donors [5]. Thus many transplantation centers and critical care societies have developed standardized donor management protocols, focusing on hemodynamic and hormonal resuscitation [6] and [7].

For many decades low-dose dopamine has been applied for prevention and treatment of acute kidney injury (AKI) in critically ill patients [8, 9]. However, several meta-analyses and prospective studies have concluded that dopamine treatment neither prevents nor ameliorates AKI in these patients [10–14]. This is in sharp contrast to the retro-and prospective studies performed by Schnuelle et al. which clearly indicate that donor dopamine treatment improves transplantation outcome in kidney and heart allograft recipients [15, 16]. The mechanism by which this occurs remains to be determined. Nonetheless, the protective effect cannot be fully explained by improved hemodynamics, as the mean blood pressure in the dopamine-treated arm was not significantly different from the untreated arm [15]. Experimental brain dead models demonstrate that hemodynamic stabilization alone is not sufficient to reduce brain death-mediated inflammation in renal allografts [17]. In line with this, Spindler et al. recently demonstrated that treatment with the hemodynamic inactive dopamine derivate *N*-octanoyl dopamine (NOD) of brain dead donor rats improves renal allograft function in recipient rats, despite the fact that it does not affect blood pressure in the brain dead donor rat [18].

Cold inflicted injury

Experimental *in vitro* and *in vivo* studies have delineated numerous potential mechanisms that collectively explain why dopamine may afford its salutary effect on transplantation outcome [19–21]. However, it remains to be elucidated which of *these* effects are responsible for the clinical findings on donor dopamine treatment as described by Schnuelle et al. [15]. Among the beneficial mechanisms, the finding that catecholamines in general can protect endothelial cells against cold inflicted injury [22] is highly intriguing and opens the possibility for novel therapeutic modalities to prevent or limit organ damage during static cold storage [15, 16] and [23–25]. The mechanism by which catecholamines protect against organ damage during hypothermic preservation is not completely understood, albeit that involvement of the H_2S pathway [26], the HO-1 pathway [27]and redox activity [22] has been postulated. With respect to the latter, Lösel et al. have demonstrated that the cryoprotective properties of catecholamines are mediated via the redox active catechol structure in conjunction with a minimal degree of hydrophobicity [28]. Importantly synthetic NADs (Fig. 1), which also carries a catechol structure, is by far more protective as compared to dopamine as a consequence of their increased hydrophobicity. Furthermore octylamide derivates of all possible dihydroxy benzoic acids revealed that only the reducing structures were protective while the non-reducing were ineffective despite comparable hydrophobicity. It thus seems that catecholamines afford cryoprotection due to their reducing properties; their efficacy is strongly influenced by their relative hydrophobicity.

Inasmuch as the catechol structure plays a pivotal role in cryoprotection independent of receptor engagement, this offers the possibility of designing compounds that are devoid of hemodynamic action and yet retain their cryoprotective properties. This might be of particular importance since approximately 12 percent of brain dead donors that are treated with low-dose dopamine may develop tachycardia or hypertension [15]. Also other dopamine-related side effects, e.g. depression of the respiratory drive or cardiac arrhythmias seem to be receptor-mediated [29, 30]. As demonstrated by Kohli et al. N-substituted dopamine derivates lack affinity to dopamine receptors and only possess a weak beta agonistic activity [31]. Hence, NADs may display protective effects in the setting of donor treatment at much lower concentrations compared to dopamine, while dopamine-like side effects would occur at much higher concentrations as required for their protective effect. However, no clinical data on NADs are yet available, which impedes drawing firm conclusions on dopamine-related side effects or safety of NADs in humans.

Nakao et al. have postulated that cytochrome P450 heme proteins are degraded during hypothermic organ preservation. This causes a detrimental increased level of intracellular free heme which subsequently leads to oxidative injury [32]. In addition to their reducing properties, catechol structures also have the propensity to coordinate with iron. Hence, it is at present unclear if the relevance of the catechol structure in preventing cold inflicted injury resides in its capacity to scavenge reactive oxygen intermediates or in preventing the formation of these intermediates via coordination with iron in the heme moiety.

Name:	Chemical structure:	Biological effects:
Dopamine	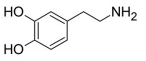	hemodynamic active [28,31], TRPV1 inactive [52], antioxidant [20], cryoprotective [21-26], HO-1 inducer [21]
N-pivaloyl dopamine	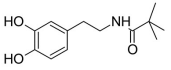	activates UPR [40]
N-octanoyl dopamine (NOD)	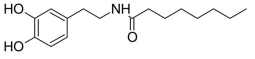	hemodynamic inactive [28], TRPV1 agonist [52], antioxidant [69], NF-κB inhibitor [68,69], cryoprotrective [40], HO-1 inducer [68], antiproliferative [40,69], activates UPR [40], protects against I/R-injury [18,52],
N-oleoyl dopamine (OLDA)	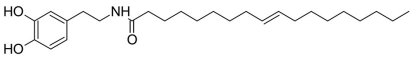	CB1 ligand [34], TRPV1 agonist [34,36], NF-κB inhibitor [66], antiproliferative [66], COX-2 inducer [63], 5-LOX inhibitor [56], protects against I/R-injury [36]
N-ararchidonoyl dopamine (NADA)	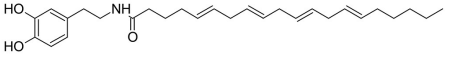	CB1 agonist [33], TRPV1 agonist [35,36], NF-κB inhibitor [66,67], antiproliferative [66], COX-2 inducer [63], PGD_2 inducer [63], PGE_2 inhibitor [63,64]
N-docosahexaenoyl (DHA) dopamine	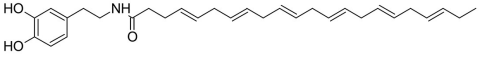	antioxidant [39]
2-arachidonoyl glycerol	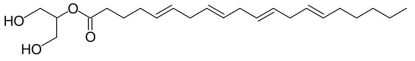	CB1 and CB2 agonist [33,61], PGD_2 inducer [62]
Anandamide	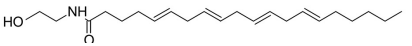	CB1 and CB2 agonist [61], TRPV1 agonist [36]

Figure 1. N-acyl dopamine derivates and endocannabinoids.

Cytoprotective properties

The cytoprotective properties of endogenous NADs have been studied mainly in relation to brain function and neuroprotection, including positive effects on hypoxic–ischemic injury or brain inflammatory processes. Their protective effect is mainly attributed to the long-chain polyunsaturated fatty acids. Apart from the fact that dopamine fatty acid conjugates can act as cannabinoid receptor ligand [33] and as TRPV1 agonist [34, 35] , Shashoua et al. reported that some of these conjugates also act as carrier to increase brain dopamine content [35]. In line with the tendency of docosahexaenoic acid (DHA) to accumulate in brain tissue [36], the DHA–dopamine conjugate is most active in increasing dopamine uptake by the brain. Bobrov et al. showed that DHA–dopamine exhibited antioxidant activity and produced a dose-dependent protective effect on cultured granular cells from rat cerebellum under conditions of oxidative stress. It also decelerated the development of Parkinson's disease-like symptoms in a MPTP (1-methyl-4-phenyl-1,2,3,6-tetrahydropyridine) mouse model [37].

The antioxidant properties of DHA-dopamine is most likely attributed to the catechol structure as it is also present in synthetic NADs with short saturated fatty acids, e.g. NOD and *N*-pivaloyl dopamine. Recently, Stamellou et al. reported that these synthetic NADs transiently activate the unfolded protein response (UPR) in endothelial cells [38]. This property is again dependent on the redox activity of these compounds. Although persistent activation of the UPR may result in apoptosis, the synthetic NADs did not affect cell viability in a µM range, yet they strongly impaired proliferation of endothelial cells [38] and smooth muscle cells [unpublished data]. Interestingly, Stamellou et al. also demonstrated that long-term treatment of endothelial cells with synthetic NADs results in hypo metabolism and thermotolerance. This is associated with decreased intracellular ATP concentrations, activation of AMP-activated protein kinase and increased resistance to cold inflicted cell injury. It thus seems that induction of the UPR by short synthetic NADs causes an adaptive response in endothelial cells. Since it has been suggested that induction of the UPR is an integral part of the protective strategies used by hibernating mammals for long term survival in a state of cold torpor [39–41], adaptation of donor organs to withstand cold ischemia via induction of the UPR would be an intriguing strategy to improve organ quality under ischemic conditions. It should be emphasized however that organ adaptation in hibernating mammals goes far beyond induction of the UPR [42].

Protection against I/R-injury

Even though our understanding in the pathophysiology of I/R-injury has improved to a large extent in the past decades, there is still a need for novel compounds that minimize the extent of tissue damage. Ischemic preconditioning (IPC) is a protective procedure accomplished by exposing the organ to a minor stress, which by itself does not cause noticeable harm. The benefit of IPC was first demonstrated by Murry et al. in dogs [43];

its protective potential on reperfusion injury is now widely accepted. When the heart was subjected to short ischemic episodes separated by short perfusion periods the myocardium was more tolerant to subsequent prolonged ischemia. Although IPC is difficult to implement as a clinical strategy, identifying effective molecules in IPC can lead to new therapeutic treatment modalities. Yet, the underlying mechanisms of IPC have been equivocally discussed [44–46].

Proteasomal iron–protein degradation has been suggested by Bulvik et al. as important mechanism of IPC. In this scenario it is postulated that expeditious cytosolic iron release alters iron homeostasis which subsequently protects the myocardium during I/R [44]. In contrast Wu et al. proposed that the benefit of IPC was mediated via suppressing excessive endoplasmic reticulum stress thereby diminishing C/EBP homologous protein (CHOP)-dependent apoptosis [45]. Also suppression of cardiac progenitor cell apoptosis has been suggested [46]. More recently Lu et al. suggested a role of TRPV1 in IPC [47]. Their data suggest that IPC upregulates arachidonate 12-lipoxygenase and consequently increases the production of the endovanilloid 12(S)-hydroxyeicosatetraenoic acid, which in turn activates TRPV1. It is believed that TRPV1 functions as polymodal sensor to detect micro-environmental changes in tissues, e.g. low pH, high temperature, or noxious stimuli [48] and [49]. These changes are likely present in ischemic tissue. The finding that NOD activates TRPV1 may explain its renoprotective properties in the setting of ischemia-induced AKI [50], yet the causality of this observation and its translation to clinical application warrants further supportive evidence. Immune modulation and inflammation

The main pharmacological functions of the endocannabinoid system include neuromodulation, controlling motor functions, cognition, emotional responses, homeostasis and motivation. In the periphery, this system is also an important modulator of immunity [51].

Several studies have unambiguously demonstrated that endocannabinoids modulate proliferation and apoptosis of T and B lymphocytes, macrophage-mediated killing, cytokine production, immune cell activation by inflammatory stimuli, chemotaxis and inflammatory cell migration [52, 53]. Most if not all of these effects have been reported to be primarily mediated via CB2 receptors causing inhibition of the cAMP/protein kinase A pathway.

NADs may modulate the immune system in a similar fashion. Yet there are a number of biological activities described for NADs related to immune modulation that are neither mediated via CB receptors nor via TRPV1. Initially NADs were described as potent inhibitors of 5-lipoxygenase [54]. This enzyme catalyses two steps in the biosynthesis of leukotrienes (LT), a group of lipid inflammatory mediators derived from arachidonic acid. LT antagonists are used in treatment of asthma; more recently a potential role in neointimal thickening and atherosclerosis has raised considerable interest [55–58]

Cyclooxygenase-2 (COX-2) is an enzyme that plays a key role in inflammatory processes. Classically, this enzyme is up-regulated in inflammatory situations and is responsible for the generation of prostaglandins (PG). One lesser-known property of COX-2 is

its ability to metabolize the endocannabinoids, *N*-arachidonoyl ethanolamine and 2-arachidonoyl glycerol, generating PG-glycerol and PG-ethanolamides [59]. Although the formation of these COX-2-derived metabolites of endocannabinoids has been known for a while, their biological effects remain to be fully elucidated. Recently, Alhouayek et al. showed that 2-arachidonoyl glycerol through its oxidation by COX-2 gives rise to the anti-inflammatory prostaglandin D2-glycerol ester [60].

Interestingly, Navarrete et al. found that *N*-arachidonoyl dopamine (NADA) activates a redox-sensitive p38 MAPK pathway that stabilizes COX-2 mRNA resulting in the accumulation of the COX-2 protein [61, 62]. Moreover, they demonstrated that NADA inhibits the expression of microsomal prostaglandin E2 synthase 1 and thus the production of the inflammatory mediator PGE2. This was paralleled by the induction of lipocalin-type prostaglandin D synthase and increased production of PGD2. Therefore even though COX-2 amplifies tissue inflammation, in conjunction with NADs, in particular NADA, it may redirect PG synthesis towards formation of PGD2 [62]. The finding of Patel et al. that selective inhibitors of COX-2 may worsen renal dysfunction and injury in conditions associated with renal ischemia supports this view [63]. Because of their redox active catechol structure NADs have the propensity to inhibit the activation of redox dependent proinflammatory transcription factors, e.g. NF-κB, AP-1 and NFAT [64, 65] and therefore they largely inhibit the expression of inflammatory mediators produced by endothelial cells [66] and proliferation of T cells [64–67].

Implementation of NAD in transplantation medicine

While the list of compounds that show beneficial effects at the pre-clinical stage is steadily increasing, only a limited number of such compounds will find a clinical use. The lack of venture capital for entering clinical phase studies is among others why only a small percentage of promising compounds will proceed, let alone will obtain FDA approval.

The multitude of beneficial effects of NADs warrants careful considerations on the application mode, e.g. donor or recipient treatment, additive to preservation solutions, and their associated ethical hurdles. Particularly donor pre-treatment may raise ethical concerns as to whether written informed consent of the recipient is required. Waiving informed consent of the recipient in the randomized donor dopamine treatment trial was justified because it was (1) strictly observational in the recipient; (2) the intervention was limited to the deceased donor and (3) limited to a fully approved drug. Clearly, as FDA approval for the use of NADs in human does not exist, similar studies with the use of NADs are not possible. Although NADs may also have the propensity to protect allografts when used as additive to the organ preservation solution, there is no supportive evidence using whole organs, albeit that it has been reported for experimental models that addition of dopamine to the preservation solutions is protective to liver [23] and renal allografts

[25]. Also the type of NADs for implementation in transplantation medicine requires careful considerations since some of the beneficial effects of NADs are meditated by the fatty acid tail and therefore not present in all NADs.

Concluding remarks

This review has summarized the potential protective properties of NADs on transplantation relevant entities. Based on their propensity to act as agonist of CB receptors and TRPV1 channels, to act as anti-oxidant and to inhibit inflammatory mediators including those derived from arachidonic acid, NADs may find clinical implementation in transplantation medicine as a mean of pre-conditioning to prevent brain death-induced inflammation and to prepare donor organs to cold ischemia. Yet it should be emphasized that most of the potential benefits of NADs mainly have been studied *in vitro* and only to a limited extent in transplantation relevant in vivo models. Nonetheless their potential as new expedient drugs should be further explored using relevant transplantation models. The composition of the NADs, i.e. the type of fatty acid that is required for a specific in vivo biological effect, as well as the pharmacokinetic of these compounds should be implemented in future studies.

All authors report no conflict of interest.

References

1. Terasaki, P.I., et al., *High survival rates of kidney transplants from spousal and living unrelated donors.* N Engl J Med, 1995. **333**(6): p. 333–6.
2. Bugge, J.F., *Brain death and its implications for management of the potential organ donor.* Acta Anaesthesiol Scand, 2009. **53**(10): p. 1239–50.
3. Wood, K.E., et al., *Care of the potential organ donor.* N Engl J Med, 2004. **351**(26): p. 2730–9.
4. Kusaka, M., et al., *Activation of inflammatory mediators in rat renal isografts by donor brain death.* Transplantation, 2000. **69**(3): p. 405–10.
5. Venkateswaran, R.V., et al., *Early donor management increases the retrieval rate of lungs for transplantation.* Ann Thorac Surg, 2008. **85**(1): p. 278–86; discussion 286.
6. Zaroff, J.G., et al., *Consensus conference report: maximizing use of organs recovered from the cadaver donor: cardiac recommendations, March 28–29, 2001, Crystal City, Va.* Circulation, 2002. **106**(7): p. 836–41.
7. Rosendale, J.D., et al., *Increased transplanted organs from the use of a standardized donor management protocol.* Am J Transplant, 2002. **2**(8): p. 761–8.
8. Duke, G.J. and A.D. Bersten, *Dopamine and renal salvage in the critically ill patient.* Anaesth Intensive Care, 1992. **20**(3): p. 277–87.
9. Kindgen-Milles, D. and J. Tarnow, *[Low dosage dopamine improves kidney function: current status of knowledge and evaluation of a controversial topic].* Anasthesiol Intensivmed Notfallmed Schmerzther, 1997. **32**(6): p. 333–42.
10. Holmes, C.L. and K.R. Walley, *Bad medicine: low-dose dopamine in the ICU.* Chest, 2003. **123**(4): p. 1266–75.
11. Bellomo, R., et al., *Low-dose dopamine in patients with early renal dysfunction: a placebo-controlled randomised trial. Australian and New Zealand Intensive Care Society (ANZICS) Clinical Trials Group.* Lancet, 2000. **356**(9248): p. 2139–43.
12. Friedrich, J.O., et al., *Meta-analysis: low-dose dopamine increases urine output but does not prevent renal dysfunction or death.* Ann Intern Med, 2005. **142**(7): p. 510–24.
13. Kellum, J.A. and M.D. J, *Use of dopamine in acute renal failure: a meta-analysis.* Crit Care Med, 2001. **29**(8): p. 1526–31.
14. Joannidis, M., et al., *Prevention of acute kidney injury and protection of renal function in the intensive care unit. Expert opinion of the Working Group for Nephrology, ESICM.* Intensive Care Med, 2010. **36**(3): p. 392–411.
15. Schnuelle, P., et al., *Effects of donor pretreatment with dopamine on graft function after kidney transplantation: a randomized controlled trial.* JAMA, 2009. **302**(10): p. 1067–75.
16. Benck, U., et al., *Effects of donor pre-treatment with dopamine on survival after heart transplantation: a cohort study of heart transplant recipients nested in a randomized controlled multicenter trial.* J Am Coll Cardiol, 2011. **58**(17): p. 1768–77.
17. Hoeger, S., et al., *Dopamine treatment in brain-dead rats mediates anti-inflammatory effects: the role of hemodynamic stabilization and D-receptor stimulation.* Transpl Int, 2007. **20**(9): p. 790–9.
18. Spindler, R.S., et al., *N-Octanoyl Dopamine for Donor Treatment in a Brain-death Model of Kidney and Heart Transplantation.* Transplantation, 2015. **99**(5): p. 935–41.

19. Kapper, S., et al., *Modulation of chemokine production and expression of adhesion molecules in renal tubular epithelial and endothelial cells by catecholamines.* Transplantation, 2002. **74**(2): p. 253–60.
20. Beck, G.C., et al., *Modulation of chemokine production in lung microvascular endothelial cells by dopamine is mediated via an oxidative mechanism.* Am J Respir Cell Mol Biol, 2001. **25**(5): p. 636–43.
21. Berger, S.P., et al., *Dopamine induces the expression of heme oxygenase-1 by human endothelial cells in vitro.* Kidney Int, 2000. **58**(6): p. 2314–9.
22. Yard, B., et al., *Prevention of cold-preservation injury of cultured endothelial cells by catecholamines and related compounds.* Am J Transplant, 2004. **4**(1): p. 22–30.
23. Koetting, M., J. Stegemann, and T. Minor, *Dopamine as additive to cold preservation solution improves postischemic integrity of the liver.* Transpl Int, 2010. **23**(9): p. 951–8.
24. Vettel, C., et al., *Dopamine and lipophilic derivates protect cardiomyocytes against cold preservation injury.* J Pharmacol Exp Ther, 2014. **348**(1): p. 77–85.
25. Gottmann, U., et al., *Effect of pre-treatment with catecholamines on cold preservation and ischemia/reperfusion-injury in rats.* Kidney Int, 2006. **70**(2): p. 321–8.
26. Talaei, F., et al., *Serotonin and dopamine protect from hypothermia/rewarming damage through the CBS/H2S pathway.* PLoS One, 2011. **6**(7): p. e22568.
27. Salahudeen, A.K., et al., *Fenoldopam preconditioning: role of heme oxygenase-1 in protecting human tubular cells and rodent kidneys against cold-hypoxic injury.* Transplantation, 2011. **91**(2): p. 176–82.
28. Losel, R.M., et al., *N-octanoyl dopamine, a non-hemodyanic dopamine derivative, for cell protection during hypothermic organ preservation.* PLoS One, 2010. **5**(3): p. e9713.
29. Zapata, P. and A. Zuazo, *Reversal of respiratory responses to dopamine after dopamine antagonists.* Respir Physiol, 1982. **47**(2): p. 239–55.
30. Katz, R.L., C.O. Lord, and K.E. Eakins, *Anesthetic-dopamine cardiac arrhythmias and their prevention by beta adrenergic blockade.* J Pharmacol Exp Ther, 1967. **158**(1): p. 40–5.
31. Kohli, J.D., et al., *Structure activity relationships of N-substituted dopamine derivatives as agonists of the dopamine vascular and other cardiovascular receptors.* J Pharmacol Exp Ther, 1980. **213**(2): p. 370–4.
32. Nakao, A., et al., *Ex vivo carbon monoxide prevents cytochrome P450 degradation and ischemia/reperfusion injury of kidney grafts.* Kidney Int, 2008. **74**(8): p. 1009–16.
33. Bisogno, T., et al., *N-acyl-dopamines: novel synthetic CB(1) cannabinoid-receptor ligands and inhibitors of anandamide inactivation with cannabimimetic activity in vitro and in vivo.* Biochem J, 2000. **351 Pt 3**: p. 817–24.
34. Huang, S.M., et al., *An endogenous capsaicin-like substance with high potency at recombinant and native vanilloid VR1 receptors.* Proc Natl Acad Sci U S A, 2002. **99**(12): p. 8400–5.
35. Shashoua, V.E. and G.W. Hesse, *N-docosahexaenoyl, 3 hydroxytyramine: a dopaminergic compound that penetrates the blood-brain barrier and suppresses appetite.* Life Sci, 1996. **58**(16): p. 1347–57.
36. Rapoport, S.I., E. Ramadan, and M. Basselin, *Docosahexaenoic acid (DHA) incorporation into the brain from plasma, as an in vivo biomarker of brain DHA metabolism and neurotransmission.* Prostaglandins Other Lipid Mediat, 2011. **96**(1–4): p. 109–13.
37. Bobrov, M.Y., et al., *Antioxidant and neuroprotective properties of N-docosahexaenoyl dopamine.* Bull Exp Biol Med, 2006. **142**(4): p. 425–7.
38. Stamellou, E., et al., *N-octanoyl dopamine treatment of endothelial cells induces the unfolded protein response and results in hypometabolism and tolerance to hypothermia.* PLoS One, 2014. **9**(6): p. e99298.

39. Mamady, H. and K.B. Storey, *Coping with the stress: expression of ATF4, ATF6, and downstream targets in organs of hibernating ground squirrels.* Arch Biochem Biophys, 2008. **477**(1): p. 77–85.
40. Krivoruchko, A. and K.B. Storey, *Activation of the unfolded protein response during anoxia exposure in the turtle Trachemys scripta elegans.* Mol Cell Biochem, 2013. **374**(1–2): p. 91–103.
41. Storey, K.B., *Out cold: biochemical regulation of mammalian hibernation-a mini-review.* Gerontology, 2010. **56**(2): p. 220–30.
42. Jani, A., et al., *Renal adaptation during hibernation.* Am J Physiol Renal Physiol, 2013. **305**(11): p. F1521–32.
43. Murry, C.E., R.B. Jennings, and K.A. Reimer, *Preconditioning with ischemia: a delay of lethal cell injury in ischemic myocardium.* Circulation, 1986. **74**(5): p. 1124–36.
44. Bulvik, B.E., et al., *Cardiac protection by preconditioning is generated via an iron-signal created by proteasomal degradation of iron proteins.* PLoS One, 2012. **7**(11): p. e48947.
45. Wu, X.D., et al., *Hypoxic preconditioning protects microvascular endothelial cells against hypoxia/reoxygenation injury by attenuating endoplasmic reticulum stress.* Apoptosis, 2013. **18**(1): p. 85–98.
46. Hu, S., et al., *Hypoxic preconditioning increases survival of cardiac progenitor cells via the pim-1 kinase-mediated anti-apoptotic effect.* Circ J, 2014. **78**(3): p. 724–31.
47. Lu, M.J., et al., *Hypoxic preconditioning protects rat hearts against ischemia-reperfusion injury via the arachidonate12-lipoxygenase/transient receptor potential vanilloid 1 pathway.* Basic Res Cardiol, 2014. **109**(4): p. 414.
48. Pan, H.L. and S.R. Chen, *Sensing tissue ischemia: another new function for capsaicin receptors?* Circulation, 2004. **110**(13): p. 1826–31.
49. Premkumar, L.S. and G.P. Ahern, *Induction of vanilloid receptor channel activity by protein kinase C.* Nature, 2000. **408**(6815): p. 985–90.
50. Tsagogiorgas, C., et al., *N-octanoyl-dopamine is an agonist at the capsaicin receptor TRPV1 and mitigates ischemia-induced [corrected] acute kidney injury in rat.* PLoS One, 2012. **7**(8): p. e43525.
51. Pandey, R., et al., *Endocannabinoids and immune regulation.* Pharmacol Res, 2009. **60**(2): p. 85–92.
52. Klein, T.W., *Cannabinoid-based drugs as anti-inflammatory therapeutics.* Nat Rev Immunol, 2005. **5**(5): p. 400–11.
53. Klein, T.W., et al., *The cannabinoid system and immune modulation.* J Leukoc Biol, 2003. **74**(4): p. 486–96.
54. Tseng, C.F., et al., *Inhibition of in vitro prostaglandin and leukotriene biosyntheses by cinnamoyl-beta-phenethylamine and N-acyldopamine derivatives.* Chem Pharm Bull (Tokyo), 1992. **40**(2): p. 396–400.
55. Werz, O. and D. Steinhilber, *Therapeutic options for 5-lipoxygenase inhibitors.* Pharmacol Ther, 2006. **112**(3): p. 701–18.
56. Dahlen, S.E., *Treatment of asthma with antileukotrienes: first line or last resort therapy?* Eur J Pharmacol, 2006. **533**(1–3): p. 40–56.
57. Peters-Golden, M. and W.R. Henderson, Jr., *Leukotrienes.* N Engl J Med, 2007. **357**(18): p. 1841–54.
58. Kabankov Iu, S., A.K. Kvasnikov, and E.D. Kvasnikova, *[Etiology of gastroenteritis in piglets].* Veterinariia, 1978(4): p. 56–8.

59. Kozak, K.R., et al., *Metabolism of the endocannabinoids, 2-arachidonylglycerol and anandamide, into prostaglandin, thromboxane, and prostacyclin glycerol esters and ethanolamides.* J Biol Chem, 2002. **277**(47): p. 44877–85.
60. Alhouayek, M., et al., *Implication of the anti-inflammatory bioactive lipid prostaglandin D2-glycerol ester in the control of macrophage activation and inflammation by ABHD6.* Proc Natl Acad Sci U S A, 2013. **110**(43): p. 17558–63.
61. Navarrete, C.M., et al., *Endogenous N-acyl-dopamines induce COX-2 expression in brain endothelial cells by stabilizing mRNA through a p38 dependent pathway.* Biochem Pharmacol, 2010. **79**(12): p. 1805–14.
62. Navarrete, C.M., et al., *Opposite effects of anandamide and N-arachidonoyl dopamine in the regulation of prostaglandin E and 8-iso-PGF formation in primary glial cells.* J Neurochem, 2009. **109**(2): p. 452–64.
63. Patel, N.S., et al., *The role of cycloxygenase-2 in the rodent kidney following ischaemia/reperfusion injury in vivo.* Eur J Pharmacol, 2007. **562**(1–2): p. 148–54.
64. Sancho, R., et al., *Immunosuppressive activity of endovanilloids: N-arachidonoyl-dopamine inhibits activation of the NF-kappa B, NFAT, and activator protein 1 signaling pathways.* J Immunol, 2004. **172**(4): p. 2341–51.
65. Sancho, R., et al., *Mechanisms of HIV-1 inhibition by the lipid mediator N-arachidonoyldopamine.* J Immunol, 2005. **175**(6): p. 3990–9.
66. Hottenrott, M.C., et al., *N-octanoyl dopamine inhibits the expression of a subset of kappaB regulated genes: potential role of p65 Ser276 phosphorylation.* PLoS One, 2013. **8**(9): p. e73122.
67. Wedel, J., et al., *N-Octanoyl dopamine transiently inhibits T cell proliferation via G1 cell-cycle arrest and inhibition of redox-dependent transcription factors.* J Leukoc Biol, 2014. **96**(3): p. 453–62.

Experimental Studies

Chapter 3

N-octanoyl dopamine treatment exerts reno-protective properties in acute kidney injury but not in renal allograft recipients

Nephrology, dialysis, transplantation. 2015 Oct 9. pii: gfv363.

Prama Pallavi*,Sarah Klotz*, Charalambos Tsagogiorgas, Fabian Zimmer, Frank G. Zöllner, Uta Binzen, Wolfgang Greffrath, Rolf-Detlef Treede, Jakob Walter, Martin C. Harmsen, Bernhard K. Krämer, Mathias Hafner, Benito A. Yard ,Simone Hoeger

* Equally contributing authors

Abstract

N-octanoyl dopamine (NOD) treatment improves renal function when applied to brain dead donors and in the setting of warm ischemia induced acute kidney injury (AKI). Because it also activates transient receptor potential vanilloid type 1 (TRPV1) channels we first assessed if NOD conveys its renoprotective properties in warm ischemia induced AKI via TRPV1 and secondly if renal transplant recipients also benefit from NOD treatment.

We induced warm renal ischemia in Lewis, wild type and TRPV1$^{-/-}$ Sprague Dawley rats by clamping the left renal artery for 45 min. Transplantations were performed in allogeneic and syngeneic donor recipient combinations (Fisher to Lewis, Lewis to Lewis) with a cold ischemia time of 20 h. Treatment was instituted directly after restoration of organ perfusion. Renal function, histology and perfusion were assessed by serum creatinine, microscopy and magnetic resonance imaging (MRI) using arterial spin labelling (ASL).

NOD treatment significantly improved renal function in Lewis rats after warm ischemia induced AKI. It was however not effective after prolonged cold ischemia. The renoprotective properties of NOD were only observed in Lewis or WT-, but not TRPV1$^{-/-}$ Sprague Dawley rats. Renal inflammation was significantly abrogated by NOD. MRI-ASL showed a significantly lower cortical perfusion in ischemic as compared to non-ischemic kidneys. No overall all differences were observed in renal perfusion between NOD and NaCl treated rats.

NOD treatment reduces renal injury in warm ischemia but is not effective in renal transplant in our experimental animal models. The salutary effect of NOD appears to be TPRV1 dependent, not involving large changes in renal perfusion.

Introduction

Acute kidney injury (AKI) is recognized as a major complication in intensive care unit patients [1-4]. Approximately thirteen percent of hospital-acquired AKI patients will progress to end stage renal disease within 3 years [5]. Innovative interventions beyond supportive therapy are currently not available for AKI patients; emphasizing the clinical need for new therapeutic approaches.

Delayed graft function (DGF) is a manifestation of AKI with attributes unique to transplantation. The diagnosis of DGF is complicated by a variety of definitions based on a range of clinical criteria depending on the local transplant centre, region, and country [6, 7]. Along with an increased use of marginal donors the incidence of DGF has increased over time, translating to a fourty percent decrease in long-term graft survival [8, 9]. Cold ischemia time is strongly associated with DGF, with a twenty-three percent increase in the risk of DGF for every 6 h of cold ischemia [10, 11].

We have recently designed *N*-octanoyl dopamine (NOD) as a possible drug candidate to overcome the limitations of dopamine treatment in brain dead donors, i.e. tachycardia and high blood pressure, which was observed in approximately twelve percent of treated donors in our prospective, randomized clinical trial to assess the salutary effect of donor dopamine treatment on DGF [12]. In contrast to dopamine (DA), NOD does not affect mean arterial blood pressure in vivo [13], yet also improves renal function in recipient rats that received a renal allograft from a NOD treated brain dead donor [14, 15]. NOD protects cultured cardiomyocytes, endothelial and renal epithelial cells against cold inflicted injury, much better as compared to dopamine. In addition to this, NOD has a profound anti-inflammatory action as it inhibits a subset of pro-inflammatory genes via impaired NFκB trans-activation [16], thus making NOD a promising drug candidate beyond its intentional use in donor management.

Indeed we have reported that NOD also has renoprotective properties in the setting of warm ischemia-induced AKI, when applied shortly before and after the induction of AKI [17]. Although *in vitro* experiments have indicated that NOD is an agonist of the transient receptor potential vanilloid type 1 channel (TRPV1) [17], it, is currently not clear if the renoprotective properties of NOD are mediated via TRPV1. Yet, other TRPV1 agonists have shown a beneficial effect on ischemia reperfusion (I/R) injury in different organs [18-20]. Activation of TRPV1 may result in the release of calcitonin gene related peptide (CGRP) and substance P (SP) [21-23] from sensory nerves, possibly causing local vasodilation in end-organs [19, 24-27].

In the present study we hypothesize that the renoprotective effect of NOD in warm ischemia-induced AKI is TRPV1 dependent. TRPV1 activation will increase renal perfusion and thus improves restoration of renal function. Because TRPV1 activation may also occur in renal allografts after prolonged static cold storage, we speculated that NOD treatment of renal allograft recipients would also benefit from NOD.

Subjects and Methods

Animals

Male Fisher (F344/DuCrl), Lewis (LEW/Crl) rats and Sprague Dawley (CD® IGS) rats weighting 200 g – 220 g were obtained from Charles River (Sulzfeld, Germany). TRPV1$^{-/-}$ Sprague Dawley rats were obtained from SAGE Labs (Boyertown, PA, US). Lewis rats were used in warm ischemia-induced AKI model to demonstrate that the NOD treatment after onset of ischemia is equally protective as the combination of pre-and post-treatment in previous study [17]. Since TRPV1$^{-/-}$ rats were bred on the Sprague Dawley background, WT Sprague Dawley were used as control. For renal transplantation the allogeneic Fisher to Lewis and syngeneic Lewis to Lewis models were used. Animals were kept under standard conditions and fed standard rodent chow and water ad libitum. All procedures were performed according to the Guide of the Care and Use of Laboratory Animals published by the National Academy of Sciences and were approved by the local authorities (Regierungspräsidium Karlsruhe AZ: 35-9185.81/G – 19/12, 35-9185.81/G – 229/12).

Experimental protocol

Ischemia-induced acute kidney injury (AKI) and renal transplantation (Tx)

All surgical procedures were performed under general anaesthesia using ketamine (100 mg/mL; Ketamin®, Intervet Deutschland GmbH, Unterschleißheim, Germany) and xylazine (6 mg/mL; Rompun®, Bayer Health Care, Leverkusen, Germany) intraperitoneal. AKI was induced by clamping the left renal artery for 45 min in unilateral nephrectomized rats. For ASL measurements the contralateral kidney was not removed but served as non-ischemic control.

Allogeneic and syngeneic renal transplantations were performed as described previously [28, 29]. After explantation, donor kidneys were stored at 4° C in University of Wisconsin solution for 20 h, before transplantation into bilaterally nephrectomized recipients.

Osmotic minipump (Alzet® 2 mL1, 10 µL/hr, Charles River Laboratories, Sulzfeld, Germany) filled with 40 µM NOD (Novaliq GmbH, Heidelberg, Germany) or NaCl (NaCl 0.9 percent Fresenius Kabi Deutschland GmbH, Bad Homburg, Germany) were implanted subcutaneously directly after induction of AKI or after transplantation as described [28, 29]. Each group consisted of a minimum of eight animals. No immunosuppression was administered in the transplantation model. Animals were treated according to the following scheme:

AKI:

Group 1: Control; ischemia time 45 min; NaCl treatment for 5 days

1A: AKI in Lewis rats

1B: AKI in wild type (WT) Sprague Dawley rats (sd)

1C: AKI in TRPV1$^{-/-}$ Sprague Dawley rats

1D: AKI (left kidney) in Lewis rats, right kidney was not removed and served as control for renal perfusion experiments

Group 2: NOD; ischemia time 45 min; NOD treatment for 5 days

2A: AKI in Lewis rats

2B: AKI in wild type (WT) Sprague Dawley rats

2C: AKI in TRPV1$^{-/-}$ Sprague Dawley rats

2D: AKI (left kidney) in Lewis rats, right kidney was not removed and served as control for renal perfusion experiments

Transplantation (Tx):

Allogeneic (Allo): Graft from Fisher donors transplanted into bilaterally nephrectomized Lewis recipients

Group 3: Allo-Tx – control; post Tx treatment with NaCl for 7 days

Group 4: Allo-Tx – NOD; post Tx treatment with NOD for 7 days

Syngeneic(Syn): Graft from Lewis donors transplanted into bilaterally nephrectomized Lewis recipients

Group 5: Syn-Tx – control; post Tx treatment with NaCl for 7 days

Group 6: Syn-Tx – NOD; post Tx treatment with NOD for 7 days

Renal function

Renal function was assessed by serum creatinine (s-crea) and serum urea (s-urea), measured on days 0, 1, 3, 5 (and 7 in Tx models) after surgery. s-crea and s-urea are expressed as mean in mg/dl ± SD.

Immunohistochemistry

The kidneys were harvested and on day 5 after AKI and on day 7 after Tx and immunohistochemical staining were performed as described before [30]. Quantification of ED1 staining was performed by morphometric analysis using software (Cell^F 5.1, Olympus Soft Imaging Solutions GmbH, Münster, Germany). For each section 20 random high magnification (400x) microscopic fields were analyzed, the results are expressed as percent ED1 stained area per microscopic field ± SD.

Real-time quantitative PCR

Total RNA was isolated from renal tissue using Trizol-Reagent (Life Technologies, Inc., Rockville, MD, USA). After DNase treatment, (RNase free DNase I, Ambion, Woodward, Austin, TX, USA) 1 µg of total RNA was reverse-transcribed into cDNA using the High-Capacity cDNA Reverse Transcription Kit (Life Technologies). TaqMan™ real-time polymerase chain reaction was used for quantitative measurement of mRNA expression of CXCL1 (Rn00578225_m1), E-Selectin (Rn00594072_m1), ICAM (Rn00564227_m1), IL-6 (Rn99999011_m1), TNF-alpha (Rn99999017_m1), VCAM1 (Rn00563627_m1). All samples were measured in triplicate. Gene expression was normalized to the housekeeping gene beta-actin (Rn006677869_m1) and expressed as fold change relative to control native kidney and calculated with the ΔΔCT method [31].

Live-cell calcium imaging

Preparation of acutely dissociated dorsal root ganglion (DRG) neurons and imaging were done as described before [32]. A cell was considered an excitable neuron and then evaluated only when significantly responding to application of capsaicin and/or depolarization by high potassium solution (140 mM). Each single slide investigated was regarded as an independent experiment. Five independent experiments were performed on acutely dissociated DRG neurons obtained from three different male WT or TRPV1$^{-/-}$ rats.

Arterial Spin Labelling-Magnetic Resonance Imaging (ASL-MRI)

Renal perfusion was measured with MRI using a flow-sensitive alternating inversion recovery (FAIR)-ASL technique [33, 34]. In brief, to acquire a perfusion-weighted image, arterial blood is labelled by inverting its magnetization. After an inflow time (inversion time) TI which allows the labelled blood to flow into the tissue of interest, it is imaged with an appropriate readout sequence. When using FAIR, the labelling is alternating between a global inversion (tag image) and a slice-selective inversion (control image). Several tag-control pairs and additional M0 images, without prior labelling are recorded. All ASL perfusion measurements were performed following the protocol and parameters described in Zimmer et al. [35]. A 3 T whole-body MR scanner (Magnetom Tim Trio, Siemens Healthcare Sector, Erlangen, Germany) was used. The total measurement time for 30 tag-control pairs and 30 M0 images was 9 min. ASL perfusion maps were calculated by analysing the acquired data with an in-house written MATLAB (Version 7.10, The MathWorks, Natick, MA, USA) script. Renal perfusion was expressed in mL/100g/min.

Statistical Analysis

Data are shown as means±standard deviation (SD). For the calcium imaging data are shown as means±standard error of the mean (SEM). For comparison of two nonparametric independent groups, Wilcoxon Rank Sum test was applied. For comparison of two parametric independent groups two-sample-t-test was performed (JMP 10.0.0; SAS Institute Inc, Cary, NC, USA). Statistical significance was defined as a p-value < 0.05.

Results

NOD treatment improves renal function after warm ischemia

NOD treatment significantly improved renal function in Lewis rats after induction of warm renal ischemia (s-crea NOD vs. NaCl): day 1 – 2.42±0.36 vs. 3.02±0.52, p=0.0406; day 3 – 1.04±0.60 vs. 3.52±1.70, p=0.0038; day 5 – 0.46±0.10 vs. 2.04±1.63, p=0.0032// s-urea NOD vs. NaCl: day 3 – 198.11±106.64 vs. 503.05±231.94, p=0,01; day 5 – 89.75±32.69 vs. 387.44±293.78, p=0.0054) (Figure 1A). While NaCl treated rats displayed a significant body weight loss, this was not observed with NOD treated rats (Figure 1B). Also the numbers of infiltrated $ED1^+$ cells assessed at day 5 were significantly decreased in NOD treated rats (Figure 1C and D). There was no difference in cytokine mRNA expression except for TNFα; IL-6 was not statistically significant Fold change TNF-α: 1.16±0.4 vs 0.69±0.19; Fold change IL6: 6.60±2.3 vs 10.52±3.91; not significant; p=0.0128; NaCl vs NOD treatment).

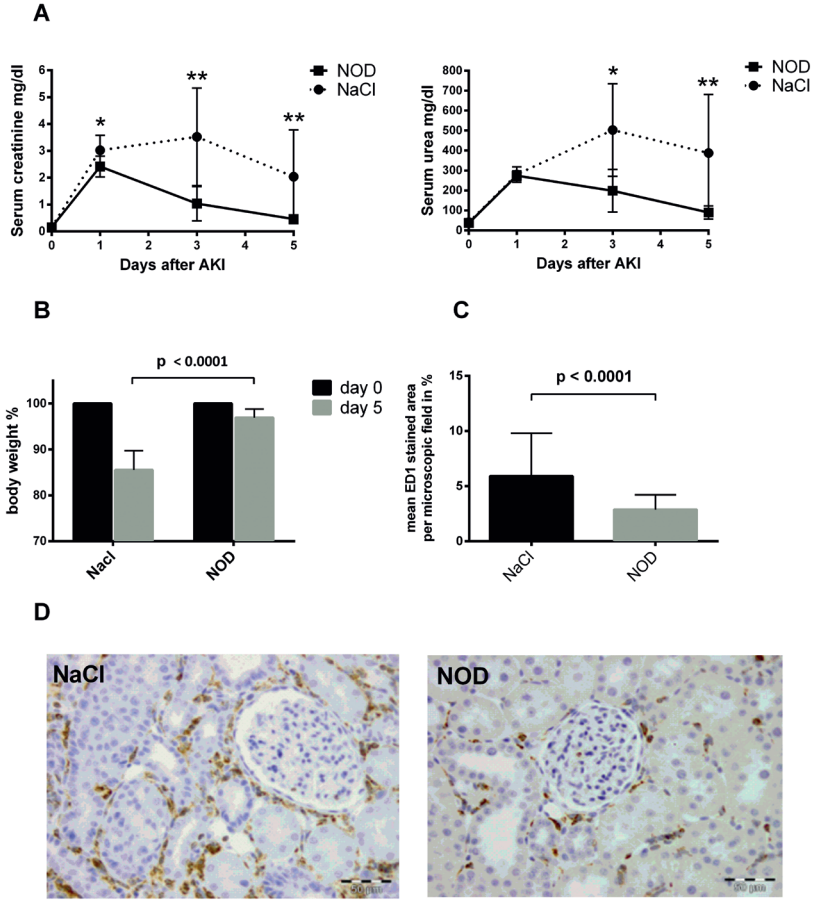

Figure 1. NOD treatment improves renal function and ameliorates inflammation in AKI (A) Serum creatinine (mg/dl) (graph to the left) and serum urea (mg/dl) (graph to the right were assessed on day 0, 1, 3, 5 after induction of AKI. The animals were treated with NOD (bold line) or NaCl (dotted line) via osmotic mini pumps over the whole experimental period. Serum creatinine was significantly lower in NOD treated rats on all days of measurements. Serum creatinine: *p=0.041 (day 1), **p=0.004 (day 3), **p=0.003 (day 5). Serum urea: p=0.344 (day 1), **p=0,010 (day 3), **p=0,005 (day 5). (B) Body weight of each of the animals was assessed directly prior to induction of AKI and 5 days thereafter. The body weight prior to AKI induction was set at 100 percent. In the NaCl treated rats a significant mean body weight loss of ~ 15 percent was observed, while in the NOD treated rats no significant differences were noticed in body weight before and 5 days after induction of AKI. (C) Renal infiltrated ED1$^+$ cells were assessed by immunohistochemistry as described in materials and methods. Quantification of ED1$^+$ was performed by quantitative morphometric analysis. For each animal at least 2 sections were evaluated using 10 randomly chosen high power (400× magnification) microscopic fields. The results are expressed as mean percent ED1$^+$ stained area per microscopic field ± SD. (D) Representative sections obtained from kidneys of the NaCl or NOD treated rats are depicted.

The salutary effect of NOD treatment in ischemia-induced AKI is mediated via TRPV1

We assessed the role of TRPV1 activation in the renoprotective properties of NOD by using TRPV1$^{-/-}$ Sprague Dawley rats. To assure that TRPV1 responses were absent in the TRPV1$^{-/-}$ Sprague Dawley rats, dorsal root ganglion cells (DRG) were isolated from wild type (WT) Sprague Dawley and TRPV1$^{-/-}$ Sprague Dawley rats and subsequently stimulated with either capsaicin or NOD. As determined by live-cell calcium imaging, neither capsaicin (10 µM, 100 µM) nor NOD (30 µM, 100 µM) were able to activate TRPV1 in DRG isolated from TRPV1$^{-/-}$ Sprague Dawley rats, while this was clearly observed in WT Sprague Dawley rats (Figure 2).

Warm ischemia-induced AKI was induced in WT Sprague Dawley and TRPV1$^{-/-}$ Sprague Dawley rats as described for Lewis rats. Impairment of renal function was observed to a similar extent in NaCl treated WT Sprague Dawley and TRPV1$^{-/-}$ Sprague Dawley rats, indicating that the absence of TRPV1 does not influence renal function in the course of AKI (Figure 3A). While NOD treatment was significantly improving renal function in the WT Sprague Dawley rats (Figure 3A, graph to the left), it was not effective in TRPV1$^{-/-}$ Sprague Dawley rats (Figure 3A, graph to the right). Loss of body weight 5 days after AKI was significantly lower in NOD treated WT Sprague Dawley rats as compared to NaCl treatment. This was not observed in TRPV1$^{-/-}$ Sprague Dawley rats (Figure 3B). Irrespective of treatment, TRPV1$^{-/-}$ Sprague Dawley rats displayed less infiltration of ED1^{+} cells as compared to WT Sprague Dawley rats. Only in WT Sprague Dawley rats NOD treatment significantly reduced the amount of infiltrated ED1^{+} cells (Figure 3C and 3D). No difference were observed in cytokine expression in renal tissue 5 days after AKI between the NOD treated and control group except for IL-6 which was significantly higher in treated WT Sprague Dawley rats (Table 1) and TRPV1$^{-/-}$ Sprague Dawley rats. Cytokine expression was significantly lower in the TRPV1$^{-/-}$ Sprague Dawley rats as compared to WT Sprague Dawley rats (Figure 3E).

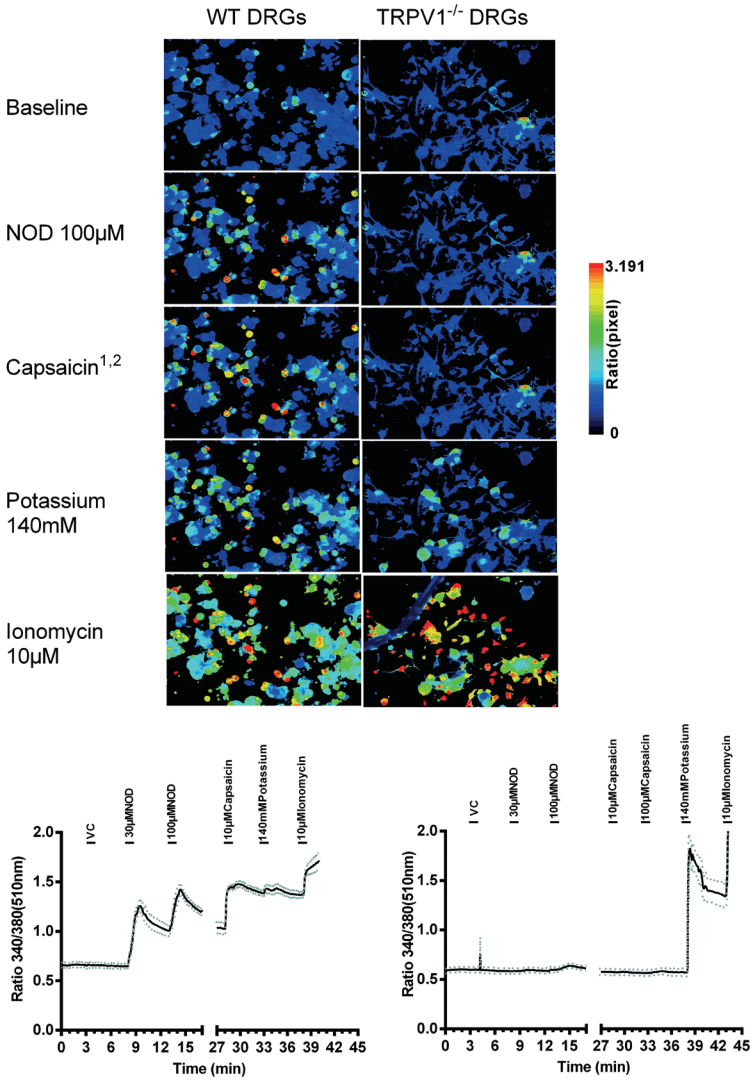

Figure 2. NOD does not activate DRG from TRPV1$^{-/-}$ rats. Live cell calcium imaging was performed on DRG isolated from wild type (WT) Sprague Dawley and TRPV1$^{-/-}$ Sprague Dawley rats. Images were recorded at baseline and after stimulation of DRG with 30 µM and 100 µM NOD, capsaicin 10 µM (1) for WT and 100 µM (2) for KO, 140 mM potassium chloride and 10 µM ionomycin subsequently. The ratio 340/380 at 510 nm is a measure proportional to free intracellular calcium. The images are false colour coded according to the amount of intracellular calcium (graph at the top where warmer colours indicate increasing calcium values). The graphs at the bottom show the mean trace ± SEM of at least 60 regions of interest (ROI) with each ROI containing 1 cell. SEM is depicted as dotted gray line.

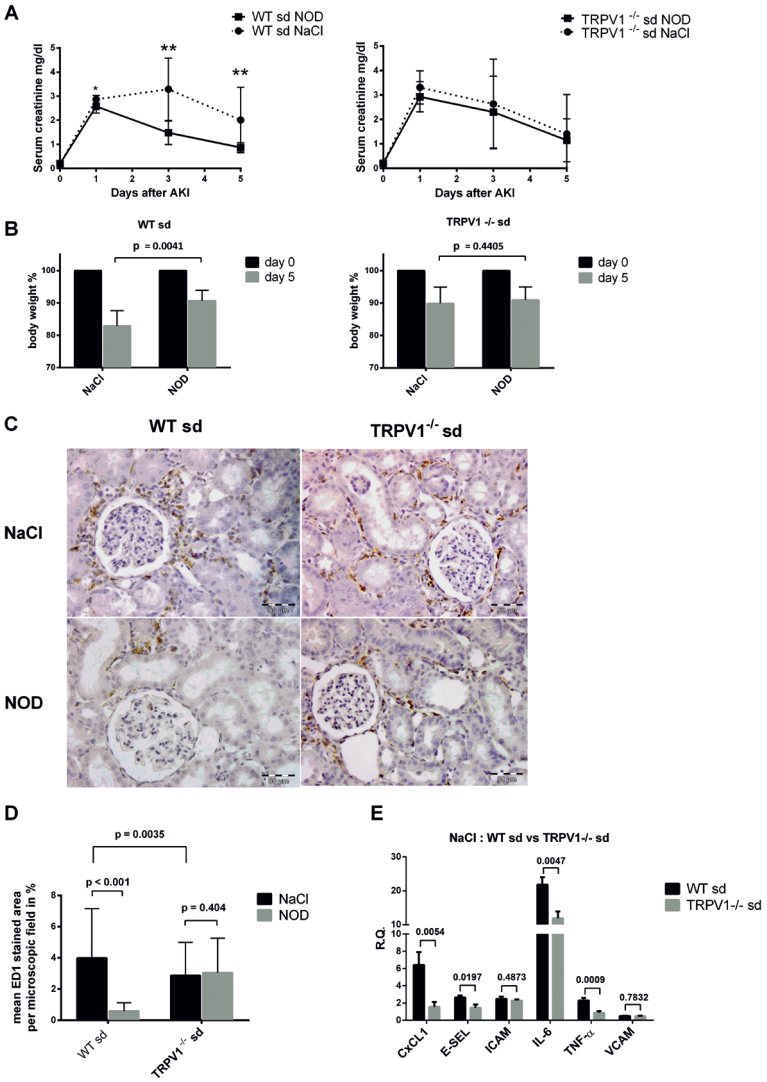

Figure 3. The renoprotective effect of NOD is abrogated in TRPV1$^{-/-}$ Sprague Dawley rats. (A) Serum creatinine (mg/dl) from WT Sprague Dawley (graph to the left) and TRPV1$^{-/-}$ Sprague Dawley rats (graph to the right) were assessed on day 0, 1, 3, 5 after induction of AKI. The animals were treated with NOD (bold line) or NaCl (dotted line) via osmotic mini pumps over the whole experimental period. Serum creatinine was significantly lower in NOD treated rats on all days of measurements in the WT rats, while in the TRPV1$^{-/-}$ Sprague Dawley rats no differences were found between NOD and NaCl treated rats. Serum creatinine/WT: *p=0.038 (day 1), **p=0.002 (day 3), **p=0.004 (day 5). Serum creatinine/TRPV1$^{-/-}$ Sprague Dawley : p=0.267 (day 1), p=0.722 (day 3), p=1.0 (day 5). (B) Body weight was measured 5 days after AKI in WT Sprague Dawley and TRPV1$^{-/-}$ Sprague Dawley rats. The results are expressed as mean percent body

Table 1. Quantification of mRNA for various cytokines was done in renal tissue obtained 5 days after AKI.

	WT Sprague Dawley rats		TRPV1$^{-/-}$ Sprague Dawley rats	
Cytokines ↓ /Treatment→	**NaCl**	**NOD**	**NaCl**	**NOD**
CxCL1	6.43±1.29	7.36±1.02	1.55±0.58	2.02±0.44
E-SEL	2.65±0.20	2.77±0.23	1.45±0.38	2.13±0.31
ICAM	2.48±0.23	3.34±0.41	2.27±0.15	2.45±0.35
IL-6	21.81±1.94	41.06±5.42†	11.88±2.04	25.99±4.11**
TNF-α	2.29±0.26	2.44±0.19	0.86±0.20	1.61±0.15***
VCAM	0.49±0.03	0.49±0.04	0.46±0.07	0.59±0.08

Results are expressed as Relative quantity±SEM relative to untreated native kidney.
(† p=0.0094; **p=0.0062, ***p=0.0096)

weight loss relative to the body weight immediately before AKI induction. In WT Sprague Dawley rats NOD treatment significantly mitigates body weight loss (p=0.0041). No difference was found in TRPV1$^{-/-}$ Sprague Dawley rats. (C) Representative sections obtained from kidneys of NaCl or NOD treated WT and TRPV1$^{-/-}$ Sprague Dawley rats are depicted. (D) Renal infiltrated ED1^{+} cells were assessed by immunohistochemistry. Quantification of ED1^{+} was performed by quantitative morphometric analysis. For each animal at least 2 sections were evaluated using 10 rando mLy chosen high power (400× magnification) microscopic fields. The results are expressed as mean percent ED1 stained area per microscopic field±SD. (E) The mRNA expression for different inflammatory cytokines was performed by qPCR on renal tissue harvested 5 days after AKI induction. Result expressed as Relative quantity±SEM relative to untreated native kidney.

Is renal perfusion influenced by NOD?

We assessed if the renoprotective effect of NOD was associated with improved renal perfusion. Renal cortical perfusion in the ischemic kidney was measured 5 days after warm ischemia-induced AKI using ASL. The non-ischemic kidney served as control. Renal cortical perfusion was significantly lower in the ischemic kidney, as reported previously [35]. NOD treatment did not influence cortical perfusion neither in the ischemic, nor in the non-ischemic control kidney (Figure 4).

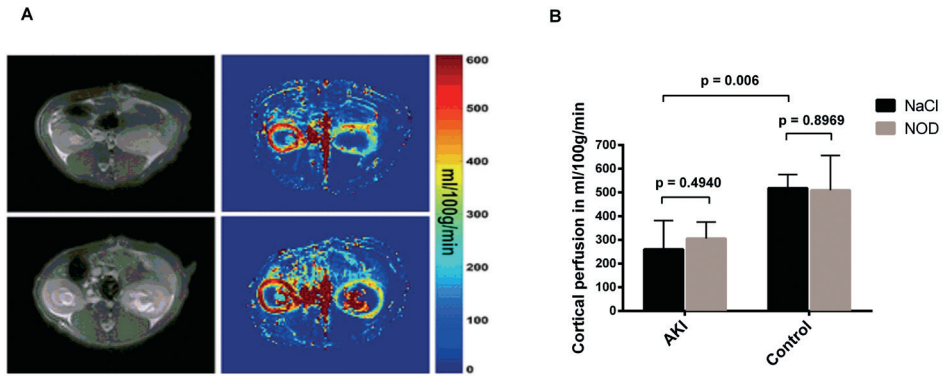

Figure 4 Renal perfusion after AKI and NOD treatment. Renal cortical perfusion was measured by ASL-MRI in a total of 10 rats. AKI was induced as described in the materials and method section. In each animal renal cortical perfusion was compared to the non-ischemic kidney **(A).** Exemplary illustrations of ASL perfusion MRI of two rats with left side AKI either treated with NOD (lower row) or NaCl (upper row) are depicted. Axial morphological images of the kidneys as recorded during the ASL measurement (M0 images) are displayed on the left. The according maps of absolute perfusion values in units of mL/100g/min are shown on the right. **(B)** Renal cortical perfusion was quantified and expressed as perfusion in mL/100g/min ± SD.

NOD does not affect renal function in NOD treated transplant recipients

We next assessed if the renoprotective effect of NOD treatment was also noted after prolonged cold ischemia and transplantation NOD treatment of the recipients did not significantly influence renal function, yet there was a trend observed towards a minor improvement (Figure 5A). Similarly, NOD did not influence body weight loss, renal inflammation (Figure 5B, C and D) or cytokine mRNA expression (data not shown). To exclude that an anti-Fisher allo-response or intrinsic strain differences have were underlying the failure of NOD to act renoprotective also syngeneic renal transplantations were performed. Similar as observed in the allogeneic transplantation model, recipient NOD treatment was not renoprotective (Figure 5E) or influenced body weight (Figure 5F). This was unlikely due to the susceptibility of TRPV1 expressing sensory nerves to prolonged cold preservation since isolated DRG that were either or not subjected to cold preservation reacted in a similar fashion to both NOD and capsaicin (Figure 5G).

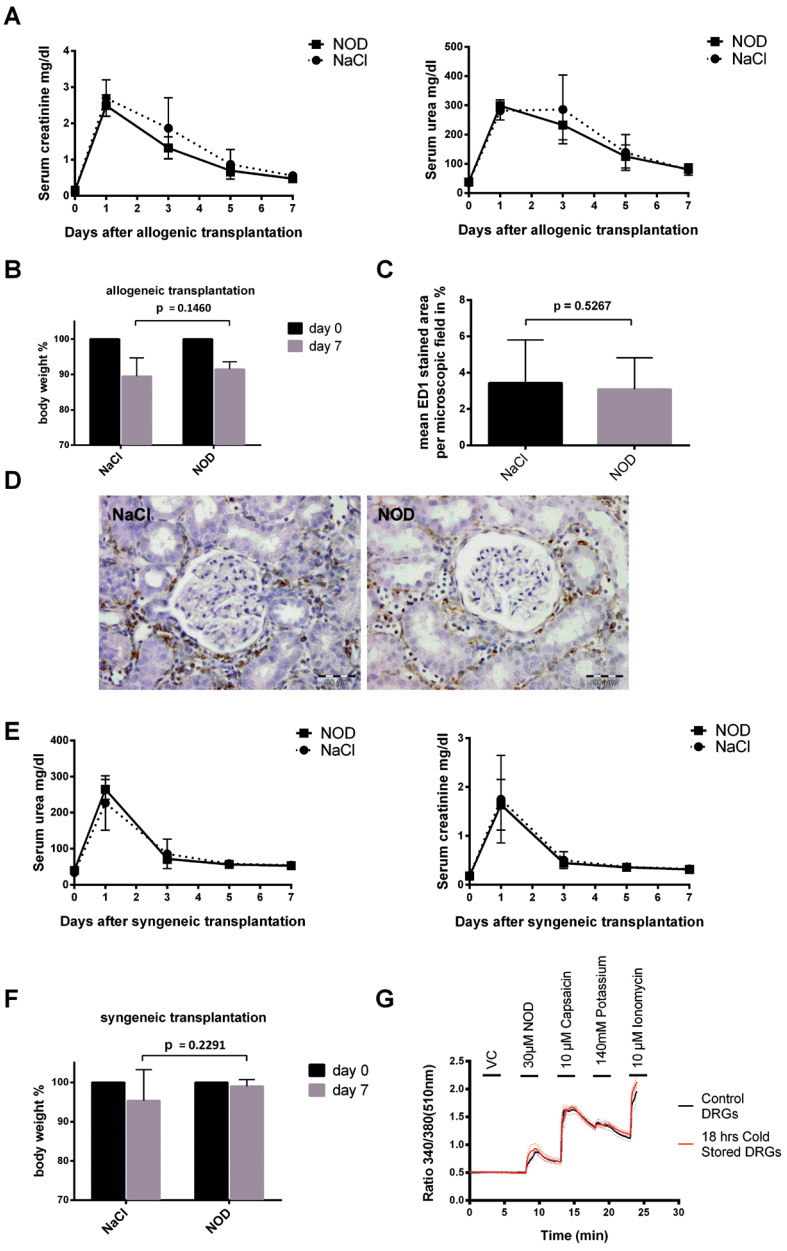

Figure 5. NOD treatment of renal allograft recipients does not improve renal function. (A) Serum creatinine (mg/dl) (graph to the left) and serum urea (mg/dl) (graph to the right) were assessed on day 0, 1, 3, 5 and 7 after transplantation of allogeneic Fischer renal allografts in Lewis recipients. The renal allografts

Discussion

In the present study we further explored the renoprotective effect of NOD in the setting of warm ischemia induced AKI in more details and assessed if renal allograft recipients may also benefit from NOD treatment. The major findings of this study are as follows. Firstly, NOD treatment improves renal function in warm ischemia induced AKI, even when treatment is started after renal ischemia. Improved renal function was not associated with large changes in renal perfusion. Secondly, the renoprotective properties of NOD are completely lost in TRPV1$^{-/-}$ Sprague Dawley rats. Thirdly, NOD treatment of renal transplant recipient rats does not improve renal function. TRPV1 responsiveness was not lost as a consequence of cold preservation since both NOD and capsaicin were able to activate DRG that were subjected to cold preservation.

Our study is in good agreement with previous publications on the protective properties of TRPV1 activation in the setting of ischemia reperfusion injury in kidney [18, 36], lung [20] and heart [37] models. Nonetheless the finding that NOD treatment did not improve kidney function in renal allograft recipient rats was unexpected. In our previous

were subjected to 20 h of cold preservation in UW solution. The recipients were treated with NOD (bold line) or NaCl (dotted line) via osmotic mini pumps over the whole experimental period. No differences in renal function between the groups were noted. Serum creatinine: p=0.494 (day 1), p=0.129 (day 3), p=0.470 (day 5), p=0.086 (day 7). Serum urea: p=0.119 (day 1), p=0.494 (day 3), p=0.939 (day 5), p=0.939 (day 7). (B) Body weight loss was measured on day 7 after allogeneic renal transplantation. The result is expressed as mean body weight loss in percent relative to the body weight on day 0. No differences in loss of body weight were found in both transplantation models. (C) Renal infiltrated ED1$^+$ cells were assessed by immunohistochemistry. Quantification of ED1$^+$ was performed by quantitative morphometric analysis. For each animal at least 10 sections were evaluated using 20 rando mLy chosen high power (400× magnification) microscopic fields. The results are expressed as mean percent ED1 stained area per microscopic field ± SD. (D) Representative sections obtained from kidneys of the NaCl or NOD treated recipient rats. (E) Serum creatinine (mg/dl) (graph to the left) and serum urea (mg/dl) (graph to the right) were assessed on day 0, 1, 3, 5 and 7 after transplantation of syngeneic Lewis renal allografts in Lewis recipients. The renal allografts were subjected to 20 h of cold preservation in UW solution. The recipients were treated with NOD (bold line) or NaCl (dotted line) via osmotic mini pumps over the whole experimental period. No differences in renal function between the groups were noted. Serum creatinine: p=0.713 (day 1), p=0.6 (day 3), p=0.96 (day 5), p=0.792 (day 7). Serum urea: p=0.227 (day 1), p=0.431 (day 3), p=1.0 (day 5), p=0.674 (day 7). (F) Body weight loss was measured on day 7 after syngeneic renal transplantation. The result is expressed as mean body weight loss in percent relative to the body weight on day 0. No differences in loss of body weight were found in both transplantation models. (G) Live cell calcium imaging was performed on freshly isolated DRG or on DRG that were subjected to 18 h of cold preservation. DRGs were subsequently stimulated with 30 µM NOD, 10 µM capsaicin, 140 mM potassium chloride and 10 µM ionomycin. Mean traces ± SEM of 200 regions of interest (ROI) with each ROI containing one cell is depicted. SEM is depicted as dotted line.

studies on NOD and AKI, NOD was applied as bolus therapy shortly before and directly after induction of warm ischemia induced AKI. Because we intuitively reasoned that pre-treatment of the recipient would not influence the function of the donor allograft, we first demonstrated that pre-treatment per se is not required for the renoprotective effect of NOD in the warm ischemia-induced AKI model. Hence both the AKI and transplantation models were similar in the sense that treatment was started after the inciting event. It could be argued that cold preservation of renal grafts is causing more damage to the kidney as compared to warm ischemia and therefore NOD might not be protective under the former condition. Yet this was not reflected by serum creatinine levels which even showed a trend towards a faster recovery of renal function in the transplantation-as compared to the warm ischemia-induced AKI model. As this was observed in both syngeneic and allogeneic donor recipient combinations, intrinsic strain differences in susceptibility to tissue ischemia also cannot explain these results. We did not study the expression of TRPV1 in renal tissue after cold storage and thus it cannot be excluded that cold storage affects the expression of TRPV1 and consequently the efficacy of NOD to improve renal function. However cold storage of isolated DRG did not impair the efficacy of capsaicin or NOD to activate TRPV1.

The renal pelvis, pelvi-ureteric junction, and ureter are heavily innervated by TRPV1-positive sensory nerves located between the layers of smooth muscles and epithelia [38, 39]. The sensory nerve endings contain amongst others vasoactive neuropeptides, e.g. calcitonin gene-related peptide (CGRP) and substance P (SP), which are released upon TRPV1 activation [40, 41]. Because CGRP and SP are vasoactive neuropeptides TRPV1-positive sensory nerve fibers may regulate local renal blood flow [42].

Mizutani et al [25] have reported that denervation of primary sensory nerves before renal ischemia/reperfusion aggravates the inflammatory response in the kidney and worsens renal function. Accordingly they postulate that TRPV1 expressing sensory nerves are activated in the pathologic process of warm ischemia/reperfusion-induced AKI and that such activation reduces acute renal injury by attenuating inflammatory responses. The finding that no significant difference in renal function impairment was found between WT and TRPV1$^{-/-}$ Sprague Dawley rats that were subjected to ischemia induced AKI and the finding that in kidneys of the latter rats consistently less infiltration of ED1^{+} monocytes/macrophages was present argues against this hypothesis. The expression of a number of chemokines was also reduced in the TRPV1$^{-/-}$ as compared to the WT Sprague Dawley rats, albeit that this might equally well be explained by a reduced number of infiltrated monocytes/macrophages. A recent study by Chen et al [43] also demonstrated that TRPV1 activation improves AKI while the absence of TRPV1 or inhibition of these channels did not further deteriorate renal function in the setting of AKI. Although our data are in good agreement with this study, it remains to be assessed why the expression of pro-inflammatory cytokines are significantly reduced in TRPV1-/- rats. Cytokine expression has been addressed in the study by Chen et al [43]. These finding also suggest that the inflammatory response in the course of AKI might not be a major critical factor that determines renal function. Also, despite the fact that *in vitro* studies clearly

have demonstrated the anti-inflammatory properties of NOD [44], with the exception of a reduction in infiltrating ED1^{+} cells NOD treatment did not have a major influence on the expression of pro-inflammatory cytokines in the kidney following AKI. In fact, we observed that the expression of IL-6 was increased by NOD in WT and TRPV1$^{-/-}$ Sprague Dawley as well as in Lewis rats, albeit that this did not reach statistical significance in the latter strain.

Although our study unambiguously demonstrates that the renoprotective effect of NOD in warm ischemia-induced AKI is strictly depending on TRPV1 expression, there are some limitations that warrant further studies. In such studies also the influence of NOD on early inflammatory parameters needs to be implemented. At present it is not clear why TRPV1 activation in warm ischemia-induced AKI models translates into improved renal function. Even though capsaicin leads to vasodilation in the renal vasculature [42], we were not able to demonstrate differences in renal perfusion in NOD treated rats using ASL. However it cannot be excluded that NOD treatment slightly increases renal perfusion not detectable by the ASL-MRI method [35]. Secondly, it is not clear why renal recipients do not benefit from NOD treatment. This seems not to be related to allogeneic differences, cold preservation or intrinsic differences in kidney from different strains, yet the role of renal denervation in NOD mediated renoprotection and kidney expression of TRPV1 over time in AKI has not been addressed. Thirdly, renoprotective effect conveyed by NOD in the warm ischemia induced AKI model cannot be extrapolated to other causes of AKI. Although, NOD treatment in pre and post bolus combination, and as continuous treatment directly after the inciting event show a protective effect, it still needs to be assessed if NOD treatment would impart protection once the degree of injury is large and manifested by already increased serum creatinine levels. Apart from this, NOD improves renal function in allograft recipients when used in BD donors [14], yet whether this is also mediated by TRPV1 is currently not known. An intriguing question which arises is as to whether donor NOD treatment can improve organ quality of renal allograft with already impaired donor renal function.

Acknowledgement

We would like to thank Susanne Behr, Katharina Prem and Handan Moerz for their excellent technical support. PP is supported by GRK880/4 and Albert und Anneliese Konanz-Stiftung. Authors declare no conflict of interest.

References

1. Levy, E.M., C.M. Viscoli, and R.I. Horwitz, *The effect of acute renal failure on mortality. A cohort analysis.* JAMA, 1996. **275**(19): p. 1489-94.
2. Chertow, G.M., et al., *Acute kidney injury, mortality, length of stay, and costs in hospitalized patients.* J Am Soc Nephrol, 2005. **16**(11): p. 3365-70.
3. Schiffl, H., S.M. Lang, and R. Fischer, *Daily hemodialysis and the outcome of acute renal failure.* N Engl J Med, 2002. **346**(5): p. 305-10.
4. Hoste, E.A., et al., *RIFLE criteria for acute kidney injury are associated with hospital mortality in critically ill patients: a cohort analysis.* Crit Care, 2006. **10**(3): p. R73.
5. Ishani, A., et al., *Acute kidney injury increases risk of ESRD among elderly.* J Am Soc Nephrol, 2009. **20**(1): p. 223-8.
6. Akkina, S.K., et al., *Similar outcomes with different rates of delayed graft function may reflect center practice, not center performance.* Am J Transplant, 2009. **9**(6): p. 1460-6.
7. Tapiawala, S.N., et al., *Delayed graft function and the risk for death with a functioning graft.* J Am Soc Nephrol, 2010. **21**(1): p. 153-61.
8. Hariharan, S., et al., *Post-transplant renal function in the first year predicts long-term kidney transplant survival.* Kidney Int, 2002. **62**(1): p. 311-8.
9. Yarlagadda, S.G., et al., *Association between delayed graft function and allograft and patient survival: a systematic review and meta-analysis.* Nephrol Dial Transplant, 2009. **24**(3): p. 1039-47.
10. van der Vliet, J.A., et al., *Influence of prolonged cold ischemia in renal transplantation.* Clin Transplant, 2011. **25**(6): p. E612-6.
11. Ojo, A.O., et al., *Delayed graft function: risk factors and implications for renal allograft survival.* Transplantation, 1997. **63**(7): p. 968-74.
12. Schnuelle, P., et al., *Effects of donor pretreatment with dopamine on graft function after kidney transplantation: a randomized controlled trial.* JAMA, 2009. **302**(10): p. 1067-75.
13. Losel, R.M., et al., *N-octanoyl dopamine, a non-hemodyanic dopamine derivative, for cell protection during hypothermic organ preservation.* PLoS One, 2010. **5**(3): p. e9713.
14. Spindler, R.S., et al., *N-Octanoyl Dopamine for Donor Treatment in a Brain-Death Model of Kidney and Heart Transplantation.* Transplantation, 2015.
15. Hoeger, S., et al., *Donor dopamine treatment in brain dead rats is associated with an improvement in renal function early after transplantation and a reduction in renal inflammation.* Transpl Int, 2008. **21**(11): p. 1072-80.
16. Hottenrott, M.C., et al., *N-Octanoyl Dopamine Inhibits the Expression of a Subset of kappa B Regulated Genes: Potential Role of p65 Ser276 Phosphorylation.* PLoS One, 2013. **8**(9).
17. Tsagogiorgas, C., et al., *N-octanoyl-dopamine is an agonist at the capsaicin receptor TRPV1 and mitigates ischemia-induced acute kidney injury in rat.* PLoS One, 2012. **7**(8): p. e43525.
18. Ueda, K., et al., *Preventive effect of TRPV1 agonists capsaicin and resiniferatoxin on ischemia/reperfusion-induced renal injury in rats.* J Cardiovasc Pharmacol, 2008. **51**(5): p. 513-20.
19. Zhong, B. and D.H. Wang, *N-oleoyldopamine, a novel endogenous capsaicin-like lipid, protects the heart against ischemia-reperfusion injury via activation of TRPV1.* Am J Physiol Heart Circ Physiol, 2008. **295**(2): p. H728-35.

20. Wang, M., et al., *TRPV1 Agonist Capsaicin Attenuates Lung Ischemia-Reperfusion Injury in Rabbits.* J Surg Res, 2010.
21. Li, J. and D.H. Wang, *Increased GFR and renal excretory function by activation of TRPV1 in the isolated perfused kidney.* Pharmacol Res, 2008. **57**(3): p. 239-46.
22. Alawi, K. and J. Keeble, *The paradoxical role of the transient receptor potential vanilloid 1 receptor in inflammation.* Pharmacol Ther, 2010. **125**(2): p. 181-95.
23. Benarroch, E.E., *CGRP Sensory neuropeptide with multiple neurologic implications.* Neurology, 2011. **77**(3): p. 281-287.
24. Harrison, S. and P. Geppetti, *Substance p.* Int J Biochem Cell Biol, 2001. **33**(6): p. 555-76.
25. Mizutani, A., et al., *Activation of sensory neurons reduces ischemia/reperfusion-induced acute renal injury in rats.* Anesthesiology, 2009. **110**(2): p. 361-9.
26. Jin, H., et al., *Involvement of perivascular nerves and transient receptor potential vanilloid 1 (TRPV1) in vascular responses to histamine in rat mesenteric resistance arteries.* Eur J Pharmacol, 2012. **680**(1-3): p. 73-80.
27. Tsuji, F. and H. Aono, *Role of Transient Receptor Potential Vanilloid 1 in Inflammation and Autoimmune Diseases.* Pharmaceuticals, 2012. **5**(8): p. 837-852.
28. Hoeger, S., et al., *Dopamine treatment in brain-dead rats mediates anti-inflammatory effects: the role of hemodynamic stabilization and D-receptor stimulation.* Transpl Int, 2007. **20**(9): p. 790-9.
29. Gottmann, U., et al., *Atorvastatin donor pretreatment prevents ischemia/reperfusion injury in renal transplantation in rats: possible role for aldose-reductase inhibition.* Transplantation, 2007. **84**(6): p. 755-62.
30. Hoeger, S., et al., *UW is superior compared with HTK after prolonged preservation of renal grafts.* J Surg Res, 2011. **170**(1): p. e149-57.
31. Schmittgen, T.D. and K.J. Livak, *Analyzing real-time PCR data by the comparative C(T) method.* Nat Protoc, 2008. **3**(6): p. 1101-8.
32. Tsagogiorgas, C., et al., *N-octanoyl-dopamine is an agonist at the capsaicin receptor TRPV1 and mitigates ischemia-induced [corrected] acute kidney injury in rat.* PLoS One, 2012. **7**(8): p. e43525.
33. Kim, S.G., *Quantification of relative cerebral blood flow change by flow-sensitive alternating inversion recovery (FAIR) technique: application to functional mapping.* Magn Reson Med, 1995. **34**(3): p. 293-301.
34. Kwong, K.K., et al., *MR perfusion studies with T1-weighted echo planar imaging.* Magn Reson Med, 1995. **34**(6): p. 878-87.
35. Zimmer, F., et al., *Quantitative renal perfusion measurements in a rat model of acute kidney injury at 3T: testing inter-and intramethodical significance of ASL and DCE-MRI.* PLoS One, 2013. **8**(1): p. e53849.
36. Ueda, K., et al., *Preventive effect of SA13353 [1-[2-(1-adamantyl)ethyl]-1-pentyl-3-[3-(4-pyridyl)propyl]urea], a novel transient receptor potential vanilloid 1 agonist, on ischemia/reperfusion-induced renal injury in rats.* J Pharmacol Exp Ther, 2009. **329**(1): p. 202-9.
37. Wang, L. and D.H. Wang, *TRPV1 gene knockout impairs postischemic recovery in isolated perfused heart in mice.* Circulation, 2005. **112**(23): p. 3617-23.
38. Rolle, U., E. Brylla, and B. Tillig, *Immunohistochemical detection of neuronal plexuses and nerve cells within the upper urinary tract of pigs.* Bju International, 1999. **83**(9): p. 1045-9.

39. Feng, N.H., et al., *Transient receptor potential vanilloid type 1 channels act as mechanoreceptors and cause substance P release and sensory activation in rat kidneys.* Am J Physiol Renal Physiol, 2008. **294**(2): p. F316-25.
40. Inoue, R., et al., *Transient receptor potential channels in cardiovascular function and disease.* Circ Res, 2006. **99**(2): p. 119-31.
41. Szolcsanyi, J., *Forty years in capsaicin research for sensory pharmacology and physiology.* Neuropeptides, 2004. **38**(6): p. 377-84.
42. Chen, L., et al., *Functional transient receptor potential vanilloid 1 and transient receptor potential vanilloid 4 channels along different segments of the renal vasculature.* Acta Physiol (Oxf), 2014.
43. Chen, L., et al., *Role of TRPV1 channels in ischemia/reperfusion-induced acute kidney injury.* PLoS One, 2014. **9**(10): p. e109842.
44. Hottenrott, M.C., et al., *N-octanoyl dopamine inhibits the expression of a subset of kappaB regulated genes: potential role of p65 Ser276 phosphorylation.* PLoS One, 2013. **8**(9): p. e73122.

Chapter 4

Analyses of Synthetic N-Acyl Dopamine Derivatives Revealing Different Structural Requirements for Their Anti-inflammatory and transient -Receptor-Potential-Channel-of-the-Vanilloid-Receptor-Subfamily-Subtype-1 (TRPV1)-Activating Properties*

Published in Journal of medicinal Chemistry 2018 Apr 2doi: 10.1021/acs.jmedchem.8b00156.

Prama Pallavi, Marc Pretze, Julio Caballero, Yingchun Li, Björn B. Hofmann, Eleni Stamellou, Sarah Klotz, Carmen Wängler, Björn Wängler, Ralf Loesel, Steffen Roth, Bastian Theisinger, Handan Morez, Uta Binzen, Wolfgang Greffrath, Rolf-Detlef Treede, Martin C. Harmsen, Bernhard K. Krämer, Mathias Hafner, Benito A. Yard, Anna-Isabelle Kälsch

*is adapted into a chapter

Abstract

We studied the chemical entities within N-octanoyl dopamine (NOD) responsible for the activation of transient-receptor-potential channels of the vanilloid-receptor subtype 1 (TRPV1) and inhibition of inflammation. The potency of NOD in activating TRPV1 was significantly higher compared with those of variants in which the ortho-dihydroxy groups were acetylated, one of the hydroxy groups was omitted (N-octanoyl tyramine), or the ester functionality consisted of a bulky fatty acid (N-pivaloyl dopamine). Shortening of the amide linker (ΔNOD) slightly increased its potency, which was further increased when the carbonyl and amide groups (ΔNODR) were interchanged. With the exception of ΔNOD, the presence of an intact catechol structure was obligatory for the inhibition of VCAM-1 and the induction of HO-1 expression. Because TRPV1 activation and the inhibition of inflammation by N-acyl dopamines require different structural entities, our findings provide a framework for the rational design of TRPV1 agonists with improved anti-inflammatory properties.

Introduction

N-acyl dopamines (NADs) are condensation products of fatty acids linked to dopamine at the amino group. They show agonistic properties at the transient receptor potential channel of the vanilloid receptor subfamily subtype 1 (TRPV1), are capable of activating the cannabinoid receptors CB1 and CB2 and show anti-inflammatory and immune modulatory effects[1–4]. TRPV1 is mainly expressed in unmyelinated C-and thinly myelinated Aδ-afferent nerve fibers[5, 6] and significantly contributes to the generation of pain signals, i.e. nociception. It is essential for selective modalities of pain sensation, e.g. tissue injury-induced thermal hyperalgesia [7] as observed in the course of inflammation [8], incision-induced postoperative pain [9], visceral nociception [10] or neuropathic pain conditions [11, 12].

There is growing evidence that supports a prominent role for inflammation in the development and maintenance of neuropathic pain. TRPV1 activation by NADs has been reported to modulate nociceptive signaling in inflammatory pain[13–15]. Independent hereof, NADs also exhibit anti-inflammatory properties on their own through inhibition of transcription factors involved in inflammation, e.g. NFκB, NFAT and AP-1 [1, 2]. We have previously demonstrated that *N*-octanoyl dopamine (NOD), a synthetic NAD, strongly inhibits Tumor necrosis factor alpha (TNFα) mediated vascular cell adhesion molecule-1 (VCAM-1) expression along with a variety of inflammatory chemo-and cytokines [16]. Moreover, like other catechol containing structures NOD induces the expression of heme oxygenase-1 (HO-1), as a consequence of Nrf-2 activation[17]. These properties make NOD an interesting molecule to ameliorate tissue damage, either caused by inflammation or oxidative stress as inciting events. Indeed we have shown that NOD has a salutatory effect on ischemia induced acute kidney injury (AKI) in rats [18] and that its use in brain dead donor rats improves renal function in recipient rats[19].

In analogy to capsaicin (CAP), an archetypic TRPV1 agonist, NADs can be structurally divided into three parts, i.e. the aromatic moiety (A-region), the linker region containing the amide bond (B-region) and the hydrophobic aliphatic side chain (C-region) [20–22]. NOD differs from CAP in structure as it contains a catechol instead of a vanilloid moiety (the A-region), is one methylene group longer (the B-region) and contains a completely saturated aliphatic chain (the C-region) (Figure 1A).

In this study we try to assess what structural elements impart NADs TRPV1 agonistic properties and what structural components confer its anti-inflammatory properties. We used NOD as a lead compound and subsequently made changes in the A-, B-and C-region to delineate to what extent this affects TRPV1 activation and its anti-inflammatory properties in terms of inhibiting TNFα mediated VCAM-1 and HO-1 induction.

Experimental procedures

Materials.

General procedures for chemical synthesis. All reagents and solvents were purchased from commercial suppliers and were used without further purification unless otherwise specified. NMR spectra were recorded on a 250 MHz Bruker AC250, a 300 MHz Varian Mercury Plus and a 500 MHz Varian NMR System spectrometer (Palo Alto, CA). Chemical shifts (δ) are given in ppm and are referenced to the residual solvent resonance signals relative to $(CH_3)_4Si$ (^1H, ^{13}C). Mass spectra were obtained on a Bruker Daltonics microflex™ MALDI-TOF mass spectrometer (Bremen, Germany). Preparative column chromatography was performed on Merck silica gel 60. Reactions were monitored by thin-layer chromatography (TLC) on Merck silica gel F254 aluminum plates, with visualization under UV (λ=254 nm). If necessary, the purity was determined by high performance liquid chromatography (HPLC). Purity of all final compounds was 95 percent or higher (Supplementary Table S2). HPLC was performed on a Dionex UltiMate 3000 HPLC system (Thermo Scientific, Dreieich, Germany), equipped with a reverse phase column (Merck Chromolith RP-18e; analytical: 100x4.6 mm plus a guard column 10x4.6mm; semipreparative: 100x10 mm plus a guard column 10x10 mm) and a UV-diode array detector (210 nm, 254 nm). The solvent system used was a gradient of acetonitrile:water (containing 0.1 percent TFA) (0–8 min: 0–100 percent MeCN) at a flow rate of 4 mL/min unless otherwise stated.

***N*-acyl dopamine synthesis** *N*-octanoyl dopamine (NOD), *N*-pivloyl dopamine (NPiD) and *N*-octanoyl tyramine (NOT) were prepared from commercially available precursors as described previously [23]. The compounds were purified by two fold recrystallization from dichloromethane, and purity of the compounds was confirmed by HPLC. Briefly, octanoic acid was converted to its mixed anhydride derivative by reaction with ethyl chloroformate in the presence of *N*-ethyl diisopropylamine. The crude mixed anhydride was incubated with dopamine hydrochloride in *N,N*-dimethylformamide and *N*-ethyl diisopropylamine to form NOD. After aqueous preparation and evaporation of the organic solvent NOD is obtained in an overall yield of sixty percent. The sample investigated by NMR (Bruker AC250) yielded spectra in accordance with the expected structure.

***N*-(3,4-dihydroxyphenethyl)pivalamide (NPiD).** Analytical HPLC: t_R=1.50 min (>97 percent). ^1H NMR (250 MHz, $CDCl_3$): δ=8.69 (s, 2H, 2xOH), 7.46 (t, ^3J=6.6 Hz, 1H, NH), 6.62 (d, $^3J_{H5,H6}$=7.9 Hz, 1H, H-5), 6.55 (dd, $^3J_{H5,H6}$=7.9 Hz, $^4J_{H2,H6}$=1.9 Hz, 1H, H-6), 6.41 (d, $^4J_{H2,H6}$=1.9 Hz, 1H, H-2), 3.14 (dt, $^3J_{H,H}$=7.4 Hz, $^3J_{NH,H}$=6.6 Hz, 2H, NCH_2), 2.50 (d, ^3J=7.4 Hz, 2H, $BnCH_2$), 1.07–1.04 ppm (m, 9H, $3xCH_3$).

4-(2-Octanamidoethyl)-1,2-phenylene diacetate (A-NOD). Acetylation of NOD was performed by suspending NOD (2 g, 7.16 mmol) of in acetic anhydride (5 mL) under magnetic stirring. When two drops of sulphuric acid were added, the suspension turned clear and stirring was continued for one hour. Diluted hydrochloric acid (5 mL) was added

and 30 min later the reaction mixture was poured into 200 mL ice water. The precipitated product was collected by vacuum filtration and dried under vacuum to yield pure A-NOD, confirmed by HPLC. Analytical HPLC: t_R=3.38 min (>97 percent). ^{1}H NMR (250 MHz, $CDCl_3$): δ=7.12 (d, $^3J_{H5,H6}$=8.1 Hz, 1H, H-5), 7.06 (dd, $^3J_{H5,H6}$=8.1 Hz, $^4J_{H2,H6}$=2.0 Hz, 1H, H-6), 7.01 (d, $^4J_{H2,H6}$=2.0 Hz, 1H, H-2), 3.49 (dt, $^3J_{H,H}$=7.5 Hz, $^3J_{NH,H}$=6.7 Hz, 2H, NCH_2), 2.81 (d, ^3J=7.5 Hz, 2H, $BnCH_2$), 2.89 (s, 6H, $2xAcCH_3$), 2.13 (t, ^3J=7.7 Hz, 2H, H-α), 1.63–1.56 (m, 2H, H-β), 1.33–1.19 (m, 8H, H-γ,δ,ε,ζ), 0.89–0.86 ppm (m, 3H, CH_3).

***N*-(3,4-Dihydroxybenzyl)octanamide** (ΔNOD). To a stirring solution of 3,4-dihydroxybenzylamine hydrobromide (300 mg, 1.36 mmol) and $NaHCO_3$ (377 mg, 4.49 mmol) in H_2O (5 mL), $CHCl_3$ was added after 30 min and after 15 min a fresh solution of octanoyl chloride (232 µL, 1.36 mmol) in $CHCl_3$ (1 mL) was added and the solution was stirred at 40° C for 18 h. Water was added (10 mL) and the solution was extracted 3× with $CHCl_3$ (10 mL). The organic phase was washed with 0.5 M HCl (10 mL) and brine (10 mL) and dried with $MgSO_4$. The $CHCl_3$ was removed and the crude product was purified by semi preparative HPLC (0–75 percent MeCN in H_2O+0.1 TFA within 6 min at 4 mL/min). The fractions containing the product were collected and lyophilized to give ΔNOD as colorless powder (66 mg, 34 percent). R_F=0.36 (EA:CH 2:1). ^{1}H NMR (300 MHz, $CDCl_3$): δ=6.87 (d, $^4J_{H2,H6}$=2.0 Hz, 1H, H-2), 6.80 (d, $^3J_{H5,H6}$=8.1 Hz, 1H, H-5), 6.62 (dd, $^3J_{H5,H6}$=8.1 Hz, $^4J_{H2,H6}$=2.0 Hz, 1H, H-6), 4.31 (d, ^3J=8.1 Hz, 2H, $BnCH_2$), 2.23 (t, ^3J=7.7 Hz, 2H, H-α), 1.67–1.57 (m, 2H, H-β), 1.27–1.22 (m, 8H, H-γ,δ,ε,ζ), 0.87–0.85 ppm (m, 3H, CH_3). ^{13}C NMR (75 MHz, $CDCl_3$): δ=174.3 (C=O), 144.5 (C-3), 144.1 (C-4), 130.1 (C-1), 119.9 (C-6), 116.9 (C-2), 114.8 (C-5), 43.5 ($BnCH_2$), 36.7 (C-α), 31.6 (C-ε), 29.1 (C-γ), 28.9 (C-δ), 25.8 (C-β), 22.6 (C-ζ), 14.0 ppm (CH_3). MS (MALDI-TOF): *m/z* (percent) 266 (100) $[M+H]^+$. Analytical HPLC: t_R=2.69 min (>96 percent). See supplementary figure 4 for NMR signal assignment.

2-(3,4-Dihydroxyphenyl)-*N*-octylacetamide (ΔNODR). (Compound 4g from Walpole et al.[24], no NMR data) To a solution of 3,4-dihydroxyphenylacetic acid (300 mg, 1.78 mmol) in dry THF (8 mL) under an argon atmosphere, Et_3N (249 µL, 1.78 mmol) and ethyl chloroformate (165 µL, 1.78 mmol) were added and stirred 3 h in the dark at ambient temperature. Then octylamine (296 µL, 1.78 mmol) was added and the solution was stirred for 18 h. To the solution was added EA and the organic phase was washed with brine and dried with $MgSO_4$. The solvent was removed and the crude product was purified by column chromatography (CH → CH:EA 4:1 → 1:1) to obtain the product ΔNODR as colorless solid (138 mg, 28 percent). R_F=0.24 (EA:CH 1:1). ^{1}H NMR (500 MHz, $CDCl_3$): δ=6.83 (d, $^3J_{H5,H6}$=8.1 Hz, 1H, H-5), 6.75 (d, $^4J_{H2,H6}$=1.7 Hz, 1H, H-2), 6.48 (dd, $^3J_{H5,H6}$=8.1 Hz, $^4J_{H2,H6}$=1.7 Hz, 1H, H-6), 3.40 (s, 2H, $BnCH_2$), 3.24 (dd, $^3J_{H,H}$=13.5 Hz, $^3J_{NH,H}$=6.7 Hz, 2H, H-α), 1.52–1.46 (m, 2H, H-β), 1.28–1.22 (m, 10H, H-γ,δ,ε,ζ,η), 0.87–0.84 ppm (m, 3H, CH_3). ^{13}C NMR (126 MHz, $CDCl_3$): δ=175.2 (C=O), 144.7 (C-3), 144.3 (C-4), 124.3 (C-1), 121.2 (C-6), 116.5 (C-5), 115.9 (C-2), 41.2 ($BnCH_2$), 40.7 (C-α), 31.7 (C-ζ), 29.1 (C-ε), 29.0 (C-δ), 28.6 (C-β), 26.8 (C-γ), 22.6 (C-η), 14.1 ppm (CH_3). MS (MALDI-TOF): *m/z* (percent) 279 (100) $[M+H]^+$. Analytical HPLC: t_R=3.12 min (>98 percent).

***(E)-N*-(3,4-dihydroxybenzyl)-8-methylnon-6-enamide (CAP-OH).** (Compound **1** from Goto et al. [25], no NMR data) To a solution of natural Capsaicin (162 mg, 0.53 mmol) and K_2CO_3 (220 mg, 1.59 mmol) in CH_2Cl_2 (30 mL), a 1 M solution of BBr_3 in CH_2Cl_2 (1.32 mL) was slowly added at-18° C within 5 min and the mixture was stirred for 60 min to reach-16° C. Water (20 mL) was added for quenching them reaction and the mixture was extracted with CH_2Cl_2 (1x) and EA (1x). The combined organic phases were washed with brine (20 mL) and dried with $MgSO_4$. The solvent was removed and the crude product was purified by column chromatography (CH → CH:EA 4:1 → 2:1 → 1:1) to obtain a yellow oil (117 mg, 76 percent). The yellow oil was further purified by semi preparative HPLC (0–50 percent MeCN in H_2O+0.1 TFA within 8 min at 4 mL/min). The fractions containing the product were collected and lyophilized to give **Cap-OH** as colorless powder (45 mg, 29 percent). R_F=0.33 (EA:CH 2:1). ^{1}H NMR (500 MHz, $CDCl_3$): δ=6.85 (s, 1H, H-5), 6.79 (s, 1H, H-2), 6.60 (d, $^3J_{H5,H6}$=8.0 Hz, 1H, H-6), 5.37–5.25 (m, 2H, HC=CH), 4.29 (s, 2H, $BnCH_2$), 2.26 (t, ^3J=7.6 Hz, 2H, H-α), 1.95 (dd, ^3J=13.9 Hz, ^4J=7.0 Hz, 1H, CH), 1.67–1.59 (m, 2H, H-δ), 1.38–1.23 (m, 4H, H-β,γ), 0.94 (s, 3H, CH_3), 0.93 ppm (s, 3H, CH_3). ^{13}C NMR (126 MHz, $CDCl_3$): δ=174.6 (C=O), 144.4 (C-3), 144.1 (C-4), 138.5 (C-ζ), 129.7 (C-1), 126.2 (C-ε), 119.9 (C-6), 115.0 (C-5), 114.9 (C-2), 43.7 (BnC), 36.4 (C-α), 32.1 (C-δ), 30.9 (C-η), 29.1 (C-γ), 25.3 (C-β), 22.6 ppm (2xCH_3). MS (MALDI-TOF): *m/z* (percent) 292 (100) $[M+H]^+$. Analytical HPLC: t_R=3.08 min (>95 percent).

General procedures for *in vitro* experiments

Chemicals

All chemical reagents were purchased from Sigma Aldrich (Sigma-Aldrich Chemie GmbH, Munich, Germany) unless otherwise indicated.

Site directed mutagenesis

A pcDNA3-rTRPV1 construct was used to generate rTRPV1-R491A (5'-gca gga aat att gaa tcc ctg cga aga aga agt aga ctc ctc-3'; 5'-gag gag tct act tct tct tcg cag gga ttc aat att tcc tgc-3); T511A (5'-gta caa aga aaa gta tct cac tgg cgc tgt cca caa aca aac tct tga-3', 5'-tca aga gtt tgt ttg tgg aca gcg cca gtg aga tac ttt tct ttg tac-3'); S512A (5'ctg tac aaa gaa aag tat ctc ata ggc gct gtc cac aaa caa act-3', 5'-gag ttt gtt tgt gga cag cgc cta tga gat act ttt ctt tgt aca-3'); T550A (5'-gta gag cat gtt ggc cca gcc cat ggc ca-3', 5'-tgg cca tgg gct ggg cca aca tgc tct ac-3'); and E570A (5'-ctg tac aaa gaa aag tat ctc agc gta gct gtc cac aaa caa act c-3', 5'-gag ttt gtt tgt gga cag cta cgc tga gat act ttt ctt tgt aca g-3') mutations using QuikChange Site-Directed Mutagenesis Kit (Agilent Technologies) as per manufactures' protocol. Sequence of all the clones was verified by using BigDye® Terminator v3.1 Cycle Sequencing Kit at the Department of Pathology by Dr. Christian Saur.

Cell culture

HEK293 cells (obtained from ATCC, LGC Standards, Teddington, UK) were cultured in T25cm^2 flasks with Dulbecco's modified Eagle's medium (DMEM; PAA, Pasching, Austria) supplemented with 10 percent fetal calf serum (FCS Gold, ;PAA), 100 U/l penicillin and 100 µg/mL streptomycin (PAA) at 37° C in a five percent CO_2 humidified atmosphere. 24 h prior to transfection, 4.0×10^5 cells per well were plated on poly-L-lysine (10 µg/mL) coated round (Ø 15 mm) coverslips, transfected with 1 µg pcDNA3-rTRPV1 or the mutated constructs using 3 µL Metafectene (metafectene® pro-Biontex Laboratories GmbH) and incubated at 34° C in a 5 percent CO_2 humidified atmosphere.

Human umbilical vein endothelial cells (HUVECs) were isolated from the freshly available umbilical cord. Cells were grown in basal endothelial cell growth medium (Provitro GmbH, Berlin Germany), supplemented with 2 percent fetal bovine serum, without antibiotics at 37ºC in a 5 percent CO_2 humidified atmosphere and experiments were conducted at approximately 80–90 percent visual confluence.

Calcium Imaging

48 h post transfection cells were transferred into extracellular solution containing NaCl 137.6 mM, KCl 5.4 mM, $MgCl_2$ 0.5 mM, $CaCl_2$ 1.8 mM, glucose 5 mM and HEPES 10 mM (Roth, Karlsruhe, Germany), loaded with the fluorescent dye FURA-2AM (3 µM; Biotrend, Köln, Germany) and 3 µM Pluronic F-127 for 45 min at RT in dark. Followed by 20 min washout in extracellular solution, fluorescence was measured using an inverted microscope (IX-81 with Cell^R, Olympus, Hamburg, Germany) and an ORCA-R2 CCD camera (Hamamatsu Corp., Bridgewater, NJ, USA). After alternating excitation with light of 340 nm and 380 nm wavelength, the ratio of the fluorescence emission intensities at 510 nm (340 nm/380 nm [510 nm]) was digitized at 0.5 Hertz and calculated. This fluorescence ratio is a relative measure of intracellular calcium concentration[26]. The concentration range at which calcium transients appeared upon stimulation with each of the compounds was established by application of increasing concentration of compounds for 1 min in a single coverslip of rTRPV1 transfected HEK293 cells followed by a washout for 1 min (inter-stimulus interval: 5 min). For EC_{50} determination a minimum of nine concentrations of each compound based on this range were used. Only one concentration per coverslip and a minimum of three separate coverslips for each concentration was used. The compound was applied to the cells for 1 min followed by 1 min washout using perfusion and 2 min rest. Repetitive application of 30 µM NOD was used to investigate tachyphylaxis. Additionally, 30 s before the second stimulus vehicle or 30 µM of the competitive TRPV1 antagonist Capsazepine was applied to block the receptor. At the end of

each experiment 10 µM CAP was used to select transfected cells. Analysis was done using cell^R software (Olympus). Each coverslip was considered as an independent experiment. Absolute change in ratio was determined by subtracting baseline value from the peak.

Protein isolation and Western blotting

HUVECs were lysed in 20 mM Tris-HCl, 150 mM NaCl, 5 mM EDTA, one percent Triton X-100, 0.5 percent sodium deoxycholate, 1 µM dithiothreitol (DTT) buffer containing proteinase and phosphatase inhibitors. Protein concentrations were measured using Coomassie-Reagent (Pierce, Rockford, USA). 15 µg of protein per condition was loaded on 10 percent SDS-polyacrylamide gel. Human anti-VCAM-1 (1:2000, BBA19, R&D Systems, Germany) or Human anti-HO-1 (1:2000, ADI-SPA-896-F, Enzo, Biochem Inc.) antibodies were used to probe the membrane. Since these compounds do not influence expression of β-Actin, equal protein loading was confirmed by stripping and re-probing membranes with monoclonal human anti-β-actin antibody (1:10,000, Abcam plc, UK). Anti-goat IgG-HRP, anti-rabbit IgG-HRP, anti-mouse IgG-HRP conjugated secondary antibodies (1:2500, Santa Cruz Biotechnology) were used. Image J ver1.5e was used for densitometry analysis. All the lanes were normalized to β-Actin. Inhibition of VCAM-1 is expressed as percentage relative to that of TNFα; induction of HO-1 is expressed as fold increase relative to that of cells grown in normal culture medium.

Luminol Assay

The redox activity of the compounds was measured using luminol assay. Serial dilutions of the compounds were prepared in distilled water, added to the luminol reaction mix (luminol 2.5 mM, p-Coumaric acid 0.9 mM and 0.3 percent $H_2O_{2)}$. HRP (0.1 µg/µL) and quenching of chemiluminescence was measured immediately using infinite® 200 PRO – Tecan microplate reader. The measurements were performed in triplicates.

Molecular modeling

Because of structural similarity between NOD and CAP the structure of TRPV1 PDB 3J5R[27], in which the TRPV1 forming complex with CAP is modelled, was taken. This structure is a reconstruction of the above mentioned complex by single particle cryo-microscopy[28]. The protein structure was processed with the Protein Preparation Wizard in the Schrödinger Suite 2005 (Maestro, Version 9.0, 2007; Schrödinger, LLC: New York, NY, USA), two chains are needed for delimiting the binding site, denoted as chain A and B in the manuscript. Hydrogen atoms were added followed by the adjustment of bond

orders. The protonation states for protonable residues were adjusted to match pH=7.4. After this, the protein was subjected to geometry optimization by using OPLS_2005 force field [29]. The structures of the different NADs were sketched by using the chemical editor at Maestro and were prepared using LigPrep (two-dimensional representations were converted into three-dimensional ones and partial charges were assigned).

Glide software was used for performing docking analyses[30]. The grid box for molecular docking was centered in the middle of the pocket, close to Y511, including the amino acids of chain A and B present in the binding site. The extra precision (XP) Glide mode was used. Glide XP has empirical scoring functions and also imposes desolvation penalties for burial of protein or ligand polar and charged groups. The method adds explicit water molecules to poses selected in previous steps, counts them, and uses these counts for performing comparisons with analogous groups in known active compounds. This process reduces false positives and increases reliability of the docking energy values. In our approach, the best docked position for each complex was determined by considering the total energy value after five runs.

Statistical analysis

All data are expressed as the means ± SEM from at least three independent experiments. Statistical significance of results was assessed by one-or two-way ANOVA followed by LSD (Prism 6 for Windows Version 6.01, $p<0.05$ was considered to be significant. For comparison, data were normalized to the respective first response.

Results

Generation of structural derivatives of NOD

To assess the molecular entities within NOD that are required for TRPV1 activation, we used NOD as a lead structure. We synthesized compounds that slightly differ from NOD at the aromatic moiety (A-region), the linker region (B-region) or the aliphatic chain (C-region). These changes included acetylation of the catechol structure, (A-NOD), omitting one hydroxyl functional group from the benzene nucleus (*N*-octanoyl tyramine (NOT)), exchanging octanoyl for the branched pivaloyl as aliphatic chain (*N*-pivaloyl dopamine (NPiD)), and shortening of the linker region by one methylene group. The later was made in two variants in which the positions of the carbonyl group were interchanged relative to the position of the amide group (ΔNOD and ΔNODR) (Figure 1B). In addition the vanilloid moiety of CAP was changed to a catechol structure (CAP-OH) (Figure 1C). We chose a different way for synthesis of CAP-OH as Goto et al [25]. Natural capsaicin was reduced and yielded saturated and unsaturated compounds with and without CH_3O-group. Only purification via semi-preparative HPLC led to the pure CAP-OH.

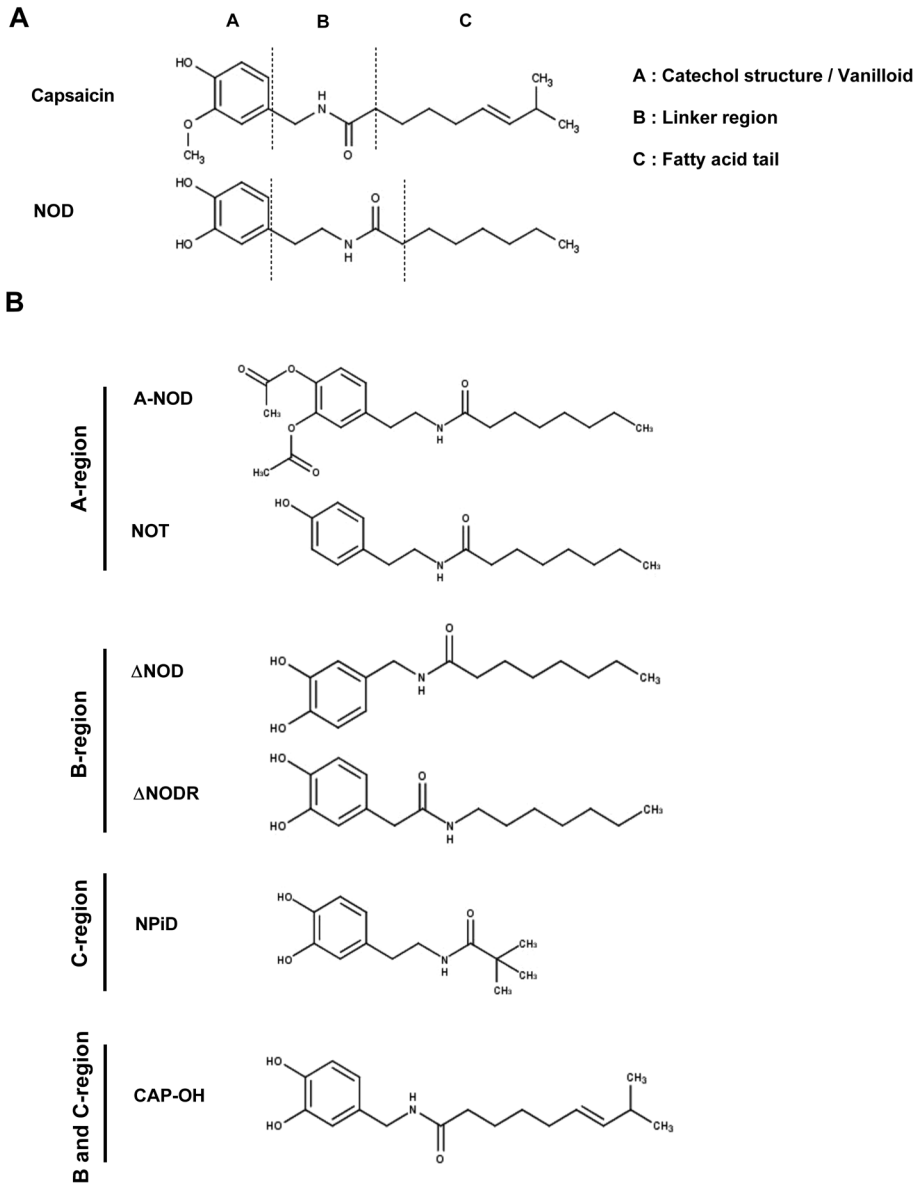

Figure 1. Chemical structures of the studied compounds. (**A**) CAP and NOD are shown with schematic representation of the different regions (A, B and C regions are shown with the dotted line). (**B**) Chemical structure of compounds used in the study, the structural region in which they vary from NOD is mentioned on the left side of the structure. NOD variants were synthesized by modifying the A-, B-and C-region region relative to that of NOD. (**C**) CAP-OH was synthesized by changing A region of CAP.

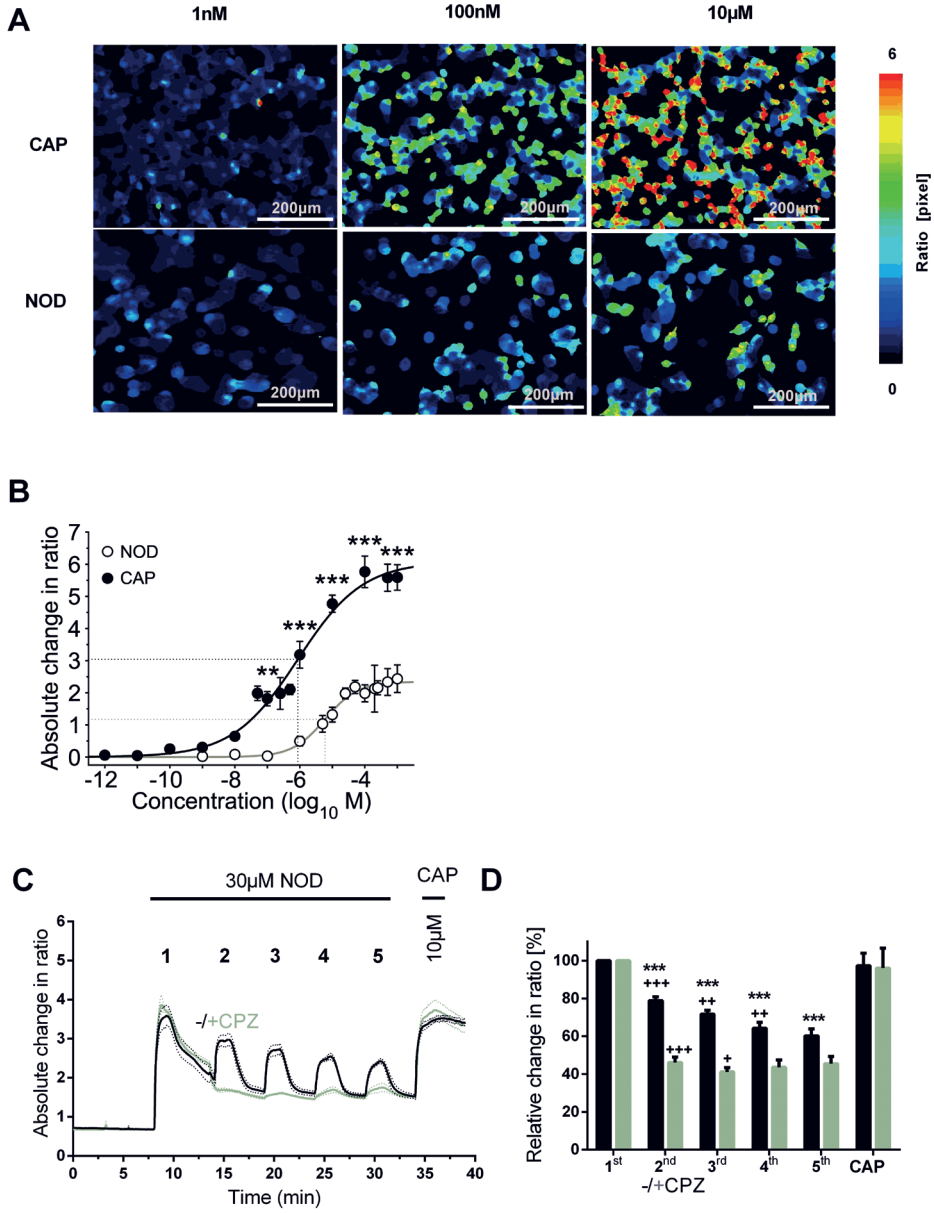

Figure 2. NOD like Capsaicin (CAP) activates rTRPV1 (A). A representative experiment showing increases in free $[Ca^{++}]_i$ in rTRPV1 transfected cells in response to 1 nM, 100 nM and 10 µM of CAP and NOD. The ratio 340/380 at 510 nm – a measure proportional to free $[Ca^{++}]_i$ – is false color coded where warmer colors indicate increasing calcium values. **(B)** Dose response curves of CAP (filled) and NOD (open circles). rTRPV1 expressing HEK293 cells were stimulated once with each concentration with at least three different measurements per concentration. The results are expressed as average ratio 340/380

NOD derivatives have differential TRPV1 activation properties

TRPV1 activation by the synthetic NADs was assessed using calcium microfluorimetry on rTRPV1 transfected HEK293 cells. Neither the synthetic NADs nor CAP induced change of intracellular calcium concentrations ($[Ca^{++}]_i$) in untransfected HEK293 cells (Supplementary Figure 1).

Even though NOD dose dependently increased $[Ca^{++}]_i$ in rTRPV1 transfected HEK293 cells (Figure 2A), it was significantly less potent and effective as compared to CAP (Figure 2 B) NOD EC_{50} 5.572 µM versus CAP EC_{50} 0.3 µM (Table 1).

The application of 30 µM NOD led to a significant increase in $[Ca^{++}]_i$ ($p<0.03$) compared to vehicle control, and these cells also responded to the specific TRPV1 agonist capsaicin CAP. With repetitive NOD application, calcium influx displayed marked tachyphylaxis and decreased to 60±6.3 percent from the first to the fifth response (Figure 2C-D; $p<0.001$). Application of TRPV1 antagonist Capsazepine (CPZ) 30 sec before the second NOD stimulus, significantly reduced responses (to 78±3.4 percent of 1st versus 35±5.1 percent of 1st without/with CPZ $p<0.001$). Interestingly, under these conditions NOD-evoked responses were persistently reduced after wash-out of CPZ, while capsaicin CAP responsiveness of these cells was not changed (Figure 2 C and D; $p=0.89$).

All synthetic NOD derivatives were able to activate TRPV1 in a concentration-dependent manner (Figure 3). ΔNODR was the most and A-NOD the least efficacious at TRPV1. EC_{50} for A-NOD, ΔNOD and ΔNODR were 20.82 µM, 2.86 µM and 0.06 µM respectively (Table 1). CAP-OH also activated TRPV1 in a dose dependent manner. Although it retained agonistic properties at TRPV1 CAP-OH has an EC_{50} value of 0.736 µM, nearly two times higher than that of CAP EC_{50} 0.3 µM (Table 1).

at 510 nm±SEM of all measurements. The EC_{50} value of CAP was about 0.87 µM and for NOD 5.93 µM (indicated as dotted lines). Two-way ANOVA indicates substance differences; $^{**}p<0.01$ and *** and $p<0.001$ LSD post-hoc test. **(C)** A series of representative experiments showing increases in free $[Ca^{++}]_i$ in rTRPV1 transfected cells in response to repetitive application of 30 µM NOD. The response displayed marked tachyphylaxis from stimulus to stimulus (black trace). Application of equimolar concentration of the competitive TRPV1 antagonist Capsazepine before and during the 2nd stimulus (CPZ; grey trace) abolished the NOD response further confirming that NOD acts as a full agonist at TRPV1. The ratios 340/380 at 510 nm – a measure proportional to free $[Ca^{++}]_i$ – was averaged from three independent experiments per condition and are shown as mean±SEM (depicted as dotted line) **(D)** Bar graph shows the maximum increases in free $[Ca^{++}]_i$ upon response to repetitive application of 30 µM NOD with or without equimolar concentration of CPZ; repeated application of NOD induced tachyphylaxis of subsequent responses, CPZ largely blocked NOD responses – both phenomena are also known for capsaicin at TRPV1. $^{***}p<0.001$, LSD post-hoc test vehicle versus CPZ group; $+p<0.05$, $++p<0.01$, $+++p<0.001$ versus preceding application within treatment group.

Because NOT and NPiD precipitated at high concentrations (1 mM) at which calcium transients were only 38 percent and 51 percent of the CAP response, EC_{50} values could not be determined. It should be mentioned however that slight calcium transients for NOT and NPiD were observed at 100 and 500 µM respectively.

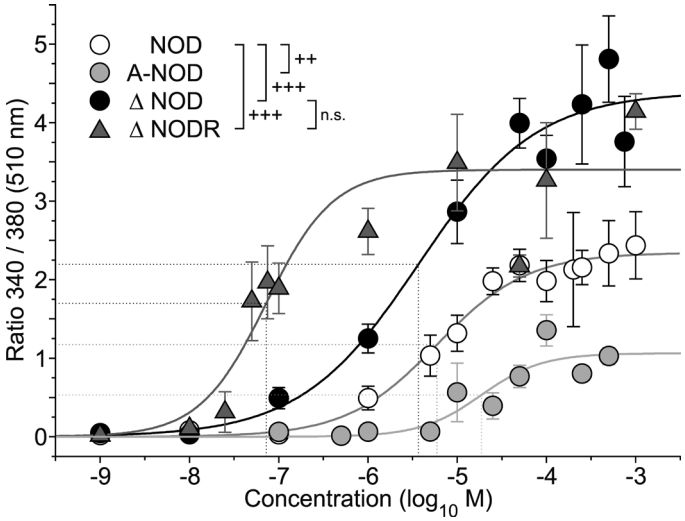

Figure 3: Dose response curves obtained with different NADs rTRPV1 transfected HEK293 cells were stimulated only once and for each concentration at least 3 different measurements were done. The results are expressed as average ratio 340/380 at 510 nm ± SEM of all measurements with EC_{50} values (indicated as dotted lines) of 5.93 µM (NOD, open circles), 18.69 µM (A-NOD, grey circles), 3.69 µM (ΔNOD, filled circles) and 0.06 µM (ΔNOD R, triangles). $^{n.s.}$ $p>0.2$, $^{++}p<0.01$, $^{+++}p<0.001$ ANOVA with LSD post-hoc test between substances.

Table 1: TRPV1 activation, anti-inflammatory, and redox properties of the compounds used in the study. For TRPV1 activation and Luminol Assay – the EC_{50} value defined as the concentration of the compound needed to evoke the response corresponding to the 50 percent of the maximum produced by that compound. The increase in ratio was fitted in equation to obtain $LogEC_{50}$ values. For TRPV1 activation assay-bottom was constrained to 0 since the baseline was subtracted from the response. Top in the equation refers to the platue observed in the dose response experiments and provides the efficacy i.e. maximum strength of TRPV1 activation.The anti-inflammatory property of the compounds was assessed at 100 µM via their ability inhibit TNFα induced VCAM-1 expression or induction of HO-1at protein level. Western blot data quantification was performed by densitometry. Inhibition of VCAM-1 is expressed as relative to that of TNFα (10ng/mL), induction of HO-1 is expressed as fold increase relative to that of cells grown in normal culture medium. For each experiment and for each quantification chemiluminescence signal was normalized using ß-actin. Statistical analysis was performed using a one way-ANOVA with Fisher's LSD test, VCAM-1 inhibition-TNFα versus treatment, HO-1 induction medium versus treatment (n.s. non-significant, *p<0.05, **p<0.01, ***p<0.001***p<0.0001,****p<0.0001).

Compound	Modified region(s) with respect to NOD	TRPV1 activation			Anti-inflammatory properties at 100 µM		Redox activity
		EC_{50} [µM]	LOG EC_{50}	TOP	VCAM-1 (Relative inhibition	HO-1 induction (fold increase)	EC_{50} Luminol Assay[µM]
Capsaicin		0.87	6.06±0.19	6.09±0.34	1.13±0.18	2.81±0.31	Not measured
NOD	none	5.93	5.23±0.08	2.34±0.08	0.40±0.05****	10.12±3.06****	9.15
A-NOD	A	18.69	4.73±0.25	1.06±0.19	0.53±0.08***	6.11±1.95*	14.80
ΔNOD	B	3.69	5.43±0.21	4.39±0.32	0.79±0.07**	3.66±0.72	6.78
ΔNODR	B	0.06	7.22±0.13	3.14±0.26	0.43±0.07****	6.98±1.49****	7.70
NOT	A	>100	>-4	N.D	0.76±0.07**	1.44±0.52	>1000
NPiD	C	>500	>-3.3	N.D	0.53±0.12***	5.93±1.55*	10.44
CAP-OH		4.93	5.31±0.25	7.81±0.66	0.46±0.11****	4.86±0.97*	37.52

(n.s. non-significant, *p<0.05, **p<0.001, ***p<0.0001)

NOD, CAP and the NOD derivatives use similar amino acids for their TRPV1 interaction

Based on the electron cryo-microscopy structure of the rTRPV1 ion channel [27], we performed docking studies with NOD, CAP, and the NOD derivatives to understand the interaction between the agonist and the channel. We observed potential hydrogen bond interactions for CAP with three amino acids Y511, T550 and E570 (Figure 4A) in the TRPV1 binding pocket. For NOD, two of these interactions were the same, i.e. T550 and E570, while no hydrogen bond interaction with Y511 was suggested (Figure 4B).

The NOD derivatives established hydrogen bond interactions with the same residues (Figure 4D-H), with the exception of A-NOD, which is oriented differently because the lack of OH substituents in its catechol group (Figure 4C). The hydrogen bond distances obtained from the docking positions of the studied compounds (without considering A-NOD) are shown in the Supplementary Table S1. It is possible to observe that NOD, CAP, and the NOD derivatives form one or two hydrogen bond interactions with the residue E570. Meanwhile, all the compounds, with the exception of NPiD, form hydrogen bond with T550. Finally, the compounds CAP, ΔNODR, NPiD and CAP-OH are hydrogen bonded to Y511.

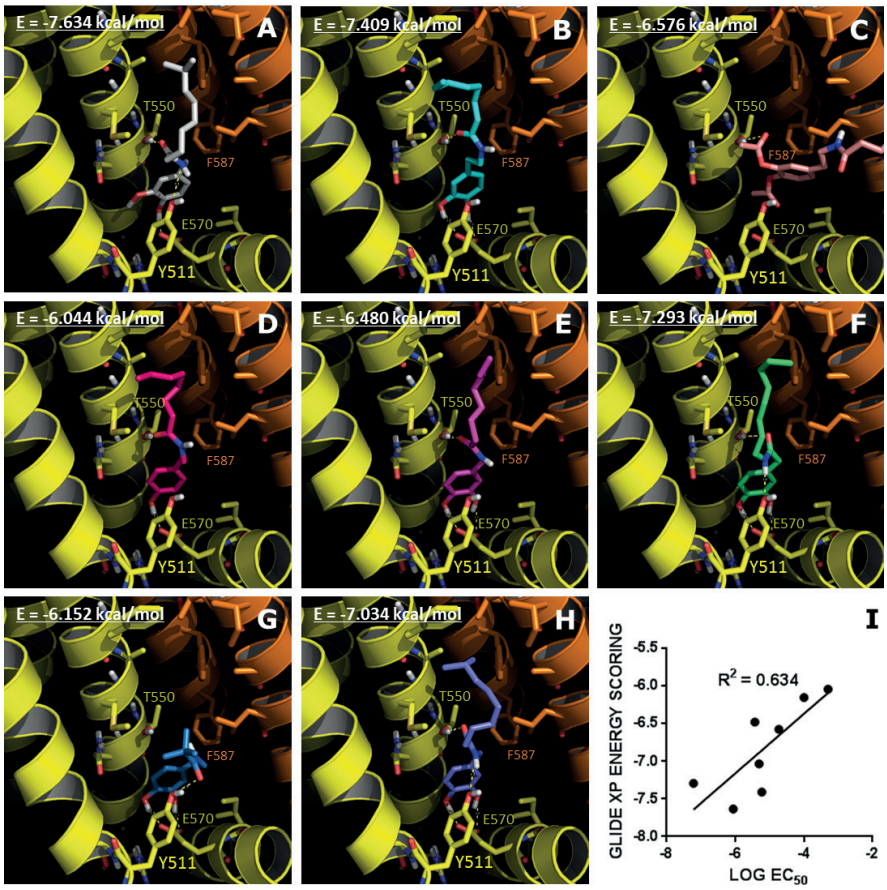

Figure 4: Docking of capsaicin, NOD, and NOD derivatives in TRPV1 channel. Conformations of the studied compounds within the binding pocket of TRPV1 for CAP (A), NOD (B), A-NOD (C), NOT (D), ΔNOD (E), ΔNODR (F), NPiD (G), and CAP-OH (H). Chain A of the protein is represented in yellow, where amino acids with hydrogen bond contributions Y511, T550 and E570 are in stick representations. Chain B of the protein is represented in orange, where amino acids with VDW contributions are also in stick representations. Glide XP scoring energy values are at the top-left corner of each docking pose picture (A-H). Correlation between these values and experimental logEC_{50} values are in (I).

The docking method Glide XP yielded a scoring energy value for each compound reported in Figure 4. Despite docking methods are not so reliable in calculating binding energy values [31] a good correlation between the Glide XP scoring energy values and experimental logEC_{50} values was found with correlation coefficient R^2=0.63 (Figure 4I). This result confirms that the selected electron cryo-microscopy structure is a good model for studying the affinities of TRPV1 ligands, and gives confidence in the ability of the Glide XP method to describe the relationship between the chemical interactions of the ligands in the binding site and their differential affinities. It is possible to extract per-residue coulombic, hydrogen bond, and van der Waals (VDW) components from the Glide XP scoring energy to get more insight in the most relevant TRPV1 amino acids involved in the differential activities (Supplementary Figure 2). The analysis of the coulombic components indicates that E570 has the major contribution, which is better when both catechol hydroxyl groups are available. The analysis of the hydrogen bond components shows that the residues Y511, T550 and E570 have different energy contributions for each compound. Finally, the analysis of the VDW contributions is more complex due to multiple residues involved. The residues with higher VDW contributions were Y511, L515, F522, F543, A546, M547, T550, N551, L553, Y554, I569, and I573 from chain A, and F587, F591, I661, L662, A665, and L669 from chain B. It is noteworthy to mention that Y511 has not only hydrogen bond contribution; it also has an important VDW contribution. This chemical role was suggested previously in the report of Lee et al.[32]: when the Y511F and Y511A mutants were generated, capsaicin EC_{50} values increased 30 times for the first mutant (where hydrogen bond contribution was lost and VDW contribution was kept), and 500 times for the second (where both hydrogen bond and VDW contributions were lost).

To evaluate the interactions revealed by the docking model and previously published anchor residues S512 and R491[33] for the CAP TRPV1 interactions, all putative interacting amino acids in rTRPV1 were changed to alanine by site-directed mutagenesis. The effect of these mutations on TRPV1 activation was studied at three different concentrations of CAP (300 nM, 1 µM, and 10 µM; Figure 5A) and NOD (15 µM, 50 µM and 200 µM; Figure 5B) corresponding to approximately 2.5, 9 and 36 (for NOD) or 1, 3 and 30 (for CAP) times the EC_{50} value. For the Y511A and E570A rTRPV1 variants the calcium responses were completely lost at the two lower concentrations of CAP or NOD and remained significantly diminished even when using excessively high concentrations of CAP or NOD (Figure 5 A-B). Also the T550A significantly diminished TRPV1 activation, which seemed to be more pronounced in the case of NOD stimulation at 15 µM (two times EC_{50}) and at 200 µM (three times EC_{50}). While in HEK cells expressing the S512A TRPV1 variant CAP was not able to evoke calcium responses when tested over a range of concentration (Supplementary figure 3), mutation of R491 to A did not affect TRPV1 activation by CAP or NOD.

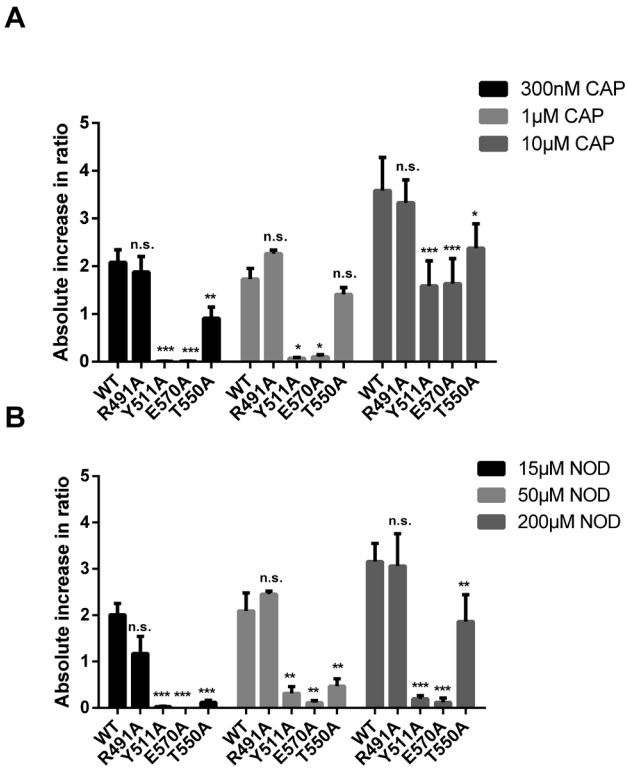

Figure 5: Point mutation of the identified binding sites dramatically changes the TRPV1 channels sensitivity to capsaicin (CAP) and NOD. HEK293 cells were transfected with different mutants of the rTRPV1 receptor. Cells were challenged with different concentrations of either capsaicin (300 nM, 1 µM, 10 µM; **A**) or NOD (15 µM, 50 µM, 200 µM; **B**). Y511A, and E570A are important for the binding of both capsaicin and NOD. Regarding T550A the effect is more pronounced after NOD application. A minimum of 3 independent experiments were done. Statistical analysis was performed using two way-ANOVA with Fisher's LSD test wild-type tested versus mutated rTRPV1 at the same concentration (n.s. non-significant, *$p<0.05$, **$p<0.001$, ***$p<0.0001$).

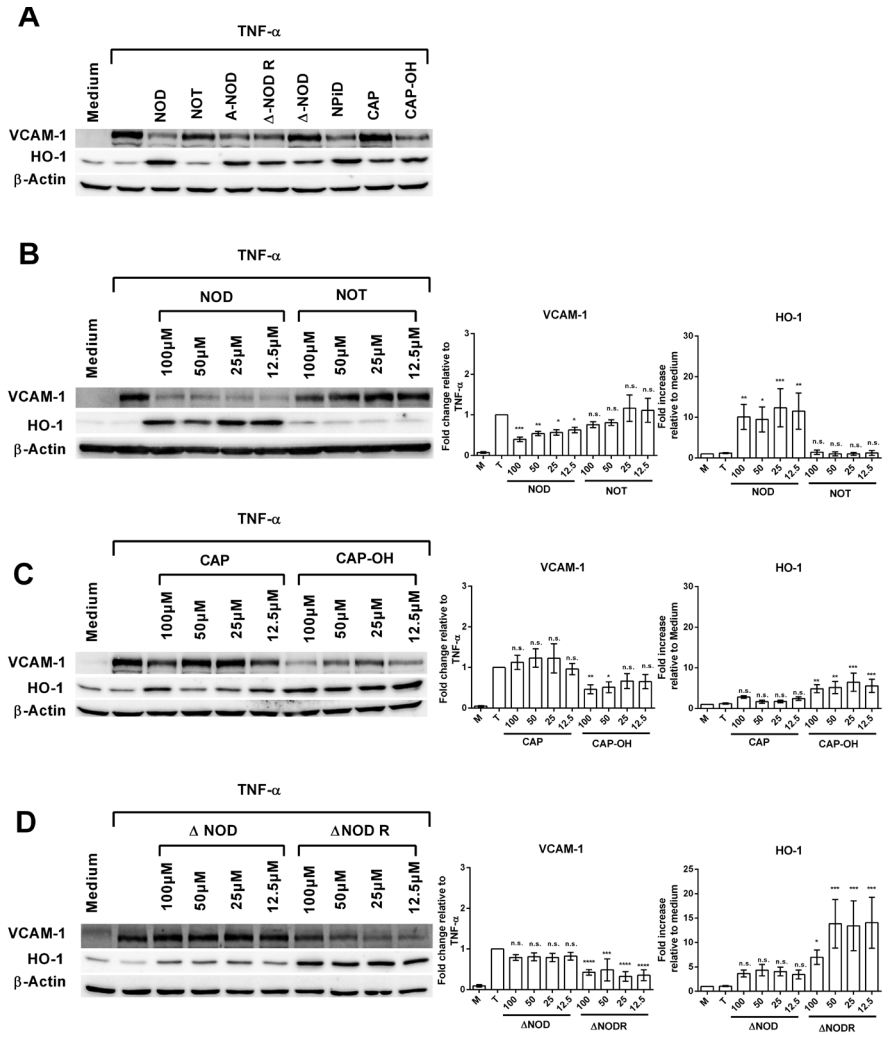

Figure 6: Anti-inflammatory property is not solely governed via catechol structure. Anti-inflammatory property is not solely governed via catechol structure. (A) HUVECs were stimulated overnight with – TNF-α (10 ng/mL) in the presence of 100 µM various compounds. The expression of VCAM-1 and HO-1 was determined by western blotting and quantified by densitometry. VCAM-1 expression is presented as fold change relative to TNFα (T) and HO-1 expression is presented as fold change relative to medium (M) (**B**-**D**) Dose-response experiments for direct comparison of NOD vs NOT (**B**), Capsaicin (CAP) vs. CAP-OH (**C**) and ΔNOD vs. ΔNODR (**D**). For all the blots equal loading of protein was ensured with ß-actin. Representative blots are shown, a total of at least 3 independent experiments were performed. Statistical analysis was performed using a one way-ANOVA with Fisher's LSD test, VCAM-1 inhibition-TNFα versus treatment, HO-1 induction medium versus treatment (n.s. non-significant, *p<0.05, **p<0.001, ***p<0.0001).

The anti-inflammatory property of NADs is not defined solely by Redox activity

To assess if the structural changes in the synthetic compounds would also affect their anti-inflammatory properties, we screened all compounds for down-regulation of TNFα mediated VCAM-1 expression and induction of HO-1 in HUVECs (Fig. 7A). Except for ΔNOD all catechol containing structures were able to inhibit TNFα mediated VCAM-1 expression, while this was neither observed for CAP nor for NOT. Inhibition of VCAM-1 expression was paralleled by a concomitant induction of HO-1 expression. Dose-response experiments for direct comparison of NOD vs NOT, CAP vs CAP-OH and ΔNOD vs. ΔNODR are depicted in figure 6 B-C. In considering that catechols contain a high redox activity which may contribute to the anti-inflammatory effects of NADs[16], we assessed for each compound the quenching properties in a peroxidase mediated luminol chemiluminescence reaction (Table 1). All compounds except for NOT were able to quench chemiluminescence in the luminol assay.

Discussion

We previously demonstrated that apart from TRPV1 activation, NOD exerts profound cyto-protective properties including prevention of cold inflicted injury [23, 34, 35], down-regulation of inflammatory mediators [16] and inhibition of platelet function[35]. In the present study we sought to dissect the molecular entities within NOD that govern TRPV1 activation and are responsible for the anti-inflammatory effect as defined by down-regulation of TNFα mediated VCAM-1 expression and induction of HO-1. The major findings of this study are as follows: firstly, NOD is an agonist at rTRPV1 in a HEK293 heterologous expression system but activates TRPV1 with lesser potency than CAP. Alterations in the A-, B-and C-regions of NOD may all affect the potency to stimulate TRPV1. While shortening of the linker region by one methylene group improved ability of NADs to activate TRPV1 (NOD $EC_{50=}$ 5.57 μM, ΔNOD $EC_{50=}$ 2.87 μM, ΔNODR $EC_{50=}$ 0.06 μM) the use of a short branched fatty acid in the C-region (NPiD) or omission of a hydroxyl group in the A region (NOT) profoundly deteriorated TRPV1 activation. Acetylation of both hydroxyl groups in the A-region (A-NOD) impaired TRPV1 activation to a much lesser extent. Secondly, docking studies suggested that amino acids (AA) Y511, E570 and T550 in TRPV1 may form hydrogen bond interactions with CAP, while only E570 and T550 form this interaction with NOD. In addition to these putative interacting AA, site directed mutagenesis also revealed the importance of S512 for TRPV1 activation by CAP or NOD. Thirdly, the anti-inflammatory effects of the compounds were not significantly affected by changes in the A-, B-and C-regions of NOD as long as the catechol moiety in the A-region was maintained. Acetylation of the ortho-dihydroxy groups (A-NOD) was equally effective as compared to NOD. Moreover attainment of catechol

structure imparted CAP-OH better anti-inflammatory property as compared to CAP. The only exception found in this study was ΔNOD which did not inhibit VCAM-1 expression despite the fact that it carries an intact catechol structure.

The CAP-bound TRPV1 structure was recently resolved by making use of cryo-EM[27, 28] and iterative computation in conjunction to systematic site-specific functional tests[36]. From these data it has been postulated that CAP takes a 'tail-up, head-down' configuration in which the vanillyl and amide groups form specific interactions with residues T550 and E570 by hydrogen bonds to anchor to its bound position. The aliphatic chain interacts with the channel through nonspecific VDW forces and contributes to the binding affinity. This is followed by a series of structural rearrangements to stabilize the activated conformation mainly by 'pulling' at E570 through hydrogen bonding and VDW forces. The Y511 residue seems not to play a role in hydrogen binding but closes the mouth of the binding pocket and thereby cradling the CAP molecule inside[36]. This model thus explains why the Y511A mutation leads to impaired TRPV1 activation, but does address the importance of S512 for TRPV1 activation by CAP [33] and NOD. Although S512 is not directly present in the binding pocket, it might contribute to the shape of the binding pocket and thus might be indirectly required for attaining the appropriate binding pocket configuration for the interaction with TRPV1 agonists. This might explain why we did not achieve TRPV1 activation by any of the TRPV1 agonist in cells expressing the S512A TRPV1 mutant. Our docking studies suggest similar interactions for NOD and TRPV1 as described for CAP, i.e. interaction of the catechol group with E570 and interaction of the amide with T550.

Acetylation of both hydroxyl groups in the A-region (A-NOD) yielded loss of TRPV1 activation potency and significantly lower 340/380-ratio for A-NOD as compared to NOD. It should be emphasized that our docking studies suggest that A-NOD would not fit in the TRPV1 pocket unless it is converted to NOD via intracellular esterases. This might as well explain why the 340/380-ratio was lower for A-NOD. Both NPiD and NOT were extremely poor TRPV1 agonists. According to docking experiments, the former does not fit in the hydrophobic region of the TRPV1 pocket because of the short bulky fatty acid tail or the short bulky fatty acid tail does not provide sufficient VDW forces in the interaction with the hydrophobic core of the channel[36]. On the other hand, NOT enters in the TRPV1 pocket but only allows one hydrogen bond with E570, as opposed to two bonds for NOD. This results in a relative loss of binding affinity and thus in impaired TRPV1 activation. Shortening of the linker region on the contrary, increased the potency of NADs to activate TRPV1 (ΔNOD $EC_{50=}$2.87 μM and ΔNODR $EC_{50=}$0.06 μM). In fact, ΔNODR was even more potent than CAP (EC_{50}=0.305 μM) in activating TRPV1. Although our TRPV1 docking model did not predict any difference between ΔNODR and CAP with respect to the total energy value, the coulombic and hydrogen bond contributions of E570 and the hydrogen bond contribution of Y511 are suggested as the more important chemical characteristics for explaining ΔNODR's lower EC_{50} value.

ΔNOD and ΔNODR also behaved differently with respect to the anti-inflammatory properties. These properties seem to depend on the presence of the catechol structure which acts as an anti-oxidant able to inhibit NFκB [16] and to activate the Nrf2-keap1 pathway[17]. In line with this, it was found that CAP-OH is more superior to CAP in inhibiting VCAM-1 and inducing HO-1 expression. Yet, despite having an intact catechol structure and high redox activity ΔNOD completely failed to inhibit TNFα mediated VCAM-1 and to induce HO-1. This underlines that redox activity alone is not determining anti-inflammatory property.

Conclusion

In conclusion, it was demonstrated that the molecular entities that govern TRPV1 activation by NOD, and presumably NADs in general, are different from the ones that provide NADs their anti-inflammatory properties. In keeping with the close relation between inflammation and pain, compounds that can desensitize TRPV1 and have anti-inflammatory properties, may offer new therapeutic avenues for the treatment of inflammatory pain. Topical application of CAP has long been clinically used to treat persistent pain, such as osteoarthritic pain, post-herpetic neuralgia of the trigeminal nerve, migraine prophylaxis, diabetic neuropathy, HIV-associated distal sensory neuropathy, and intractable pain in cancer patients[37–41]. Nonetheless its use is associated with complete denervation and impaired nerve regeneration [42] as a consequence of strong TRPV1 activating properties. Moreover, it may not, or only indirectly, address the inflammatory component of pain. Our findings may thus provide a framework for the rational design of moderate TRPV1 agonists with improved anti-inflammatory properties for the treatment of inflammatory pain.

Disclosure

All other submitting authors declare that they do not have any conflict of interest with this publication.

Ethical Statement

Umbilical cords for isolation of human umbilical vein endothelial cells (HUVECs) were received from donors in the Department of Obstetrics and Gynecology, University Medical Center Mannheim, Heidelberg University, Mannheim, Germany. This was approved by the local ethics committee (Medizinische Ethikkommission II der Medizinischen Fakultät Mannheim) and all donors gave their written informed consent (Ethics Application No. 2015–518N-MA).

Acknowledgements

We would like to thank Prof. Dr. Hans-Günter Schmalz and Dr. Nikolay Sitnikov from Department of Chemistry, University of Cologne, for their invaluable discussion on the chemical structures and findings of this study We like to acknowledge Dr. Christian Saur, from Department of Pathology, University Hospital Mannheim, for his help with the sequencing of the mutants. This study was supported by grants from the Deutsche Forschungsgemeinschaft (GRK880/3) and Albert und Anneliese Konanz-Stiftung.

Author Contribution

PP, ES, JC, MP, SR ,BH, YL, HM and BT performed the experiments. PP, JC, MP, BAY, CW, RL, WG UB BKK and AIK analyzed the results. PP, WG, UB, BAY, MH and SK were involved in the design of the study. PP, BW, WG, UB, MCH, BKK, MH, RDT, BAY, and AIK wrote the paper.

Refrences

1. Navarrete, C.M., et al., *Endogenous N-acyl-dopamines induce COX-2 expression in brain endothelial cells by stabilizing mRNA through a p38 dependent pathway.* Biochem Pharmacol, 2010. **79**(12): p. 1805–14.
2. Sancho, R., et al., *Immunosuppressive activity of endovanilloids: N-arachidonoyl-dopamine inhibits activation of the NF-kappa B, NFAT, and activator protein 1 signaling pathways.* J Immunol, 2004. **172**(4): p. 2341–51.
3. Chu, C.J., et al., *N-oleoyldopamine, a novel endogenous capsaicin-like lipid that produces hyperalgesia.* J Biol Chem, 2003. **278**(16): p. 13633–9.
4. Bisogno, T., et al., *N-acyl-dopamines: novel synthetic CB(1) cannabinoid-receptor ligands and inhibitors of anandamide inactivation with cannabimimetic activity in vitro and in vivo.* Biochem J, 2000. **351 Pt 3**: p. 817–24.
5. Kaufman, M.P., et al., *Effects of capsaicin and bradykinin on afferent fibers with ending in skeletal muscle.* Circ Res, 1982. **50**(1): p. 133–9.
6. Belmonte, C., et al., *Excitation by irritant chemical substances of sensory afferent units in the cat's cornea.* J Physiol, 1991. **437**: p. 709–25.
7. Caterina, M.J., et al., *Impaired nociception and pain sensation in mice lacking the capsaicin receptor.* Science, 2000. **288**(5464): p. 306–13.
8. Fischer, M.J., J. Btesh, and P.A. McNaughton, *Disrupting sensitization of transient receptor potential vanilloid subtype 1 inhibits inflammatory hyperalgesia.* J Neurosci, 2013. **33**(17): p. 7407–14.
9. Pogatzki-Zahn, E.M., et al., *Heat hyperalgesia after incision requires TRPV1 and is distinct from pure inflammatory pain.* Pain, 2005. **115**(3): p. 296–307.
10. Cervero, F. and J.M. Laird, *Understanding the signaling and transmission of visceral nociceptive events.* J Neurobiol, 2004. **61**(1): p. 45–54.
11. Baron, R., *Neuropathic pain: a clinical perspective.* Handb Exp Pharmacol, 2009(194): p. 3–30.
12. Butera, J.A., *Current and emerging targets to treat neuropathic pain.* J Med Chem, 2007. **50**(11): p. 2543–6.
13. Spicarova, D. and J. Palecek, *The role of the TRPV1 endogenous agonist N-Oleoyldopamine in modulation of nociceptive signaling at the spinal cord level.* J Neurophysiol, 2009. **102**(1): p. 234–43.
14. Farkas, I., et al., *The antinociceptive potency of N-arachidonoyl-dopamine (NADA) and its interaction with endomorphin-1 at the spinal level.* Pharmacol Biochem Behav, 2011. **99**(4): p. 731–7.
15. De Petrocellis, L., et al., *Actions of two naturally occurring saturated N-acyldopamines on transient receptor potential vanilloid 1 (TRPV1) channels.* Br J Pharmacol, 2004. **143**(2): p. 251–6.
16. Hottenrott, M.C., et al., *N-octanoyl dopamine inhibits the expression of a subset of kappaB regulated genes: potential role of p65 Ser276 phosphorylation.* PLoS One, 2013. **8**(9): p. e73122.
17. Kim, H., et al., *Caffeic acid phenethyl ester activation of Nrf2 pathway is enhanced under oxidative state: structural analysis and potential as a pathologically targeted therapeutic agent in treatment of colonic inflammation.* Free Radic Biol Med, 2013. **65**: p. 552–62.
18. Tsagogiorgas, C., et al., *N-octanoyl-dopamine is an agonist at the capsaicin receptor TRPV1 and mitigates ischemia-induced [corrected] acute kidney injury in rat.* PLoS One, 2012. **7**(8): p. e43525.

19. Spindler, R.S., et al., *N-Octanoyl Dopamine for Donor Treatment in a Brain-death Model of Kidney and Heart Transplantation.* Transplantation, 2015. **99**(5): p. 935–41.
20. Walpole, C.S., et al., *Analogues of capsaicin with agonist activity as novel analgesic agents; structure-activity studies. 1. The aromatic "A-region".* J Med Chem, 1993. **36**(16): p. 2362–72.
21. Walpole, C.S., et al., *Analogues of capsaicin with agonist activity as novel analgesic agents; structure-activity studies. 3. The hydrophobic side-chain "C-region".* J Med Chem, 1993. **36**(16): p. 2381–9.
22. Walpole, C.S., et al., *Analogues of capsaicin with agonist activity as novel analgesic agents; structure-activity studies. 2. The amide bond "B-region".* J Med Chem, 1993. **36**(16): p. 2373–80.
23. Losel, R.M., et al., *N-octanoyl dopamine, a non-hemodyanic dopamine derivative, for cell protection during hypothermic organ preservation.* PLoS One, 2010. **5**(3): p. e9713.
24. Walpole, C.S.J., et al., *Analogues of Capsaicin with agonist activity as novel analgesic agents; Structure-activity studies. 1. The aromatic "A-region".* J. Med. Chem., 1993. **36**: p. 2362–2372.
25. Goto, M., et al., *^{11}C-labeled Capsaicin and its in vivo molecular imaging in rats by positron emission tomography.* Food Nutr. Sci., 2015. **6**(2): p. 216–220.
26. Grynkiewicz, G., M. Poenie, and R.Y. Tsien, *A new generation of Ca2+indicators with greatly improved fluorescence properties.* J Biol Chem, 1985. **260**(6): p. 3440–50.
27. Liao, M., et al., *Structure of the TRPV1 ion channel determined by electron cryo-microscopy.* Nature, 2013. **504**(7478): p. 107–12.
28. Cao, E., et al., *TRPV1 structures in distinct conformations reveal activation mechanisms.* Nature, 2013. **504**(7478): p. 113–8.
29. Jorgensen, W.L., D.S. Maxwell, and J. Tirado-Rives, *Development and Testing of the OPLS All-Atom Force Field on Conformational Energetics and Properties of Organic Liquids.* Journal of the American Chemical Society, 1996. **118**(45): p. 11225–11236.
30. Friesner, R.A., et al., *Extra precision glide: docking and scoring incorporating a model of hydrophobic enclosure for protein-ligand complexes.* J Med Chem, 2006. **49**(21): p. 6177–96.
31. Ramirez, D. and J. Caballero, *Is It Reliable to Use Common Molecular Docking Methods for Comparing the Binding Affinities of Enantiomer Pairs for Their Protein Target?* Int J Mol Sci, 2016. **17**(4).
32. Lee, J.H., et al., *Structural insights into transient receptor potential vanilloid type 1 (TRPV1) from homology modeling, flexible docking, and mutational studies.* J Comput Aided Mol Des, 2011. **25**(4): p. 317–27.
33. Jordt, S.E. and D. Julius, *Molecular basis for species-specific sensitivity to "hot" chili peppers.* Cell, 2002. **108**(3): p. 421–30.
34. Vettel, C., et al., *Dopamine and lipophilic derivates protect cardiomyocytes against cold preservation injury.* J Pharmacol Exp Ther, 2013. **348(1):**: p. 77–85.
35. Ait-Hsiko, L., et al., *N-octanoyl-dopamine is a potent inhibitor of platelet function.* Platelets, 2013. **24**(6): p. 428–34.
36. Yang, F., et al., *Structural mechanism underlying capsaicin binding and activation of the TRPV1 ion channel.* Nat Chem Biol, 2015. **11**(7): p. 518–24.
37. Backonja, M., et al., *NGX-4010, a high-concentration capsaicin patch, for the treatment of postherpetic neuralgia: a randomised, double-blind study.* Lancet Neurol, 2008. **7**(12): p. 1106–12.
38. Haanpaa, M. and R.D. Treede, *Capsaicin for neuropathic pain: linking traditional medicine and molecular biology.* Eur Neurol, 2012. **68**(5): p. 264–75.

39. Sharma, S.K., A.S. Vij, and M. Sharma, *Mechanisms and clinical uses of capsaicin.* Eur J Pharmacol, 2013. **720**(1–3): p. 55–62.
40. Knotkova, H., M. Pappagallo, and A. Szallasi, *Capsaicin (TRPV1 Agonist) therapy for pain relief: farewell or revival?* Clin J Pain, 2008. **24**(2): p. 142–54.
41. Mason, L., et al., *Systematic review of topical capsaicin for the treatment of chronic pain.* BMJ, 2004. **328**(7446): p. 991.
42. Polydefkis, M., et al., *The time course of epidermal nerve fibre regeneration: studies in normal controls and in people with diabetes, with and without neuropathy.* Brain, 2004. **127**(Pt 7): p. 1606–15.

Chapter 5

Radiofluorinated *N*-Octanoyl Dopamine ([18F]F-NOD) as a Tool to Study Tissue Distribution and Elimination of NOD *in vitro* and *in vivo*

Journal of medicinal chemistry 2016 Nov 10;59(21):9855–9865.

Prama Pallavi*, Marc Pretze*, Mareike Roscher, Sarah Klotz, Julio Caballero, Uta Binzen, Wolfgang Greffrath, Rolf-Detlef Treede, Martin C. Harmsen, Mathias Hafner, Benito A.Yard, Carmen Wängler, Björn Wängler

* Equally contributing author

Abstract

To mitigate pre-transplantation injury in organs of potential donors *N*-octanoyl dopamine (NOD) treatment might be considered as it does not affect hemodynamic parameters in braindead (BD) donors. To better assess optimal NOD concentrations for donor treatment we report on the fast and facile radiofluorination of the NOD-derivative [^{18}F]F-NOD [^{18}F] compound **5** for *in vivo* assessment of NOD's elimination kinetics by means of PET imaging. [^{18}F] compound **5** was synthesized with reproducible high radiochemical yield and purity (> 98 percent) as well as high specific activities (> 20 GBq/µMol). Stability tests showed no decomposition of [^{18}F]**5** over a period of 120min in rat plasma. *In vitro*, low cell association was found for [^{18}F] compound **5** indicating no active transport mechanism. *In vivo*, [^{18}F] compound **5** exhibited a fast blood clearance, predominantly eliminated by liver. Although these data suggest that also NOD might be subjected to a fast clearance, further pharmacokinetic evaluation is warranted.

Introduction

Current evidence suggests that low dose dopamine treatment of braindead (BD) donors improves transplantation outcome in recipients of renal and heart allografts [1–3]. Although the salutary effect of donor dopamine treatment has not been completely delineated, it has been suggested that the hemodynamic properties of dopamine do not play an essential role herein.[4, 5] *In vitro* studies have identified three putative mechanisms by which dopamine may convey its protective properties in transplantation settings. Firstly, dopamine can protect cells against cold inflicted injury as tested *in vitro* on endothelial cells, renal epithelial cells and cardiomyocytes. [6],[7, 8] Secondly, dopamine is able to activate the transcription factor Nrf2 which regulates the expression of the tissue protective protein Heme oxygenase 1 (HO-1).[9] Thirdly, dopamine has anti-inflammatory properties, reflected by down-regulation of adhesion molecules and chemokines.[9–11]

Even though both prospective and retrospective studies have advocated the use of dopamine in BD donors as a meaningful modality to improve transplantation outcome [1, 2], it has not been implemented in general guidelines for donor management. Currently dopamine is used in donor management to stabilize blood pressure, albeit that in clinical practice (nor)adrenaline is more frequently used for blood pressure stabilization of BD donors. In approximately 12 percent of treated donors dopamine treatment needs to be discontinued as a consequence of tachycardia or hypertension. Moreover, the potential impact of inotropic agents on cardiomyocytes, i.e. increased cytosolic calcium concentration [12, 13] and opening of the mitochondrial permeability transition pore [14, 15], may raise further concerns on the use of such agents in donor management.[16, 17] This underscores the need for dopamine-like compounds that are devoid of hemodynamic action and yet have a similar or higher efficacy to protect organ allografts from pre-transplantation injury. By *N*-acylation of dopamine, which largely abrogates adrenoceptor and dopaminergic receptor binding, a class of synthetic compounds was developed lacking hemodynamic actions while retaining the protective properties of dopamine.[3, 8] As representative of *N*-acyl dopamines we have shown that *N*-octanoyl dopamine (NOD) is superior to dopamine *in vitro* [18, 19] and is highly effective *in vivo* to protect rat kidneys from ischemia induced acute kidney injury (AKI).[20, 21] The latter seems to be a consequence of the interaction with the transient receptor potential cation channel subfamily V member 1 (TRPV1) [22] as NOD was not renoprotective in TRPV1$^{-/-}$ rats.[23] Recently it was also demonstrated that NOD treatment of BD donor rats reduced inflammation in the donor kidney and improved renal function when such grafts were transplanted into allogeneic recipients [24].

Although these pre-clinical findings are promising tissue distribution and pharmacokinetics of NOD have not been addressed so far. As a first step we developed in the present study a NOD based radiotracer to study the *in vivo* tissue distribution and elimination kinetics of NOD by means of PET imaging.

In this work, we developed a fluorinated derivative of NOD, 2-fluoro-*N*-octanoyl dopamine **5** (F-NOD) and compared the *in vitro* behaviour of F-NOD with NOD in various assays in order to prove whether F-NOD could act as an analogue to NOD. In brief, we compared the induction of HO-1, redox activity, TRPV1 activation and EC_{50}. Further we performed a catechol *O*-methyl transferase (COMT) assay with NOD and F-NOD in order to investigate the cell intern metabolism. We developed a precursor **10** for radiofluorination in order to obtain the radiotracer [^{18}F]F-NOD. Next, we performed an *in vitro* cell assay with [^{18}F]F-NOD at HUVECs for the determination of cell association. After this, we evaluated the *in vivo* behaviour of radiolabelled [^{18}F]F-NOD in three Lewis rats.

Experimental Section

General procedures. All reagents and solvents were purchased from commercial suppliers and were used without further purification unless otherwise specified. NMR spectra were recorded on a 300 MHz Varian Mercury Plus and a 500 MHz Varian NMR System spectrometer (Palo Alto, CA). Chemical shifts (δ) are given inppm and are referenced to the residual solvent resonance signals relative to $(CH_3)_4Si$ (^{1}H, ^{13}C) and the internal standard $CFCl_3$ (^{19}F). Mass spectra were obtained on a Bruker Daltonics microflex™ MALDI-TOF mass spectrometer (Bremen, Germany). Preparative column chromatography was performed on Merck silica gel 60. Reactions were monitored by thin-layer chromatography (TLC) on Merck silica gel F254 aluminium plates, with visualization under UV (λ=254nm) or by evaluation using ninhydrin and heating. If necessary, the purity was determined by high performance liquid chromatography (HPLC). Purity of all final compounds was 95 percent or higher. Analytical (radio-)HPLC was performed on a Dionex UltiMate 3000 HPLC system (Thermo Scientific, Dreieich, Germany), equipped with a reverse phase column (Merck Chromolith® RP-18e; 100x4.6 mm plus a guard column 10x4.6mm), a UV-diode array detector (210nm, 254nm) and a scintillation radiodetector Gabi Star (Raytest, Straubenhardt, Germany). The solvent system used was a gradient of acetonitrile:water (containing 0.1 percent TFA) (0–8min: 0–100 percent MeCN) unless otherwise stated at a flow rate of 4 mL/min. All radioactive compounds were identified using analytical radio-HPLC by comparison of the retention time of the reference compound and also by co-injection with the reference substance. A difference of 0.11min between UV and γ-trace occurs as a function of the HPLC setup. Decay-corrected RCYs were quantified by calculation from QMA-eluted activity against C_{18}-eluted activity with respect to the purity of the final product in radio-HPLC and radio-TLC using a radio-TLC scanner (BAS-2500, Raytest). Catridge purification was performed with Waters C_{18} light cartridges. [^{18}F] Fluoride was purchased from ZAG Zyklotron AG (Karlsruhe, Germany).

Cell culture

Human umbilical vein endothelial cells HUVECs were isolated from the freshly available umbilical cord. Cell were grown in basal endothelial cell growth medium (Provitro GmbH, Berlin, Germany), supplemented with 2 percent fetal bovine serum and antibiotics. Cultures were maintained at 37ºC in a 5 percent CO_2 humidified atmosphere and experiments were conducted on cells at approximately 80–90 percent confluence.

HEK293 cells were cultured in T25cm^2 flask with DMEM supplemented with 10 percent FCS, 1 percent Penicillin Streptomycin at 37° C with 5 percent CO_2 humidified atmosphere.

Calcium Imaging and data analysis

HEK293 cells were seeded on 15 mm round glass coverslips in 12 well plates. 24 hours post plating, cells were transfected with rTRPV1 using Metafectane (metafectene® pro-Biontex Laboratories GmbH, Germany). 48 hours post transfection, cells were transferred into extracellular solution containing 137.6 mM NaCl, 5.4 mM KCl, 0.5 mM $MgCl_2$, 1.8 mM $CaCl_2$, 5 mM glucose, and 10 mM HEPES (Roth, Karlsruhe, Germany), loaded with the fluorescent dye FURA-2AM (1 µM; Biotrend, Cologne, Germany). Fluorescence was measured using an inverted microscope (IX-81 with Cell^R, Olympus, Hamburg, Germany) and an ORCA-R2 CCD camera (Hamamatsu Corp., Bridgewater, NJ, USA). After alternating excitation with light of 340nm and 380nm wavelength, the ratio of the fluorescence emission intensities at 510nm (340nm/380nm [510nm]) was calculated and digitized at 0.5 Hertz. This fluorescence ratio is a relative measure of intracellular calcium concentration [25]. Analysis was done using cell^R software (Olympus). All the cells that responded to Capsaicin were taken as region of interest and each coverslip was taken as an independent experiment. To determine the absolute change in ratio, the baseline value was subtracted from the peak. The data was analyzed using 2-way ANOVA with fixed effects for substance and concentration (STATISTICA Vs. 4.5, StatSoft, Inc.), LSD post-hoc test was used to identify substance differences at a given concentration.

Protein isolation and Western Blotting

HUVEC cell lysates were generated by lysing in lysis buffer consisting of 10 mM Tris-HCl, 150 mM NaCl, 5 mM EDTA, 1 percent Triton X-100, 0.5 percent sodium deoxycholate, 1 µM dithiothreitol (DTT), proteinase inhibitor cocktail and phosphatase inhibitor. Protein concentration was measured using Coomassie-Reagent (Pierce, Rockford, USA). Samples (15 µg protein extract) were heated to 95° C for 5mins, loaded and separated on 10 percent SDS-polyacryamide gels followed by semi-dry blotted onto PVDF membranes (Roche, Mannheim, Germany). The membranes were incubated with 5 percent w/v non-fat dry milk in TBS/Tween 0.5 percent to block unspecific background staining

and hereafter incubated overnight at 4° C with anti-VCAM-1-(AF643, R&D Systems, Wiesbaden, Germany) or anti-HO-1-antibodies (ADI-SPA-895, Enzo, Biochem Inc, USA). Subsequently, the membranes were thoroughly washed with TBS-Tween 0.1 percent and incubated with the appropriate horseradish peroxidase conjugated secondary antibody, followed by five wash steps in TBS/Tween 0.1 percent. Proteins were visualized using enhanced chemiluminescence technology, according to the manufacturer's instructions (Pierce, Rockford, IL, USA). To confirm equal protein loading, membranes were stripped and re-probed with monoclonal anti-β-actin antibody (clone AC-74, ascites fluid, Sigma Aldrich, USA).

Luminol Assay

The redox activity of the NOD and F-NOD was measured using luminol assay. Serial dilutions of the compounds were prepared in distilled water and added to Luminol reaction mix (luminol 2.5mM, p-Coumaric acid 0.9 mM and 0.3 percent H_2O_2). HRP (0.1 µg/µL) was added to the reaction mix and quenching of chemiluminescence was measured immediately using infinite® 200 PRO – Tecan microplate reader. The measurements were performed in triplicates.

COMT assay (for hydrophilic substrate-dopamine)

The assay is performed with manufacturer specifications. In brief, the assay solution consists of 1 mM SAM in 100 µL of 20 mM tracepure HCl mixed with 100 µL of 10 mM $MgCl_2$ in tracepure water and 100 µL of 5 mM dithiothreitol in tracepure water and 200 µL of 0.5 M Tris buffer (pH 8.0 at 37° C). The substrate (10 mM dopamine) is added in 200 µL tracepure water. 100 µL of this assay solution were mixed with 100 µL freshly prepared COMT-solution (10units) in 1 percent BSA (bovine serum albumin) and incubated at 37° C for 1 hr. Afterwards, 100 µL of HCl conc. were added and the mixture was cooled on ice for 5mins, centrifuged and the supernatant was analysed with analytical HPLC.

COMT assay (for hydrophobic substrate).

The assay solution consists of 100 µL of 10 mM $MgCl_2$ in tracepure water and 100 µL of 5 mM dithiothreitol in tracepure water and 500 µL of 0.5 M Tris buffer (pH 8.0 at 37° C). 100 µL of this assay solution were mixed with 10 µL Tween20 and 20 µL of 14.6 mM SAM (300nmol). 3 µL (300nmol) of the substrate (100mM NOD or F-NOD in EtOH) is added and finally 100 µL freshly prepared COMT-solution (75units) in 1 percent BSA (bovine serum albumin) is added. The assay mixture is incubated at 37° C for 2–4h. Afterwards, the mixture was cooled on ice for 5mins, centrifuged and the supernatant was extracted 3× with $CHCl_3$. The organic solvent is removed in vacuum and the residue is dissolved in 1:1 MeCN/water and analysed with analytical HPLC.

Cell uptake assay

Cells were incubated with ~450 kBq [^{18}F]**5** per well on a six-well plate for different time points at 37° C under normal atmosphere. Therefore, 9.11 MBq [^{18}F] compound **5** was added to 20 mL cell medium, mixed and 1 mL from that solution was added to every well containing cells. After incubation, the supernatant was collected, the cells were washed three times with 1 mL PBS and the third washing solution was collected and finally 50 µL lysis buffer was added to the cells and cells were scratched from the bottom of the well and collected for gamma counting.

Animal experiments and data analysis

Lewis rats (LEW/Crl, Charles River Laboratories, Sulzfeld, Germany), aged 10 weeks and with a weight of 270–280 g, were employed for the initial PET experiments. The rats were anesthetized by isoflurane (2–2.5 percent delivered at 3.5L/min) and a catheter was implanted in the V. femoralis for administration of the radiotracer. First experiments were set-up as terminal experiments in order to assess the biodistribution after injection of different doses of [^{18}F]F-NOD (4.8, 5.9 and 13.2 MBq, in 0.9 percent NaCl solution, 150 µL, respectively).

All experiments were performed in compliance with the National Guidelines for Animal Protection, Germany, and the approval of the animal care committee. Small-animal PET experiments were conducted on the Albira PET System (Bruker Biospin MRI GmbH, Ettlingen, Germany). On injection of the radiotracer a 120-min dynamic scan was initiated. The protocol comprised 31 frames (10× 60, 10× 120, 5× 300, and 6× 600 sec). Reconstruction was performed using maximum likelihood expectation maximization (MLEM) algorithm with a matrix size of 20×20 and a pixel size of 0.5 mm (12 iterations) with the Albira Suite Reconstructor (Bruker Biospin MRI GmbH, Ettlingen, Germany) with the data output in kBq/cc. For data analysis volumes of interests (VOI) were drawn in PMOD (version 3.608) to quantify the injected dose (PMOD Technologies Ltd, Zurich, Switzerland).

Materials

(*E*)-1-Fluoro-4,5-dimethoxy-2-(2-nitrovinyl)benzene (2). 3,4-Dimethoxy-2-fluorobenzaldehyde (**1**, 552 mg, 3.00 mmol) and ammonium acetate (58 mg, 0.75 mmol) were dissolved in nitromethane (5 mL) and the mixture was stirred at 80° C for 6 h. After cooling to room temperature (r. t.) excess nitromethane was removed and substituted with Et_2O. This solution was washed with water (2× 10 mL), dried with $MgSO_4$ and the yellow product (555 mg, 81 percent) was crystallized from a solution of Et_2O/petroleum ether (PE) 1:1. The purity of **2** was>97 percent and the product was used without further purification. R_F=0.47 (Et_2O:PE 1:1). ^{1}H NMR (500 MHz, $CDCl_3$): δ=8.04 (d, $^3J_{H,H}$=13.7Hz, 1H,-HC=CH-NO_2), 7.64 (d, $^3J_{H,H}$=13.7Hz, 1H,-HC=CH-NO_2), 6.87 (d, $^4J_{H,F}$=6.7Hz, 1H, H-6), 6.71 (d, $^3J_{H,F}$=11.7Hz, 1H,

H-3), 3.93 (s, 3H, 4-OCH_3), 3.90ppm (s, 3H, 5-OCH_3). ^{13}C NMR (126 MHz, $CDCl_3$): δ=157.6 (d, $^1J_{C,F}$=251.9Hz, C-1), 153.7 (d, $^3J_{C,F}$=10.5Hz, C-4), 146.0 (d, $^4J_{C,F}$=2.2Hz, C-5), 137.1 (d, $^3J_{C,F}$=10.5Hz, C-3), 132.6 (d, $^5J_{C,F}$=1.0Hz, C=C-NO_2), 111.1 (d, $^4J_{C,F}$=4.4Hz, C=C-NO_2), 100.5 (d, $^2J_{C,F}$=27.9Hz, C-6), 56.5ppm (2xOCH_3). ^{19}F NMR (282 MHz, $CDCl_3$): δ=-114.6ppm. MS (MALDI-TOF): *m/z* (percent) 228 (30) $[M+H]^+$, 250 (30) $[M+Na]^+$. See Figure 1 for NMR signal assignment.

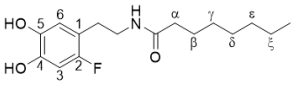

Figure 1. F-NOD **7** as an example for NMR signal assignment.

2-(2-Fluoro-4,5-dimethoxyphenyl)ethan-1-amine (3). To a solution of **2** (2.43 g, 10.69 mmol) in anhydrous THF (40 mL) under an N_2 atmosphere a fresh solution of $LiAlH_4$ (1.02 g, 26.9 mmol) in THF (40 mL) was slowly added at 0° C. The mixture was stirred for 15min and the reaction was quenched with ice-cold water. THF was removed under reduced pressure at 30° C, brine was added and the aqueous phase was extracted with ethyl acetate (EA) (3× 50 mL). The organic phase was dried with $MgSO_4$, concentrated and the crude product **3** was obtained as yellow oil (2.11 g, 99 percent). R_F=0.16 (EE). ^{1}H NMR (300 MHz, $CDCl_3$): δ=6.68 (d, $^4J_{H,F}$=7.1Hz, 1H, H-6), 6.61 (d, $^3J_{H,F}$=11.0Hz, 1H, H-3), 3.85 (s, 3H, 5-OCH_3), 3.84 (s, 3H, 4-OCH_3), 2.98 (t, ^3J=6.1Hz, 2H, NCH_2), 2.77 (t, ^3J=6.9Hz, 2H, CCH_2), 2.33ppm (br s, 2H, NH_2). ^{13}C NMR (75 MHz, $CDCl_3$): δ=155.2 (d, $^1J_{C,F}$=237.8Hz, C-1), 148.4 (d, $^3J_{C,F}$=9.9Hz, C-4), 145.1 (d, $^4J_{C,F}$=2.6Hz, C-5), 116.2 (d, $^2J_{C,F}$=17.5Hz, C-1), 113.3 (d, $^3J_{C,F}$=6.5Hz, C-6), 100.2 (d, $^2J_{C,F}$=28.5Hz, C-3), 56.5 (OCH_3), 56.1 (OCH_3), 42.0 (NCH_2), 31.9ppm (CCH_2). MS (MALDI-TOF): *m/z* (percent) 223 (100) $[M+Na]^+$.

***N*-(2-Fluoro-4,5-dimethoxyphenethyl)octanamide (4).** To a solution of **3** (2.07 g, 10.40 mmol) in CH_2Cl_2 (20 mL), a solution of octanoyl chloride (1.6 mL, 9.36 mmol) in CH_2Cl_2 (25 mL) was slowly added at 0° C. To the resulting dark orange suspension Et_3N (2.2 mL, 15.6 mmol) was added and the mixture was stirred for 15min at 0° C. The resulting pale yellow solution was washed with water and brine and dried with $MgSO_4$. The solvent was removed and the crude product was purified by column chromatography (PE → PE:EA 10:1 → 5:1 → 4:1 → 1:1) to obtain compound **4** as pale yellow solid (1.41 g, 42 percent). R_F=0.33 (PE:EA 1:2). Hot petroleum ether was used for recrystallization of **4**. ^{1}H NMR (500 MHz, DMSO-d_6): δ=6.66 (t, $^4J_{H,F}$=7.1Hz, 1H, H-6), 6.61 (d, $^3J_{H,F}$=11.0Hz, 1H, H-3), 5.49 (s, 1H, NH), 3.85 (s, 3H, OCH_3), 3.84 (s, 3H, OCH_3), 3.48 (dt, $^3J_{H,H}$=6.8Hz, $^3J_{NH,H}$=6.1Hz, 2H, NCH_2), 2.79 (t, ^3J=6.9Hz, 2H, CCH_2), 2.13 (t, ^3J=7.6Hz, 2H, H-α), 1.62–1.56 (m, 2H, H-β), 1.31–1.23 (m, 8H, H-ɣ,δ,ε,ζ), 0.89–0.86ppm (m, 3H, CH_3). ^{13}C NMR (126 MHz, DMSO-d_6): δ=173.2 (C=O), 155.1 (d, $^1J_{C,F}$=237.7Hz, C-2), 148.4 (d, $^3J_{C,F}$=9.9Hz, C-4), 145.2 (d, $^4J_{C,F}$=2.7Hz, C-5), 116.1 (d, $^2J_{C,F}$=17.4Hz, C-1), 113.0 (d, $^3J_{C,F}$=6.4Hz, C-6), 100.1 (d, $^2J_{C,F}$=28.5Hz, C-3), 56.4 (OCH_3), 56.4

(OCH_3), 39.7 (NCH_2), 36.9 (C-α) 31.7 (C-ε), 29.2 (C-γ), 29.0 (C-δ), 28.8 ($C\underline{C}H_2$), 25.7 (C-β), 22.6 (C-ζ), 14.1ppm (CH_3). ^{19}F NMR (282MHz, $CDCl_3$): δ=-126.1ppm. MS (MALDI-TOF): *m/z* (percent) 326 (100) $[M+H]^+$. Analytical HPLC: t_R=4.54min.

***N*-(2-Fluoro-4,5-dihydroxyphenethyl)octanamide (5).** To a solution of **4** (734 mg, 2.26 mmol) in CH_2Cl_2 (100 mL), a solution of BBr_3 (11.3 mL, 11.3mmol, 1M) in CH_2Cl_2 was slowly added at-12° C within 5min. The mixture was stirred for 135min at-10° C and was allowed to reach r. t. for 60min. Water (30 mL) was added for quenching the reaction and the mixture was extracted with CH_2Cl_2 (1x) and EA (2x). The combined organic phases were dried with $MgSO_4$, concentrated under reduced pressure and the crude product was purified by column chromatography (PE → PE:EA 1:1) to obtain compound **5** as pale yellow solid (602mg, 90 percent). R_F=0.44 (PE:EA 1:3), 0.85 (methanol). ^{1}H NMR (300 MHz, DMSO-d_6): δ=9.09 (s, 1H, OH), 8.72 (s, 1H, OH), 7.81 (t, ^3J=5.7Hz, 1H, NH), 6.54 (d, $^4J_{H,F}$=7.8Hz, 1H, H-6), 6.48 (d, $^3J_{H,F}$=10.9Hz, 1H, H-3), 3.18–3.11 (m, 2H, NCH_2), 2.52 (t, ^3J=7.3Hz, 2H, CCH_2), 2.01 (t, ^3J=7.2Hz, 2H, H-α), 1.48–1.43 (m, 2H, H-β), 1.27–1.23 (m, 8H, H-γ,δ,ε,ζ), 0.88–0.83ppm (m, 3H, CH_3). ^{13}C NMR (75 MHz, DMSO-d_6): δ=171.9 (C=O), 153.3 (d, $^1J_{C,F}$=233.2Hz, C-2), 144.2 (d, $^3J_{C,F}$=11.2Hz, C-4), 141.3 (d, $^4J_{C,F}$=2.3Hz, C-5), 116.5 (d, $^3J_{C,F}$=6.0Hz, C-6), 115.0 (d, $^2J_{C,F}$=17.2Hz, C-1), 102.8 (d, $^2J_{C,F}$=26.4Hz, C-3), 39.0 (NCH_2), 35.3 (C-α) 31.1 (C-ε), 28.5 (C-γ), 28.4 (C-δ), 28.1 ($C\underline{C}H_2$), 25.2 (C-β), 22.0 (C-ζ), 13.9ppm (CH_3). ^{19}F NMR (282 MHz, DMSO-d_6): δ=-129.7ppm. MS (MALDI-TOF): *m/z* (percent) 298 (100) $[M+H]^+$. Analytical HPLC: t_R=3.96min.

4-(2-Aminoethyl)-5-nitrobenzene-1,2-diol (8). 6-Nitrodopamine compound **8** was prepared according to the literature.[26] In brief, to a solution of dopamine hydrochloride (1.50g, 7.91mmol) in water (45 mL) at 0° C $NaNO_2$ (1.89g, 27.39mmol) was added and the mixture was stirred for 15min. To the pale yellow solution an ice-cold solution of 20 percent H_2SO_4 (3.5 mL) was slowly added. The yellow product starts to precipitate from the brown solution. The product was filtered, washed with cold water and methanol and dried with high vacuum to obtain compound **8** as yellow solid (1.21g, 77 percent). NMR and MS analyses were consistent with the literature.[26]

4-Nitro-5-(2-octanamidoethyl)-1,2-phenylene dioctanoate (9). To a solution of compound **8** (500 mg, 2.52 mmol) in CH_2Cl_2 (10 mL), a solution of octanoyl chloride (1.19 mL, 6.98mmol) in CH_2Cl_2 (3 mL) was slowly added at 0° C. Et_3N (1.23 mL, 8.82mmol) was added and the mixture was stirred at r. t. for 16h. CH_2Cl_2 was removed and the residue was redissolved in EA (20 mL) and washed with brine. The organic phase was dried with Na_2SO_4, concentrated under reduced pressure and the crude product was purified by column chromatography (PE → PE:EA 5:1 → 3:1) to obtain compound **9** as pale yellow solid (431mg, 33 percent). R_F=0.59 (PE:EA 1:1). Hot acetonitrile was used for recrystallization of compound **9**. ^{1}H NMR (500 MHz, $CDCl_3$): *δ*=7.89 (s, 1H, H-3), 7.21 (s, 1H, H-6), 5.79 (s, 1H, NH), 3.61–3.57 (dt, $^3J_{H,H}$=6.8Hz, $^3J_{NH,H}$=6.4Hz, 2H, NCH_2), 3.12 (t, ^3J=6.8Hz, 2H, CCH_2), 2.55 (t, ^3J=7.5Hz, 2H, 2-O(CO)CH_2), 2.54 (t, ^3J=7.5Hz, 2H, 1-O(CO)CH_2), 2.17 (t, ^3J=7.7Hz, 2H, N(CO)CH_2), 1.70–1.63 (m, 4H, O(CO)$CH_2C\underline{H}_2$), 1.56–1.50 (m, 2H, N(CO)$CH_2C\underline{H}_2$), 1.44–1.22 (m, 24H, 3xH-γ,δ,ε,ζ), 0.92–0.85ppm (m, 9H, 3xCH_3). ^{13}C NMR (126 MHz, $CDCl_3$): δ=173.7 (NC=O), 170.5 (2-OC=O), 170.2 (1-OC=O), 146.0 (C-1), 145.8 (C-2), 140.9 (C-4), 133.2 (C-5),

127.5 (C-6), 120.9 (C-3), 39.7 (NCH_2), 36.6 (N-C-α), 34.0 (2-O-C-α), 33.9 (1-O-C-α), 32.8 (CCH_2), 31.7 (N-C-ε), 31.6 (2xO-C-ε), 29.0 (6xC-ɣ,δ), 25.6 (N-C-β), 24.8 (2xO-C-β), 22.6 (3xC-ζ), 14.0ppm (3xCH_3). MS (MALDI-TOF): *m/z* (percent) 577 (60) $[M+H]^+$. Analytical HPLC: t_R=7.75min.

***N*-(4,5-Dihydroxy-2-nitrophenethyl)octanamide (10).** Compound **9** (150 mg, 0.26 mmol) was dissolved in acetonitrile (25 mL) at 30° C. The mixture was cooled to 0° C and a solution of 0.1M NaOH (2.6 mL, 0.26 mmol) was added dropwise. The mixture was then stirred for 4 h at 50° C. Water was added and the mixture was extracted with EA (2x). The organic phase was dried with $MgSO_4$, concentrated under reduced pressure and the crude product was purified by column chromatography (PE → PE:EA 1:1) to obtain compound **10** as yellow solid (83 mg, 99 percent). R_F=0.20 (PE:EA 1:1). ^{1}H NMR (500 MHz, DMSO-d_6): δ=10.33 (s, 1H, OH), 9.81 (s, 1H, OH), 7.84 (t, ^3J=5.7Hz, 1H, NH), 7.48 (s, 1H, H-6), 6.68 (s, 1H, H-3), 3.27–3.23 (m, 2H, NCH_2), 2.88 (t, ^3J=7.1Hz, 2H, CCH_2), 1.99 (t, ^3J=7.5Hz, 2H, H-α), 1.47–1.41 (m, 2H, H-β), 1.28–1.17 (m, 8H, H-ɣ,δ,ε,ζ), 0.87–0.84ppm (m, 3H, CH_3). ^{13}C NMR (126 MHz, DMSO-d_6): δ=171.9 (C=O), 151.7 (C-5), 143.9 (C-4), 139.0 (C-2), 128.1 (C-1), 118.1 (C-6), 111.9 (C-3), 39.7 (NCH_2), 35.3 (C-α) 32.8 (C-ε), 31.0 (CCH_2), 28.5 (C-ɣ), 28.3 (C-δ), 25.1 (C-β), 22.0 (C-ζ), 13.8ppm (CH_3). MS (MALDI-TOF): *m/z* (percent) 325 (100) $[M+H]^+$. Analytical HPLC: t_R=4.06min.

***N*-(4-Hydroxy-3-methoxyphenethyl)octanamide (12).** 3-Methoxytyramine (3-MT) (50mg, 0.25 mmol) was mixed with octanoic acid (40 µL, 0.25mmol) and BOP (110mg, 0.25mmol) in 2 mL anhydrous THF. The solution was cooled to 0° C and Et_3N (105 µL, 0.75mmol) dissolved in 400 µL THF was added dropwise within 15min. The reaction was allowed to stir at r. t. for 16h. THF was substituted with 10 mL Et_2O and the organic phase was washed 3× with HCl (3 mL, 1 M), 2× with $NaHCO_3$-solution (5 mL, 1 M) and 2× with brine (5 mL). The organic phase was dried with $MgSO_4$ and the product was recrystallized in Et_2O/hexane to obtain a pale yellow solid (70 mg, 95 percent). R_F=0.30 (PE:EE 1:2). ^{1}H NMR (500 MHz, $CDCl_3$): *δ*=6.85 (d, ^3J=7.9Hz, 1H, H-2), 6.71–6.66 (m, 2H, H-5,6), 5.50 (s, 1H, NH), 3.88 (s, 3H, OCH_3), 3.49 (t, ^3J=6.8Hz, 2H, NCH_2), 2.74 (t, ^3J=6.9Hz, 2H, CCH_2), 2.21 (d, ^3J=2.9Hz, 1H, OH), 2.13 (t, ^3J=7.6Hz, 2H, $(CO)CH_2$), 1.63–1.54 (m, 2H, $N(CO)CH_2CH_2$), 1.32–1.22 (m, 8H, H-ɣ,δ,ε,ζ), 0.89–0.86ppm (m, 3H, CH_3). ^{13}C NMR (126 MHz, $CDCl_3$): δ=173.1 (NC=O), 146.6 (C-3), 144.3 (C-4), 140.9 (C-1), 121.3 (C-6), 114.4 (C-5), 111.1 (C-2), 55.9 (OCH_3), 40.6 (NCH_2), 36.9 (CCH_2), 35.4 (C-α), 31.7 (N-C-ε), 29.2 (C-ɣ), 29.0 (C-δ), 25.8 (C-β), 22.6 (C-ζ), 14.1ppm (CH_3). MS (MALDI-TOF): *m/z* (percent) 294 (70) $[M+H]^+$. Analytical HPLC: t_R=6.13min (0–8min: 0–50 percent MeCN).

Radiochemistry

***N*-(2-[^{18}F]Fluoro-4,5-dihydroxyphenethyl)octanamide[^{18}F]5.** No-carrier-added aqueous [^{18}F]fluoride (3.43GBq) was trapped on a Waters QMA cartridge, which was preconditioned with 1M $NaHCO_3$ (5 mL) and tracepure H_2O (10 mL). [^{18}F]Fluoride was eluted with a freshly prepared Kryptofix®-solution (12.5mg K2.2.2, 800 µL MeCN, 200 µL tracepur H_2O, 10 µL 1M K_2CO_3) into the reaction vessel and dried via azeotropic distillation with

a gentle stream of helium (2 mL/min) at 100° C for 4min at 600mbar, followed by addition of anhydrous acetonitrile (2 × 0.8 mL;3min at 600mBar) and 4min at full vacuum. Afterwards, compound **10** (1.5mg, 4.62 µMol) dissolved in anhydrous DMSO (500 µL) was added, and the reaction mixture was stirred at 120° C for 30min. Water (15 mL) was added, the solution was passed through a SepPak® tC_{18} plus light cartridge (145 mg sorbent, preconditioned with 5 mL Et_2O), the cartridge was washed with water (10 mL, cartridge kept wet) followed by elution of [^{18}F]**5** with diethylether (3 mL, the first yellow 1.1 mL were discarded until the eluted fraction was colourless). The solvent was evaporated at 80° C at 900mbar in a gentle stream of helium for 4–5min to afford 880MBq (RCY=45 percent, d.c.) [^{18}F]**5** with a RCP>99 percent within approx. 90min and a specific activity=28±6GBq/µMol (n=5). Radio-HPLC: t_R=4.07min. Radio-TLC: R_F=0.85 (methanol). For injection purposes, [^{18}F]**5** is redissolved in a suitable amount (0.4 – 1.0 mL) of 0.9 percent NaCl solution for injection+0.9 percent EtOH and purified by a sterile filter (0.22 µM) with a final pH 7.57±0.3.

Results and discussion

Synthesis of F-NOD

F-NOD was synthesized from 3,4-dimethoxy-2-fluorobenzaldehyde compound **1** as outlined in Scheme 1. It was successfully converted to the β-nitrostyrene derivative compound **2** by the method of Milhazes et al.[27] To this end, nitromethane was used as solvent and ammonium acetate as base for generation of compound **2** (yield>81 percent), which was subsequently reduced with $LiAlH_4$ to the corresponding amine **3**. This was followed by introduction of an octanoyl group at the primary amine using octanoyl chloride in excess and selective removal of both methoxy groups with 5 eq. BBr_3 at-12° C [28].

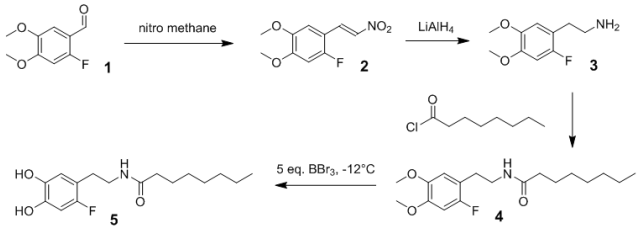

Scheme 1. Synthesis pathway of the non-radioactive reference compound **5.**

In vitro studies with F-NOD and NOD

Several *in vitro* studies were conducted to test if F-NOD compound **5** displayed similar relevant biological properties as NOD compound **7**, i.e. inhibition of TNFα mediated vascular cell adhesion molecule 1 (VCAM-1) expression, induction of HO-1, redox activity [29, 30] and the ability to activate TRPV1. [31] At higher concentrations both NOD **7** and F-NOD compound **5** inhibited VCAM-1 expression almost to a similar extent, while at low concentrations F-NOD compound **5** seemed to be less effective. This was more pronounced for induction of HO-1 (Figure 2A). We have previously demonstrated that the redox activity of NOD compound **7** is crucial for its ability to inhibit VCAM-1 expression.[32] In essence this redox activity is provided by the ortho dihydroxy moiety on the benzene structure. Since these functional groups are also present in F-NOD compound **5**, this largely explains its ability to inhibit VCAM-1 expression and induce HO-1. We made use of peroxidase based luminol reaction, to assess if a difference existed in redox activity of the compounds Dose response experiments revealed highly significant effects of concentration ($F(15,559)=194.42$, $p<0.001$; two-way ANOVA, fixed effects) as well as of substance $F(1,559)=26.78$, $p<0.001$. Although both NOD **7** and F-NOD **5** were able to completely quench chemiluminescence, for NOD **7** (EC_{50} : 12.12 **µM**) it was achieved at lower concentration as compared to F-NOD compound **5** (EC_{50} : 32.6 µM) (Figure 2B Interaction: $F(15,559)=5.98$, $p<0.001$ two-way ANOVA, fixed effects). This suggests a small difference in redox activity between both compounds and might explain why F-NOD **5** is less efficiently inhibiting VCAM-1 and inducing HO-1 expression at low concentrations. In agreement with their redox activity it was found that both compounds were able to protect endothelial cells against cold inflicted injury (Figure S1).

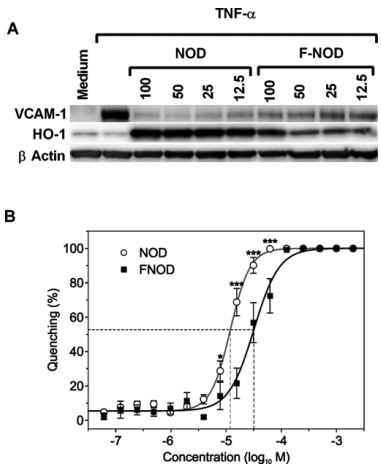

Figure 2. *In vitro F*-NOD **5** shows similar biological activities as NOD **7**: (A) Influence of F-NOD and NOD on TNFα mediated VCAM-1 expression and induction of HO-1. Cells were stimulated overnight with TNFα 10ng/mL in the presence of different concentrations of F-NOD **5** or NOD (0–100 µM). Cell lysates were prepared and 15 µg of total protein was loaded on a 10 percent SDS PAGE. The gel was blotted and stained for VCAM-1 and HO-1. Equal loading of protein was confirmed with ß-Actin. Note that at higher concentrations inhibition of VCAM-1 and induction of HO-1 are comparable but not at lower concentrations to NOD in terms of its anti-inflammatory properties. (B) Redox activity of NOD and F-NOD: F-NOD **5** similar to NOD **7** was able to quench the luminol assay. Serial dilutions of NOD **7** or F-NOD **5** were added to 100 **µL** of reaction mixture containing 0.005U of horseradish peroxidase (HRP), 2.5 mM luminol and 0.9 mM p-Coumaric acid. Chemiluminescence was measured directly after addition of 0.03 percent H_2O_2. The ability to quench peroxidase mediated chemiluminescence was tested and results are expressed as relative to the control to which neither NOD nor F-NOD was added along with ± SEM of all measurements. For each concentration and for each compound at least 3 independent measurements were performed. EC_{50} of NOD **7** was determined to be 12.12 **µM** and EC_{50} of F-NOD **5** 32.60 **µM** indicated by dashed lines, $^{*}p<0.05$, $^{***}p<0.001$ ANOVA with LSD post-hoc test.

The TRPV1 activating properties were assessed in a heterologous cell assay. F-NOD compound **5** like NOD compound **7** was able to activate TRPV1 (Figure 3A). Dose response experiments revealed highly significant effects of concentration ($F_{(11,137)=}17.86$, $p<0.001$; two-way ANOVA, fixed effects) as well as of substance ($F_{(1,137)=}12.38$, $p<0.001$). Thus, both substances were able to activate TRPV1 in a concentration dependent manner but NOD ($EC_{50=}7.10$ µM [-5.15±0.08]) was much more effective as compared to F-NOD ($EC_{50=}45.94$ µM [-4.34±0.12]) (Figure 3B).

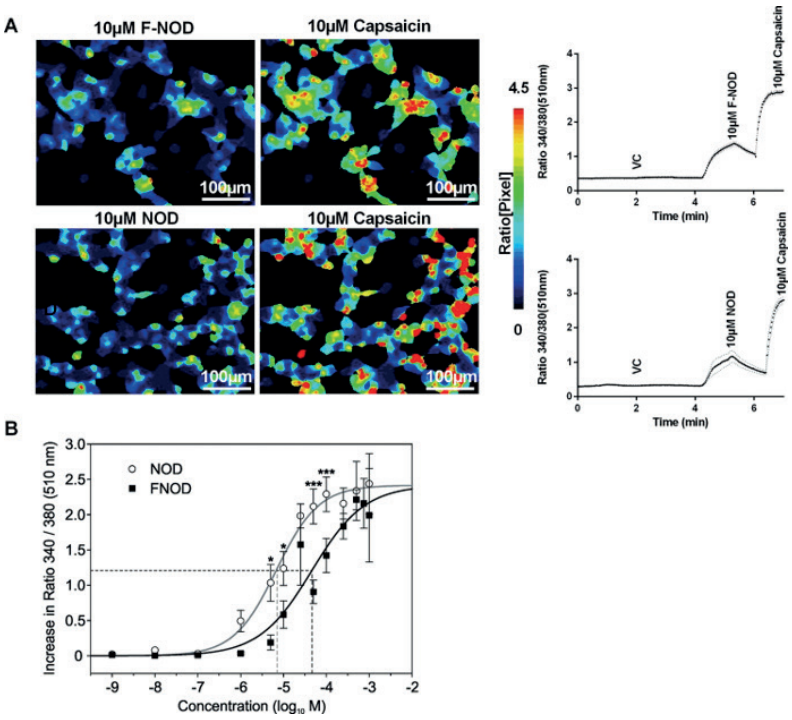

Figure 3. TRPV1 activation by F-NOD and NOD: (A) Representative images of a calcium imaging experiment using rTRPV1 transfected HEK293 cells (Left panel). The ratio 340/380 at 510nm – a measure proportional to free intracellular calcium – is false colour coded where warmer colours indicate increasing calcium values. Average time course traces are shown on the right panel. Cells were first either stimulated with 10 **µM** NOD compound 7 or 10 **µM** of F-NOD compound 5, followed by 10 **µM** capsaicin to select rTRPV1 transfected cells and to see maximum response after washing away of the first substance; (B) rTRPV1 transfected HEK293 cells were stimulated with different concentrations of NOD compound 7 or F-NOD compound 5: For each concentration and for each compound at least 3 independent measurements were performed. The results are expressed as average ratio 340/380 at 510nm ± SEM of all measurements (n=3 to 13). EC50 of F-NOD compound 5 was determined to be 45.94 **µM** and EC50 of NOD compound 7 7.10 **µM**; EC_{50} values (NOD **7**: 7.10 µM and F-NOD **5**: 45.94 µM) indicated by dashed lines, *p<0.05, ***p<0.001 ANOVA with LSD post-hoc test.

It was further investigated, whether F-NOD also interacted with TRPV1 binding pocket in similar fashion as NOD via computational molecular modelling. No differences in putative interactions with amino acids inside the TRPV1 binding pocket were found between NOD compound **7** and F-NOD compound **5** (Figure S2). The 6-fold increase in EC_{50} value of F-NOD for TRPV1 activation could be explained by the insertion of fluorine as substituent in the aromatic ring. Fluorine might exert an inductive (-I) effect, thereby reducing the negative charge density in the aromatic ring, which in turn may influence the ability of F-NOD to access the TRPV1 binding site [33].

Radiochemistry

For radiolabelling purposes we initially tried to synthesize the precursor **10** by introduction of a nitro group into NOD **7** (Scheme 2). Although synthesis of NOD compound **7** was successful [34], the subsequent nitration step to generate precursor compound **10** failed under various conditions.[26, 35–37] This was most likely due to the acidic conditions during the nitration, which caused hydrolysis of the octanoyl group yielding only small amounts (<10 percent) of nitro dopamine **8**. Therefore precursor compound **10** was synthesized from 5-nitrified dopamine compound **8**, which was subsequently reacted with an excess of octanoyl chloride in order to maximize the yield of compound **9** (Scheme 2). The *O*-octanoyl groups of compound **9** were removed selectively by NaOH.

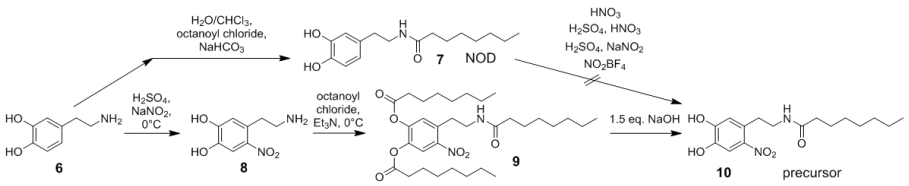

Scheme 2. Synthesis pathway of precursor **10.**

The optimization procedure for radiolabelling of precursor compound **10** (0.5–1.8 mg) was performed at 20–120°C in CH_3CN, DMF or DMSO (0.5–1.0 mL) for 20–60 minutes, respectively, using [^{18}F]KF/K2.2.2/K_2CO_3 (Table 1). Scheme 3 depicts the best radiolabelling conditions, which were obtained with 1.5 mg compound **10** in 0.5 mL DMSO for 30min reaction time at 120° C (radiochemical yield (RCY)=45 percent (decay corrected – d.c.) (Figure 4A); specific activity 21.9–34.5GBq/µMol for [^{18}F]F-NOD [^{18}F]**5**). Purification was performed by tC_{18} light cartridges resulting in a radiochemical purity (RCP)>99 percent and absolute amount of activity of 880MBq after 90min (starting from 3.43 GBq [^{18}F]fluoride) (Figure 4B). The identity of the product was checked by comparison of retention times on HPLC and TLC with that of the reference compound **5**.

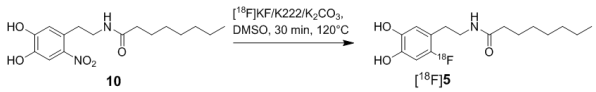

Scheme 3. Radiosynthesis scheme of radiotracer [18F]F-NOD [18F]**5**.

Radiolabelling with acetonitrile as solvent resulted in a comparable RCY (38 percent, d.c.) but under formation of a more lipophilic side product (>29 percent). Removal of this side product was only possible by semi-preparative HPLC which ended in prolonged overall synthesis time and lower product activity. Radiolabelling utilizing DMF resulted in much lower RCY (6 percent, d. c.) (Table 1).

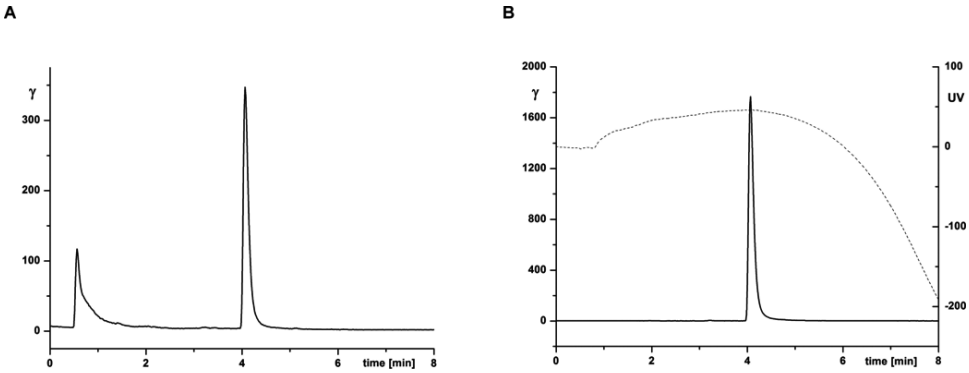

Figure 4. Synthesis and purification of [18F]F-NOD: (A) Representative chromatogram of the radiolabelling reaction and 18F-incorporation (t_R=0.65min) into [18F]F-NOD (t_R=4.07min) after 30min at 120° C in DMSO; (B) Representative chromatogram of the purity of [18F]F-NOD (t_R=4.07min) after purification with SepPak light cartridge: γ-trace (thick line) is depicting the radiochemical purity>99 percent, UV-trace at 210**nm** (dashed line) is depicting the chemical purity>96 percent.

Table 1. Optimization of the radiolabelling of precursor 10 reaction time, temperature, solvent and concentration of precursor.

amount of 10 [mg]	solvent	volume [mL]	temperature [° C]	labelling time [min]	RCY [percent]*	RCP [percent] of crude [^{18}F]**5**
1.5	MeCN	0.5	20	30	10	25
1.5	MeCN	0.5	100	10	19	42
1.8	MeCN	0.5	100	40	18	55
1.8	MeCN	1.0	100	60	38	61
1.5	DMF	0.5	100	40	6	65
0.5	DMSO	0.5	110	40	16	83
1.5	DMSO	0.5	100	40	33	58
1.5	DMSO	0.5	120	40	45	69

*Unless otherwise stated RCYs are all corrected for decay

Lipophilicity and in vitro stability tests of [18F]F-NOD

The lipophilicity of a pharmacologically active compound is a fundamental physicochemical parameter. Hence, logP/logD determinations are of utmost importance and relevance to evaluate structure-activity relationships in medicinal chemistry as well as in radio pharmacy.[38] The lipophilicity (logD) of [^{18}F] compound **5** was determined at pH 7.5 to be 3.35 ± ± 0.04 (n=3) using PBS and *n*-octanol according to the shake-flask method (OECD guideline).[39] Next, the stability of [^{18}F] compound **5** was elaborated *in vitro*. To this end, a solution of [^{18}F]**5** in PBS/3 percent EtOH (100 µL) was incubated with rat plasma (200 µL) and shaken for at least 120min at 37° C. Radio-TLC as well as radio-HPLC analyses were performed after 30, 60 and 120min, respectively, and showed no decomposition or radiodefluorination of [^{18}F]**5** (RCP≥98 percent) in the supernatant fraction, which showed a recovery rate of [^{18}F] compound **5** of 77–85 percent after precipitation of the incubation solution (100 µL) with acetonitrile (100 µL) at 0° C. The precipitate contained 15–23 percent of the remained activity.

Cell uptake and stability studies

Cell uptake studies were performed with HUVECs to assess to what extent [^{18}F] compound **5** is taken-up by the cells, and if so whether it is further metabolized. As depicted in Figure 5A [^{18}F] compound **5** cell associated activity was approximately 0.14–0.21 percent of the applied dose (ID) after 120 minutes of incubation at 37° C. HPLC analysis of the cell lysate extracts revealed only one radioactive peak at t_R=4.07min, corresponding to the intact [^{18}F] compound **5**, indicating that [^{18}F] compound **5** was not metabolized intracellularly within the time-frame of the experiment.

In order to investigate the stability of [^{18}F] compound **5** in more detail, a catechol *O*-methyl transferase [40] (COMT) assay was performed [41] to assess if [^{18}F]**5** is a genuine substrate for COMT. COMT is a ubiquity intracellular enzyme which deactivates catechols by addition of a methyl group to one of the hydroxyl groups.[42] The assay was optimized using dopamine as gold standard, which is converted to 3-methoxythyramine (3-MT) compound (**11**) (Scheme 4).

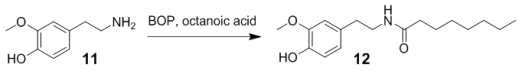

Scheme 4. Synthesis for *O*-methylated metabolite compound **12** of NOD in COMT assay.

Because of the high lipophilicity of both NOD and F-NOD, 10 µL of Tween20 was added and higher concentrations of the methyl donor *S*-adenosyl-L-methionine (SAM) and COMT were used with elongated reaction times (120–240min) in order to allow the formation of 3-MNOD compound **12** and $(OMe)_2$-F-NOD compound **4**. Figure 5 displays the HPLC chromatograms of combined injections of different NOD and F-NOD derivatives (Figures 5 B,D) and the performed COMT assay (Figures 5 C,E) at different time points.

The conversion to the methylated derivatives proceeded slower in comparison to dopamine which was totally converted to 3-MT after 120 minutes using low concentration of SAM and COMT. Methylation of NOD and F-NOD occurred at both hydroxy groups resulting in double methylated derivatives. The rate of conversion to the methylated derivatives of F-NOD was slightly faster in comparison to NOD (see chromatograms C and E at 180 minutes in Figure 5). This might be explained by the strong negative inductive effect of the fluorine.

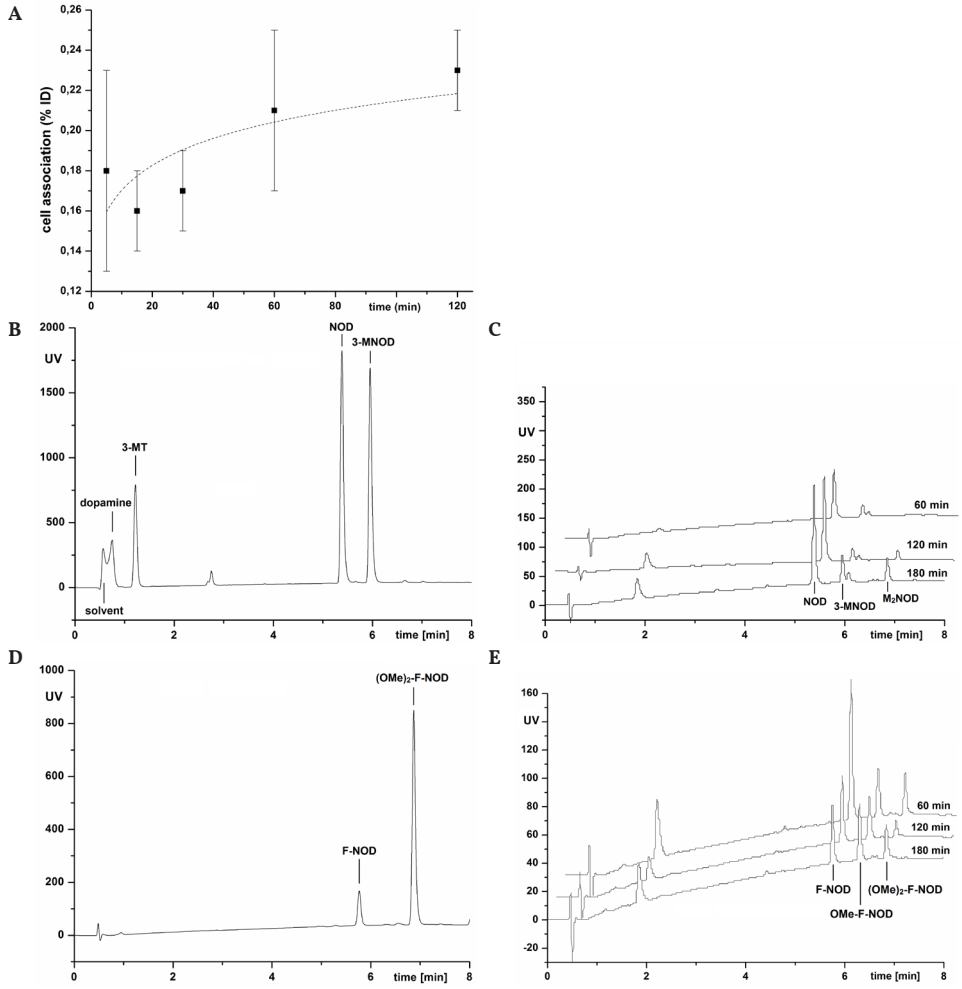

Figure 5. (A) Uptake of [18F]**5** by endothelial cells over a period of 120 min at 37° C (values represent means ± SD of three independent experiments); Representative chromatograms of: (B) NOD and its derivatives; (C) COMT assay for NOD, indicating a new more lipophilic peak (16 percent) at the same retention time like 3 - O - methoxy N - octanoyl dopamine compound **12**; (D) F - NOD and its derivative; (E) COMT assay for F - NOD; HPLC condition: 0 – 50 percent MeCN + 0.1 percent TFA within 8 minutes.

In vivo evaluation of [18F]5

For assessment of the elimination kinetics of [^{18}F] compound **5** in three Lewis rats different amounts of activity (4.8, 5.9 and 13.2 MBq) were injected to find the optimal dose for PET imaging (13.2MBq). Elimination of [^{18}F] compound **5** was characterized by a fast

blood clearance and substantial renal and hepatobiliary elimination (Figure 6A) comparable with lipophilic radiotracers.[43, 44] The activity is flowing through the kidneys without higher accumulation of activity within 5–10 minutes (SUV_{bw}=8±5g/mL) which was subsequently reallocated from the renal pelvis into the bladder within 30min. Most of the injected activity accumulated in the liver after 8min (SUV_{bw}=21±10g/mL) possibly because of the lipophilic nature of [^{18}F] compound **5**. It seems that in the liver might be substantial oxidative defluorination [45] of [^{18}F]**5** by rat specific dehalogenase [46, 47] as reflected by a gradual accumulation of activity in bones starting at 60 minutes. After 120 minutes most of the activity was found in the bladder (SUV_{bw}=38.5 g/mL) and bones (SUV_{bw}=9.8g/mL). Time-activity curves of different organs are illustrated in Figure 6B. The activity remains at a certain level (SUV_{bw}=8g/mL) within the renal pelvis and slowly eliminates into the bladder after 30 minutes. The liver activity is higher but also shows a faster elimination then the renal pelvis with no formation of a plateau.

A

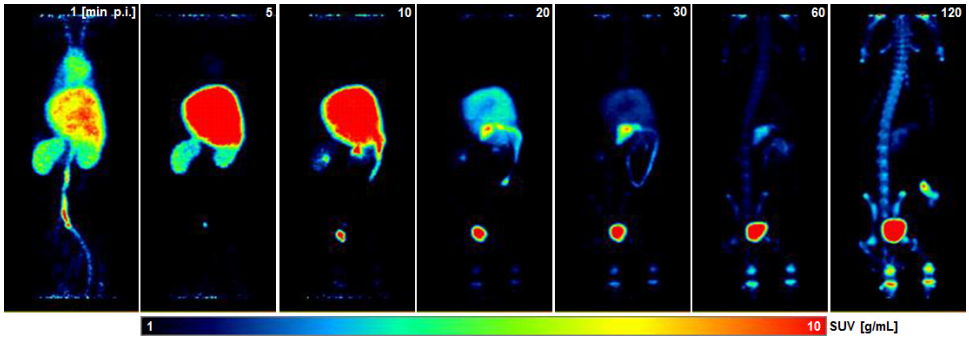

B

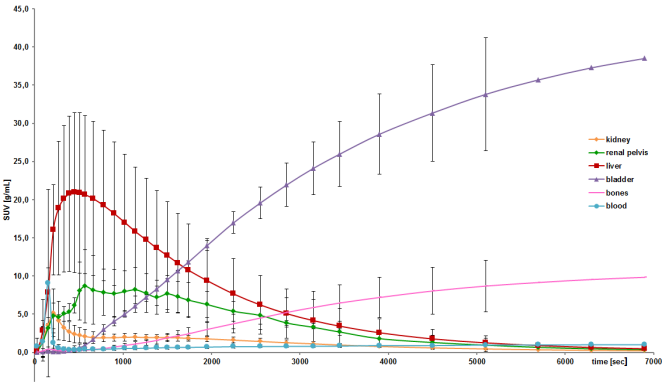

Figure 6. (A) PET images (MIP - maximal intensity projection) of Lewis rat with injected 13.2 MBq [18F]**5**; (B) Distribution of [18F]**5** within 120 min (n=3). Most of activity accumulates in liver. Some of the activity remains at a certain level inside the renal pelvis for 30 min.

Conclusion

In summary, we compared the *in vitro* behavior of F-NOD compound **5** with NOD compound **7** in various assays in order to prove, whether F-NOD compound **5** could act as an analogue to NOD compound **7**. The results of F-NOD compared to NOD were similar at induction of HO-1, redoxactivity, TRPV1 activation and EC_{50}. NOD and F-NOD are both substrates for COMT. At both derivatives *O*-methylation takes place but in comparison to dopamine, NOD and F-NOD have a higher stability. This might be due to the higher lipophilicity of compound **5** and compound **7**, which hinders the *O*-methylation by the enzyme. These data suggested that the radiolabelled [^{18}F]F-NOD could act as a tool for further determination of the behaviour of NOD. *In vitro* cell assay with [^{18}F]F-NOD at HUVECs revealed low cell association (0.14–0.21 percent), which means that there is no active transport mechanism into the cell. The cell experiment suggests, that the concentration of NOD must be at least 500× higher in order to get a 1× concentration inside the cell after 2 h.

The *in vivo* experiments reveal a fast renal and hepatobiliary clearance of [^{18}F] F-NOD. Since the concentration of the radiotracer is very low, the metabolism of such small doses can be faster in comparison to a higher concentration of non-radioactive NOD. Due to the fast clearance it is recommended to use a high concentration of NOD as bolus injection or semi-high in continuous injection in order to reach a renoprotective level in the kidneys for transplantation purposes.

In conclusion, we herein report on the fast and facile radiofluorination of the NOD-derivative [^{18}F]F-NOD [^{18}F] compound **5** for *in vivo* assessment of NOD's elimination kinetics by means of PET imaging. We demonstrated that F-NOD **5** and NOD **7** behave similar in different *in vitro* assays and that both are substrates for COMT. [^{18}F] compound **5** was synthesized with reproducible high radiochemical yield and purity (>98 percent) as well as high specific activities (>20 GBq/µMol). After a synthesis time of approximately 90 minutes, the radiotracer was ready for injection. Stability tests show no decomposition of [^{18}F]**5** over a period of 120 minutes in rat plasma. Fast blood clearance and a predominant Elimination by liver and kidneys was found for [^{18}F] compound **5** *in vivo*. Although these data suggest that also NOD might be subjected to a fast clearance, further pharmacokinetic evaluation is warranted. However, [^{18}F] compound **5** is useful for studying pharmacokinetics via biodistribution for period up to 30 minutes, due to the fast renal and hepatobiliary elimination and degradation *in vivo* between 30–60min. [^{18}F]**5** might not be suitable for elongated pharmacokinetics and biodistribution studies in rodents as it likely underlies oxidative defluorination after 60min.

Conflict of Interests

The authors declare no conflicts of interest.

Ethical Statement

Umbilical cords for isolation of were Human umbilical vein endothelial cells (HUVECs) were received from donors in the Department of Obstetrics and Gynaecology, University Medical Center Mannheim, Heidelberg University, Heidelberg, Germany. This was approved by local ethics committee (Medizinische Ethikkommission II der Medizinischen Fakultät Mannheim) and all donors gave their written informed consent (Ethic Application No. 2015–518N-MA).

Author Contributions

The manuscript was written through contributions of all authors. All authors have given approval to the final version of the manuscript. ‡These authors contributed equally. *These authors are sharing correspondence.

Acknowledgment

The excellent technical assistance of Ms. Anne-Maria Suhr in the animal experiments and of Ms. Handan Moerz in calcium imaging experiments is gratefully acknowledged. We would like to thank Tobias Timmermann for measuring the NMR spectra and Uwe Seibold for measuring the MALDI-MS. The funding „Perspektivförderung des Ministeriums für Wissenschaft und Kunst Baden-Württemberg“ is gratefully acknowledged.

References

1. Schnuelle, P., et al., *Effects of donor pretreatment with dopamine on graft function after kidney transplantation.* J. Am. Med. Assoc., 2009. **302**(10): p. 1067–1075.
2. Benck, U., et al., *Effects of donor pre-treatment with dopamine on survival after heart transplantation: a cohort study of heart transplant recipients nested in a randomized controlled multicenter trial.* J. Am. Coll. Cardiol. , 2011. **58**(17): p. 1768–1777.
3. Lösel, R.M., et al., *N-octanoyl dopamine, a non-hemodyanic dopamine derivative, for cell protection during hypothermic organ preservation.* PLoS ONE, 2010. **5**(3): p. e9713.
4. Hoeger, S., et al., *Dopamine treatment in brain-dead rats mediates anti-inflammatory effects: the role of hemodynamic stabilization and D-receptor stimulation.* Transplant Int., 2007. **20**(9): p. 790–799.
5. Hoeger, S., et al., *Donor dopamine treatment in brain dead rats is associated with an improvement in renal function early after transplantation and a reduction in renal inflammation.* Transplant Int., 2008. **21**(11): p. 1072–1080.
6. Kassmann, M., et al., *Transient receptor potential vanilloid 1 (TRPV1), TRPV4, and the kidney.* Acta Physiol., 2013. **207**(3): p. 546–564.
7. Yard, B., et al., *Prevention of cold-preservation injury of cultured endothelial cells by catecholamines and related compounds.* Am. J. Transplant., 2004. **4**(1): p. 22–30.
8. Vettel, C., et al., *Dopamine and lipophilic derivates protect cardiomyocytes against cold preservation injury.* J. Pharmacol. Exp. Ther. , 2014. **348**(1): p. 77–85.
9. Berger, S.P., et al., *Dopamine induces the expression of heme oxygenase-1 by human endothelial cells in vitro.* Kidney Int., 2000. **58**(6): p. 2314–2319.
10. Beck, G., et al., *Clinical review: immunomodulatory effects of dopamine in general inflammation.* Crit. Care, 2004. **8**(6): p. 485–491.
11. Kapper, S., et al., *Modulation of chemokine production and expression of adhesion molecules in renal tubular epithelial and endothelial cells by catecholamines.* Transplantation, 2002. **74**(2): p. 253–260.
12. van der Heyden, M.A., T.J. Wijnhoven, and T. Opthof, *Molecular aspects of adrenergic modulation of cardiac L-type Ca2+channels.* . Cardiovasc. Res., 2005. **65**(1): p. 28–39.
13. Mann, D.L., et al., *Adrenergic effects on the biology of the adult mammalian cardiocyte.* Circulation, 1992. **82**: p. 790–804.
14. Halestrap, A.P., et al., *Elucidating the molecular mechanism of the permeability transition pore and its role in reperfusion injury of the heart.* Biochim. Biophys. Acta, 1998. **1366**(1–2): p. 79–94.
15. Leung, A.W. and A.P. Halestrap, *Recent progress in elucidating the molecular mechanism of the mitochondrial permeability transition pore.* Biochim. Biophys. Acta, 2008. **1777**(7–8): p. 946–952.
16. Roy, N., et al., *Dopamine induces postischemic cardiomyocyte apoptosis in vivo: an effect ameliorated by propofol.* Ann. Thorac. Surg., 2006. **82**(6): p. 2192–2199.
17. Nixon, J.L., et al., *Impact of high-dose inotropic donor support on early myocardial necrosis and outcomes in cardiac transplantation.* Clin. Transplant., 2012. **26**(2): p. 322–327.
18. Shashoua, V.E. and G.W. Hesse, *N-docosahexaenoyl, 3-hydroxytyramine: A dopaminergic compound that penetrates the blood-brain barrier and suppresses appetite.* Life Sci., 1996. **58**(16): p. 1347–1357.
19. Liu, Z., et al., *Donor dopamine pretreatment inhibits tubulitis in renal allografts subjected to prolonged cold preservation.* Transplantation, 2007. **83**(3): p. 297–303.

20. Tsagogiorgas, C., et al., *N-octanoyl-dopamine is an agonist at the capsaicin receptor TRPV1 and mitigates ischemia-induced acute kidney injury in rat.* PLoS ONE, 2012. **7**(8): p. e43525.
21. Waikar, S.S., K.D. Liu, and G.M. Chertow, *Diagnosis, epidemiology, and outcomes of acute kidney injury.* Clin. J. Am. Soc. Nephrol., 2008. **3**: p. 844–861.
22. Westaway, S.M., *The potential of transient receptor potential vanilloid type 1 channel modulators for the treatment of pain.* J. Med. Chem., 2007. **50**: p. 2589–2596.
23. Klotz, S., et al., *N-octanoyl dopamine treatment exerts renoprotective properties in acute kidney injury but not in renal allograft recipients.* Nephrol. Dial. Transplant., 2015. **31**: p. 564–573.
24. Spindler, R.S., et al., *N-Octanoyl Dopamine for Donor Treatment in a Brain-death Model of Kidney and Heart Transplantation.* Transplantation, 2015. **99**(5): p. 935–41.
25. Grynkiewicz, G., M. Poenie, and R.Y. Tsien, *A new generation of Ca^{2+} indicators with greatly improved fluorescence properties*.* J. Biol. Chem., 1985. **260**(6): p. 3440–3450.
26. Napolitano, A., et al., *A new oxidation pathway of the neurotoxin 6-aminodopamine. Isolation and characterisation of a dimer with a tetrahydro[3,4a]iminoethanophenoxazine ring system.* Tetrahedron, 1992. **48**(39): p. 8515–8522.
27. Milhazes, N., et al., *Synthesis and cytotoxic profile of 3,4-methylenedioxymethamphetamine ("Ecstasy") and its metabolites on undifferentiated PC12 cells: a putative structure-toxicity relationship.* Chem. Res. Toxicol., 2006. **19**: p. 1294–1304.
28. Punna, S., S. Meunier, and M.G. Finn, *A hierarchy of aryloxide deprotection by boron tribromide.* Org. Lett., 2004. **6**(16): p. 2777–2779.
29. Stratford, M.R., P.A. Riley, and C.A. Ramsden, *Rapid halogen substitution and dibenzodioxin formation during tyrosinase-catalyzed oxidation of 4-halocatechols.* Chem. Res. Toxicol., 2011. **24**(3): p. 350–356.
30. Li, J., et al., *Emerging disinfection byproducts, halobenzoquinones: Effects of isomeric structure and halogen substitution on cytotoxicity, formation of reactive oxygen species, and genotoxicity.* Environ. Sci. Technol., 2016. **50**(13): p. 6744–6752.
31. Darré, L. and C. Domene, *Binding of capsaicin to the TRPV1 ion channel.* Mol. Pharm., 2015. **12**(12): p. 4454–4465.
32. Hottenrott, M.C., et al., *N-octanoyl dopamine inhibits the expression of a subset of kB regulated genes: potential role of p65 Ser276 phosphorylation.* PLoS ONE, 2013. **8**(9): p. e73122.
33. Gillis, E.P., et al., *Applications of fluorine in medicinal chemistry.* J. Med. Chem., 2015. **58**(21): p. 8315–8359.
34. Wang, B., et al., *Highly efficient synthesis of capsaicin analogues by condensation of vanillylamine and acyl chlorides in a biphase $H_2O/CHCl_3$ system.* Tetrahedron, 2009. **65**(27): p. 5409–5412.
35. Uchida, M., et al., *Orally active factor Xa inhibitors: investigation of a novel series of 3-amidinophenylsulfonamide derivatives using an amidoxime prodrug strategy.* Bioorg. Med. Chem. Lett., 2008. **18**(16): p. 4682–4687.
36. Kolasa, T. and M.J. Miller, *Synthesis of the chromophore of pseudobactin, a fluorescent siderophore from Pseudomonas.* J. Org. Chem., 1990. **55**: p. 4246–4255.
37. Lee, J.E., et al., *A novel bicyclic hexapeptide, RA-XVIII, from Rubia cordifolia: structure, semi-synthesis, and cytotoxicity.* Bioorg. Med. Chem. Lett., 2008. **18**(2): p. 808–811.

38. Wilson, A.A., et al., *An admonition when measuring the lipophilicity of radiotracers using counting techniques.* Appl. Radiat. Isot., 2001. **54**: p. 203–208.
39. Schaffler, K., et al., *An oral TRPV1 antagonist attenuates laser radiant-heat-evoked potentials and pain ratings from UV(B)-inflamed and normal skin.* Br J Clin Pharmacol, 2013. **75**(2): p. 404–14.
40. Zajac, D., et al., *Metabolism of N-acetylated-dopamine.* PLoS ONE, 2014. **9**(1): p. e85259.
41. Smit, N., et al., *O-Methylation of L-dopa in melanin metabolism and the presence of catechol-O-methyltransferase in melanocytes.* Pigm. Cell Res., 1994. **7**: p. 403–408.
42. Kiss, L.E. and P. Soares-da-Silva, *Medicinal chemistry of catechol O-methyltransferase (COMT) inhibitors and their therapeutic utility.* J. Med. Chem., 2014. **57**(21): p. 8692–8717.
43. Tu, Z., et al., *Synthesis and evaluation of 15-(4-(2-[^{18}F]fluoroethoxy)phenyl)pentadecanoic acid: A potential PET tracer for studying myocardial fatty acid metabolism.* Bioconjugate Chem., 2010. **21**: p. 2313–2319.
44. Hendricks, J.A., et al., *In vivo PET imaging of histone deacetylases by ^{18}F-suberoylanilide hydroxamic acid (^{18}F-SAHA).* J. Med. Chem., 2011. **54**(15): p. 5576–5582.
45. Morgan, P., et al., *Oxidative dehalogenation of 2-fluoro-17a-ethynyloestradiol in vivo.* Biochem. Pharmacol., 1992. **44**(9): p. 1717–1724.
46. Choi, J.Y., et al., *Effective microPET imaging of brain 5-HT(1A) receptors in rats with [^{18}F]MeFWAY by suppression of radioligand defluorination.* Synapse, 2012. **66**(12): p. 1015–1023.
47. Rietjens, I.M.C.M., et al., *Reaction pathways for biodehalogenation of fluorinated anilines.* Eur. J. Biochem., 1990. **194**: p. 945–954.

Chapter 6

N-octanoyl dopamine treatment of endothelial cells induces the unfolded protein response and results in hypo metabolism and tolerance to hypothermia

(Public Library of Science. 2014 Jun 13;9(6):e99298)

Eleni Stamellou, Johann Fontana, Johannes Wedel, Emmanouil Ntasis, Carsten Sticht, Anja Becker, **Prama Pallavi,** Kerstin Wolf, Bernhard K Krämer, Mathias Hafner, Willem J. van Son, Benito A. Yard

Abstract

N-acyl dopamines (NAD) are gaining attention in the field of inflammatory and neurological disorders. Due to their hydrophobicity, NADD may have access to the endoplasmic reticulum (ER). We therefore investigated if NAD induce the unfolded protein response (UPR) and if this in turn influences cell behaviour.

Genome wide gene expression profiling, confirmatory qPCR and reporter assays were employed on human umbilical vein endothelial cells (HUVEC) to validate induction of UPR target genes and UPR sensor activation by *N*-octanoyl dopamine (NOD). Intracellular ATP, apoptosis and induction of thermo tolerance were used as functional parameters to assess adaptation of HUVEC.

NOD, but not dopamine dose dependently induces the UPR. This was also found for other synthetic NAD. Induction of the UPR was dependent on the redox activity of NADD and was not caused by selective activation of a particular UPR sensor. UPR induction did not result in cell apoptosis, yet NOD strongly impaired cell proliferation by attenuation of cells in the S-G2/M phase. Long-term treatment of HUVEC with low NOD concentration showed decreased intracellular ATP concentration paralleled with activation of AMPK. These cells were significantly more resistant to cold inflicted injury.

We provide for the first time evidence that NAD induce the UPR *in vitro*. It remains to be assessed if UPR induction is causally associated with hypometabolism and thermotolerance. Further pharmacokinetic studies are warranted to address if the NAD concentrations used *in vitro* can be obtained in vivo and if this in turn shows therapeutic efficacy.

Introduction

The endoplasmic reticulum (ER) can be considered as the gatekeeper for protein synthesis, assuring appropriate protein folding and maturation of secreted and transmembrane proteins. These functions are highly regulated and require checkpoint for allowing that only correctly folded proteins can leave the ER. Whenever the folding capacity of the ER is too low to meet the cellular demand for newly synthesized proteins, unfolded or misfolded proteins start to accumulate in the ER, which in turn, triggers a set of responses known as the unfolded protein response (UPR) [1–4].The function of the UPR can be divided into two major objectives, i.e. restoration of ER homeostasis and secondly induction of apoptosis if the first objective fails. The UPR accomplishes its function by increasing the expression of chaperone proteins to assist in protein folding, transient inhibition of mRNA translation to decrease protein influx into the ER, increasing ER associated degradation to remove misfolded proteins and induction of apoptotic genes to eliminate cells that are beyond repair.

The UPR consist of three different branches, each of which containing a specific transmembrane ER sensor protein that, upon activation, sets a series of responses in motion resulting in the transcription of typical UPR target genes [3, 4]. These so called UPR sensor proteins are the inositol requiring kinase 1 (IRE1), double-stranded RNA-activated protein kinase (PKR)-like ER kinase (PERK) and activating transcription factor 6 (ATF6)[1–3], all of which are associated with the ER chaperone glucose-regulated protein BiP. If misfolded proteins accumulate, BiP dissociates from the ER sensors, leading to their activation [1–3, 5]. UPR sensor activation is characterized by cleavage of X-box-binding protein 1 (Xbp1) mRNA (IRE1), phosphorylation of the translation initiation factor 2 α subunit (eIF2α) (PERK) and processing of ATF6 in the Golgi apparatus[6–12].The UPR has been implicated in a variety of diseases including cancer, metabolic, neurodegenerative and inflammatory disease [13]. In addition it might be an integral part of the protective strategies used by hibernating mammals for long term survival in a state of cold torpor[14]. Signalling components of the UPR are emerging as potential targets for intervention and treatment of human disease[15].

Long chain polyunsaturated fatty acids are able to form conjugates with amines, e.g. ethanolamine, serotonin or dopamine. Since these conjugates can influence a variety of biological systems, they are gaining increased attention as promising new leads in the field of inflammatory and neurological disorders and for other pharmacological applications[16]. Endogenous *N*-acyl dopamines (NAD), e.g. *N*-arachidonoyl-, *N*-oleoyl-, *N*-palmitoyl-and *N*-stearoyl-dopamine are present in brain tissue and are known to modulate the endocannaboid system. It has also been reported that NAD are able to activate transient receptor potential (TRP) vanilloid subfamily member 1 (TRPV1) [16, 17]. We recently described *N*-octanoyl-dopamine (NOD), a short synthetic NAD, as a potent

protective compound in acute kidney injury [18]. In addition it prevents hypothermic preservation injury[19, 20] strongly inhibits platelet function [21] and impairs NFκB activation [22]. Yet, it should be underscored that its increased hydrophobicity, as compared to dopamine, may allow NOD to cross intracellular membranes much easier where it may severely change the redox milieu within subcellular compartments [19]. Changes in redox milieu are either caused by donation of reduction equivalents as a consequence of quinone formation or by the iron chelating properties of the catechol structure[23]. In keeping with the importance of redox homeostasis in the ER for oxidative protein folding [24, 25], the present study was conducted to assess if synthetic *N*-acyl dopamine derivatives are able to activate the UPR. In addition we sought to identify the structural entities within NOD that might be important for UPR activation. To this end we made use of synthetic NAD that were either changed at the aromatic ring or in the aliphatic chain. We also sought to address if activation of the UPR by NOD compromises cell viability or if it represents a protective response, allowing cells to adapt to more aggravating conditions such as hypothermic preservation.

Materials and Methods

Reagents

Reagents were obtained from the sources as indicated: endothelial cell culture medium (Provitro, Berlin, Germany), PBS, trypsin solution, ethanol (GIBCO, Invitrogen, NY, USA), FBS Gold (PAA laboratories GmbH, Pasching, Austria), Actinomycin D, β-mercaptoethanol, tunicamycin, ethidium bromide, EDTA solution, DMSO, Tween 20, phospahatase inhibitor cocktail 2, Igepal 10 percent, collagenase, HEPES, Triton X-100, DTT, sodium deoxycholate, Tris-base, ammonium persulphate, SDS, TEMED, glycine, MTT, hexadimethrine bromide, acrylamid 40 percent, gelatine (Sigma-Aldrich, Taufkirchen, Germany), bovine serum albumin (SERVA, Heidelberg, Germany), protease inhibitor cocktail, first strand cDNA synthesis Kit (Roche Diagnostic, Mannheim, Germany), Dual-Glo Luciferase Assay System (Promega, Mannheim, Germany), Coomassie protein assay reagent (Pierce, Rockford, IL, USA), Trizol (Invitrogen, Carlsbad, CA, USA), chloroform, isopropanol, tetrahydrofuran, (Merck, Darmstadt, Germany), anti-eIF2α, anti-phospho-eIF2α (Cell Signalling, Boston, USA), anti-β-actin (Sigma, Taufkirchen, Germany), Proteostat PDI assay kit (Enzo, Lörrach, Germany), Cignal Lenti ERSE/ATF6/positive control Reporter (luc) kit (Qiagen, Düsseldorf, Germany). Chemiluminescence reagent was purchased from PerkinElmer LAS Inc. (Boston, MA, USA). Primers and all reagents were purchased for TaqMan PCR (ABI, Darmstadt, Germany). Secondary antibodies conjugated with horseradish peroxidase, anti-CHOP and anti-phospho-AMPK were purchased from Santa Cruz Biotechnology (Heidelberg, Germany).

Cell culture

Human umbilical vein endothelial cells (HUVECs) were purchased from Promo Cell, Heidelberg, Germany and cultured in basal endothelial medium supplemented with 10 percent fetal bovine serum (FBS), essential growth factors and antibiotics. Cultures were maintained at 37° C, 5 percent CO_2 humidified atmosphere and experiments were conducted on cells in passage 2–6 at approximately 80–90 percent confluence.

Synthesis of N-acyl dopamines (NAD)

N-octanoyl dopamine (NOD), *N*-pivloyl dopamine (NPiD) and *N*-octanoyl tyramine (NOT) were synthesized from commercially available precursors as previously described [19]and purified by twofold recrystallization from dichloromethane as demonstrated by thin layer chromatography (TLC). Octanoic or pivalic acid were converted to their mixed anhydride derivate by reaction with ethyl chloroformate in the presence of *N*-ethyl diisopropylamine. The crude mixed anhydrides were incubated with dopamine hydrochloride (Sigma-Aldrich, Taufkirchen, Germany) in *N,N*-dimethylformamide and *N*-ethyl diisopropylamine to form NOD or NPiD. NOT was synthesized according to NOD using the analog mixed anhydride coupled to tyramine as reaction component. After aqueous preparation and evaporation of the organic solvent NOD in an overall yield of approximately 60 percent is obtained. The sample investigated by NMR (Bruker AC250) yielded spectra in accordance with the expected structure. Acetylation of NOD (A-NOD) was performed by suspending two grams of NOD in 5 mL acetic anhydride under magnetic stirring. When two drops of sulphuric acid were added, the suspension turned clear and stirring was continued for one hour. Diluted hydrochloric acid (5 mL) was added and 30 min later the reaction mixture was poured into 200 mL ice water. The precipitated product was collected by vacuum filtration and dried under vacuum to yield A-NOD, pure as judged by thin layer chromatography (TLC).

Gene expression profiling

Sample preparation and processing was performed according to the Affymetrix GeneChip Expression Analysis Manual (http://www.Affymetrix.com). Total RNA was isolated from HUVECs using Trizol-Reagent (Life Technologies, Inc., Rockville, MD, USA). DNase treatment was carried out, using RNase free DNase I (Ambion, Woodward, Austin, TX, USA). RNA concentration and quality were assessed by RNA 6000 nano assays on a Bioanalyser 2100 system (Agilent, Waldbronn, Germany). 5 µg of RNA was converted into cDNA using T7-(dT)24 primers and the SuperScript Choice system for cDNA synthesis (Life Technologies, Inc., Rockville, MD, USA). Biotin-labelled cDNA was prepared by *in vitro* transcription using the BioArray high yield RNA transcript labeling kit (Enzo Diagnostics, Farmingdale, NY, USA). The resulting cDNA was purified, fragmented and hybridized to

U133A gene chips (Affymetrix, Santa Clara, CA, USA). After hybridization the chips were stained with streptavidin–phycoerythrin (MoBiTec, Goettingen, Germany) and analysed on a GeneArray scanner (Hewlett Packard Corporation, Palo Alto, CA, USA).

Microarray processing and statistical analysis

Gene expression profiling was performed using arrays of HG_U133A 2.0-type from Affymetrix. A Custom CDF Version 13 with Entrez based gene definitions was used to annotate the arrays. The Raw fluorescence intensity values were normalized applying quantile normalization. Differential gene expression was analysed OneWay-ANOVA using a commercial software package SAS JMP7 Genomics, version 4, from SAS (SAS Institute, Cary, NC). A false positive rate of $\alpha=0.05$ with FDR correction was taken as the level of significance. The raw and normalized data are deposited in the Gene Expression Omnibus database (http://www.ncbi.nlm.nih.gov/geo/; accession No. GSE-56285).

RNA isolation, PCR and RNA stability

Total RNA was isolated as described above. 1 µg of total RNA was reverse-transcribed into cDNA using the 1st Strand cDNA Synthesis Kit. cDNA was diluted in 20 µL DEPC-treated water and stored at –20° C until use. qPCR was performed on a ABI-Prism 7700 sequence detection system using TaqMan universal PCR master mix AmpErase UNG (part no. 4324018). The following Taqman assays were used: BiP (part No. Hs00607129_gH), CHOP (part No. Hs00358796_g1), PDIA4 (part No. Hs00202612_m1), ERO1L (part No. Hs00205880_m1) and GAPDH (part No. Hs02758991_g1). Samples were run under the following conditions: initial denaturation for 10 min at 95° C followed by 40 cycles of 15 s at 95° C and 1 min at 60° C. The levels of gene expression in each sample were determined with the comparative cycle threshold method. PCR efficiency was assessed from the slopes of the standard curves and was found to be between 90 percent and 100 percent. Linearity of the assay could be demonstrated by serial dilution of all standards and cDNA. All samples were normalized for an equal expression of GAPDH. For RT-PCR 1 µL of cDNA was amplified in a 20 µL reaction mix containing 2.5 mmol·L–1 dNTPs, 25 pmol·L–1 of each primer, 0,125 units Taq polymerase and 0,5 mmol·L–1 MgCl2. The following primers were used: : GAPDH forward: 5′-GTC TTC ACC ACC ATG GAG AA-3′ and reserve: 5′-ATC CAC AGT CTT CTG GGT GG-3′, Xbp1 forward: 5′-CCT TGT AGT TGA GAA CCA GG-3′ and reverse 5′-GGG GCT TGG TAT ATA TGT GG-3′. The cycling conditions used for various primers were as follows: 4 min of denaturation at 94° C, followed by 30 (Xbp1) or 25 (GAPDH) cycles of amplification, each consisting of denaturation for 30 s at 94° C, annealing for 30 s at 58° C (Xbp1) and 55° C (GAPDH) and extension for 1 min at 72° C. In all experiments GAPDH was used as housekeeping gene, no differences were found for the conditions tested when β-actin was used. After the last amplification a final extension for 10 min at 72° C was performed for each reaction. PCR products were analyzed on a 4 percent NuSieve agarose gel containing ethidium bromide and run at 50 V for 6 h.

Lentiviral transduction and reporter assays

To evaluate activation of UPR pathways, cells were transfected with commercially available reporter constructs as ready-to use transducer lentiviral particles (Qiagen, Düsseldorf, Germany). One day before transduction cells were seeded in 96-well plates (10^4/well) and cultured overnight. Hereafter, the cells were transduced at an MOI of 5 using 8 percent polybrene. Five h after transduction 3 volumes of fresh cell growth medium was added and the cells were incubated overnight. Cell growth medium was replaced the next day and 24 h hereafter the cells were treated with NAD according to the specific experiment. Luciferase activity was evaluated by a commercially available luciferase assay system (Promega, Mannheim, Germany) according to the manufacturer's protocol.

Protein extraction and Western blot Analysis

HUVEC lysed in 20 mM Tris-HCl, 150 mM NaCl, 5 mM EDTA, 1 percent Triton X-100, 0.5 percent sodium deoxycholate, 1 µM dithiothreitol (DTT) buffer containing proteinase and phosphatase inhibitors. In some experiments, nuclear proteins were isolated as previously described [26]. Protein concentrations were measured using Coomassie-Reagent (Pierce, Rockford, USA). Samples (20 µg protein extract) were heated to 95° C for 5 minutes, loaded and separated on 10 percent SDS-polyacryamide gels followed by semi-dry blotting onto PVDF membranes (Roche, Mannheim, Germany). The membranes were incubated with 5 percent w/v non-fat dry milk or bovine serum albumin in TBS/Tween 0.5 percent to block unspecific background staining and hereafter incubated overnight at 4° C with the specific mono-or polyclonal eIf2α and p-eIf2α (Cell Signalling, Boston, USA), anti-CHOP and anti-pAMPK (Santa Cruz, Heidelberg, Germany). Subsequently, the membranes were thoroughly washed with TBS-Tween 0.1 percent and incubated with the appropriate horseradish peroxidise conjugated secondary antibody (Santa Cruz, Heidelberg, Germany), followed by five times wash in TBS/Tween 0.1 percent. Proteins were visualized using enhanced chemo luminescence technology, according to the manufacturer's instructions (Pierce, Rockford, IL). To confirm equal protein loading, membranes were stripped and re-probed with monoclonal anti-β-actin antibody (Sigma, Taufkirchen, Germany).

PDI activity assay

PDI activity was assessed in a test tube using a commercially available assay ProteoStat PDI assay kit (Enzo Life Sciences, Lörrach, Germany). The assay was performed as recommended by the manufacturer.

FACS analysis

Cell apoptosis and cell cycle analysis were assessed by FACS. For cell apoptosis HUVEC were stimulated with NOD (100 µM) or Tunicamycin (1 µg/mL) for 24 h followed by Annexin V/PI staining (Life Technologies, Darmstadt, Germany). For cell cycle analysis HUVEC were stimulated with NOD (100 µM) for 24 h. After stimulation the cells were harvested by trypsin, washed three times with phosphate-buffered saline (PBS), and stained for 15 min at room temperature with 5 µL of Annexin V–FITC and 10 µL of PI (5 µg/mL) in 1 binding buffer (10 mMHEPES, pH 7.4, 140 mM NaOH, 2.5 mM $CaCl_2$). For cell cycle analysis the cells were stained with DRAQ5 (Biostatus Lim., Shephsed, UK) at a final concentration of 10 µM according to the supplier's protocol. For all experiments cells were analyzed on a FACS Calibur flow cytometer (BD Biosciences, Heidelberg, Germany). At least 50,000 gated events were collected per sample and data were analysed by Flowjo software (Tree Star, Inc., Ashland, OR, USA).

Proliferation assay

HUVECs were seeded in multiple cell densities (2×10^3–8×10^3) in a 96-well plate and cultured in 100 µL of complete medium for 24 h. Hereafter cells were treated with different concentrations of NOD for 24 h and pulsed with 0.2 µCi of [6–3H] thymidine/well (Perkin Elmer, Groningen, The Netherlands) during the last 16 h of culture. All conditions were tested on six replicates culture wells. Incorporated ^{3}Hthymidine was assessed by scintillation counting in a liquid scintillation counter (LS 6500, Beckman Coulter, Krefeld, Germany).

Intracellular ATP measurement

Cells were cultured from passage 2 till passage 6 in the presence or absence of NOD (1 µM). At passage 6 the cells were seeded in 6-well plates and were cultured for additional 2 days. Hereafter cells were harvested by trypsin, counted and 500.000 cells pro condition were lysed in 200 µL of lysis buffer (100 mM Tris, 4 mM EDTA, pH 7.7). Lysates were collected and ATP concentrations were assessed directly hereafter using a commercially available ATP-driven luciferase assay according to the manufacturer's instruction (Roche Diagnostics, Mannheim, Germany). All experimental conditions were tested in triplicates in at least 3 different experiments.

LDH assay

Tolerance to hypothermia associated cell damage was assessed by lactate dehydrogenase (LDH) release. To this end, HUVEC were cultured from passage 2 till passage 6 in the presence or absence of NOD (1 µM). At passage 6 the cells were seeded in 24-well plates and

were cultured for additional 2 or 5 days in the absence of NOD. Shortly before subjecting the cells to cold storage the medium was changed to phenol red free and cells were stored for 24 h at 4° C. Cell damage was assessed by LDH release in the supernatant, according to manufacturer's instructions (Roche diagnostics, Mannheim, Germany). All experimental conditions were tested in triplicate in at least 3 different experiments.

Statistical analysis

All data are expressed as the means ± SD from at least three independent experiments. Statistical significance was assessed by one-way ANOVA (Dunnett's and Tukey test) and $p<0.05$ was considered to be significant.

Results

Induction of the UPR by NOD

To investigate if *N*-octanoyl dopamine (NOD) induces the UPR, we screened by genome wide gene expression profiling in HUVECs for genes that were up regulated by NOD. To this end, three different primary cultures of HUVECs were treated with 100 µM NOD for 24 h or left untreated. The results of the top 30 genes that showed up-regulation are depicted in Table 1. Thirteen out of these have been reported to be UPR target genes [3, 11, 27]. Up-regulation of the 5 most influenced UPR target genes was confirmed in independent experiments by qPCR (data not shown). The raw and normalized data are deposited in the Gene Expression Omnibus database (http://www.ncbi.nlm.nih.gov/geo/; accession No. GSE-56285).

To further substantiate our affymetrix findings and to confirm that NOD treatment induces the UPR we made use of a cis acting ER-stress response element (ERSE)-containing luciferase reporter construct. Luciferase expression increased upon NOD treatment in lentiviral transduced HUVEC in a dose-dependent fashion (Figure 1a). Since these cis acting elements are present in the promoter of BiP, we assessed the influence of NOD on BiP mRNA expression. In line with the ERSE reporter assay it was found that BiP mRNA transiently increased upon NOD treatment, with maximal expression occurring at 8 h of stimulation (Figure 1b).

NOD did not selectively activate one particular proximal UPR sensor as PERK, IRE1 and ATF6 were all transiently activated. Phosphorylation of eIF2α was in most experiments evident after 24 h of NOD treatment. In some experiments phosphorylation was also noted at 8 h, but was persistently absent at later time points (Figure 1c). Similarly, IRE1 and ATF6 were transiently activated upon NOD treatment. Xbp1 splicing (Figure 1d) and ATF6 induced luciferase expression (Figure 1e) were maximal at 4 and 8 h respectively, with decreasing tendency at later time points.

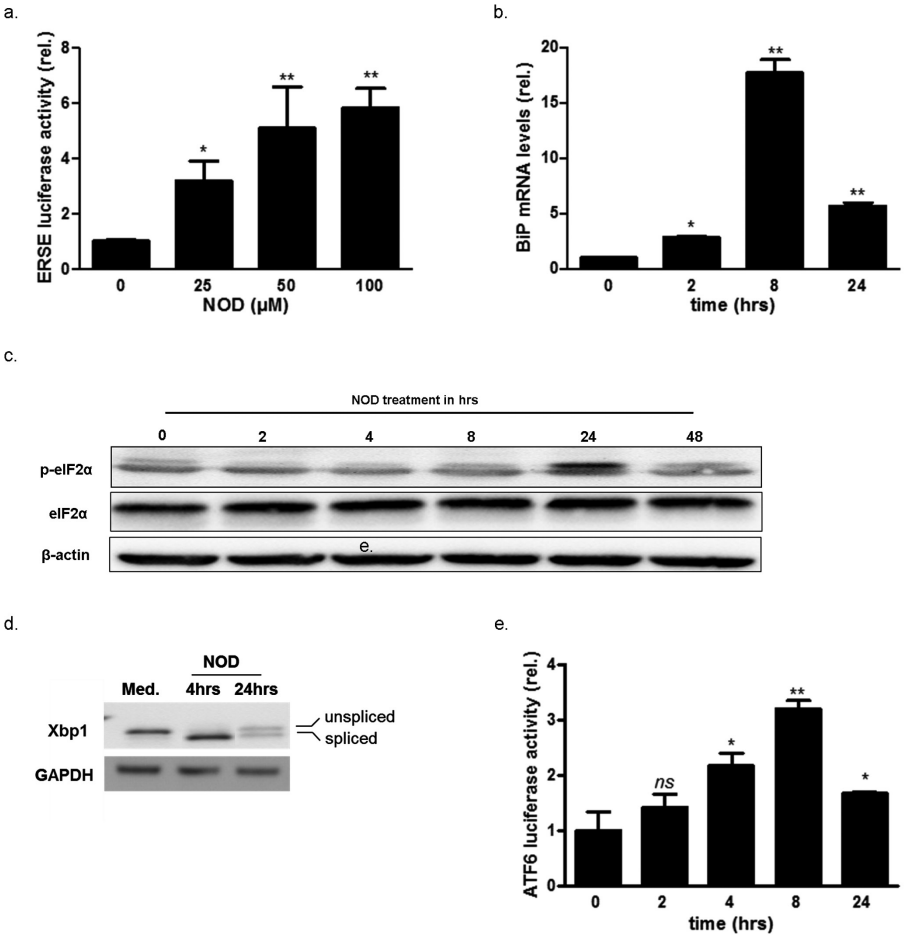

Figure 1. Induction of the UPR by NOD. (a) HUVECs were transduced by lentiviral particles containing either an ERSE-luciferase reporter or a luciferase construct under control of a CMV driven promoter as transduction efficiency control. The cells were stimulated for 8 h with 25 μM, 50 μM and 100 μM of NOD as indicated. Luciferase activity was assessed as described in materials and methods and normalized for constitutively expressed luciferase. The results are expressed as normalized ESRE luciferase activity relative to untreated (0 μM) cells. Values represent mean±SD from three independent experiments. *p<0.05, **P<0.01 vs. untreated control. (b) HUVECs were treated with 100 μM NOD for the indicated time periods. Total RNA was isolated and the expression of BiP and GAPDH was assessed by qPCR. The results are expressed as BiP mRNA levels, normalized for GAPDH and relative to cells that were not treated. *p<0.05, **p<0.01 vs. untreated control. (c) HUVECs were treated with 100 μM NOD for the indicated time periods. Hereafter protein extracts were made and phosphorylation of eIF2α was assessed by Western blotting. The blots were stripped and re-probed with antibodies directed against total eIF2α and β-actin to test for equal loading. The results of a representative blot are depicted, a total of 4 independent experiments were performed. (d) HUVECs were treated for 4 and 24 h with 100 μM of NOD

before total RNA was isolated. Cells that were not treated (Med.) served as control. Spliced and unspliced xbp-1 mRNA were detected by PCR. The spliced and unspliced amplification products differ by 26 bp. (e) Cells were transduced with lentiviral particle containing an ATF-6-driven luciferase reporter or a luciferase construct under control of a CMV driven promoter as transduction efficiency control. The cells were stimulated for different time periods with NOD 100 µM. Luciferase activity was assesses as described in materials and methods and normalized for constitutively expressed luciferase. The results are expressed as normalized ATF6 luciferase activity relative to time point 0. Values represent mean ± SD from three independent experiments. $^{**}p<0.01$, $^{*}p<0.05$ vs. untreated control, ns: no significant.

Table 1. Up-regulation of genes by NOD (NOD-treated vs. not treated cells).

Gene	Fold Change	p-value[a]
FAM129A	9.46	2.75
HMOX1	8.56	3.51
DNAJB9	8.22	3.97
SLC3A2	7.73	5.54
AKR1C1	7.37	2.25
DDIT3	6.69	3.89
IL13RA2	5.99	2.85
ASNS	5.68	2.39
HERPUD1	5.63	3.20
GDF15	5.26	3.21
SQSTM1	4.58	3.16
RRAGD	4.52	2.31
HYOU1	4.36	2.52
IL8	4.20	4.22
PDIA4	4.17	2.19
LBH	3.94	2.57
BLVRB	3.92	2.52
WARS	3.79	2.27
HSPA5	3.54	2.41
SDF2L1	3.46	3.17
TRIB3	3.44	2.64
P4HA2	3.38	3.39
MANF	3.27	2.83
SEL1L	3.24	2.31
CTNS	3.23	3.12
CCRL2	3.15	4.10
TM6SF1	3.08	2.48
DERL2	3.08	2.70

a: p-values for the comparison are given as log10 value. UPR target genes are depicted in bold.

Structural requirements of NOD for UPR induction

To assess the structural requirements for UPR induction by NOD we used NOD as lead compound and subsequently changed the functional groups at the aromatic ring or exchanged the octanoyl-for the more bulky pivaloyl moiety. The changes at the aromatic ring included, omission of one hydroxyl group (*N*-octanoyl tyramine (NOT) and acetylation of the hydroxyl-groups (A-NOD). While NOT has a significant lower redox activity compared to NOD, in A-NOD oxidation of the masked catechol structure can only occur intracellular. Moreover acetylation of the hydroxy groups makes the molecule more polar which may facilitate cellular uptake. The presence of the bulky pivaloyl moiety in *N*-pivaloyl dopamine (NPiD) makes the ester more resistant to hydrolysis [28] (Figure 2).

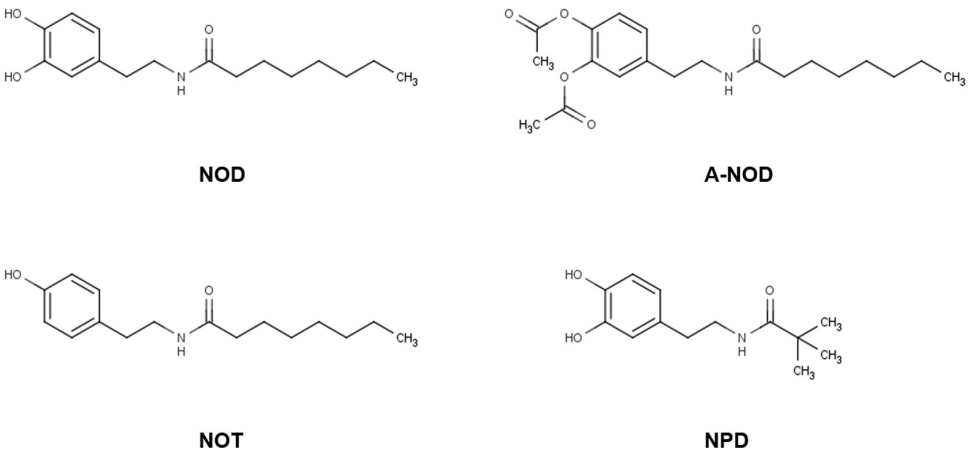

Figure 2. Molecular structure of NAD used in the study.

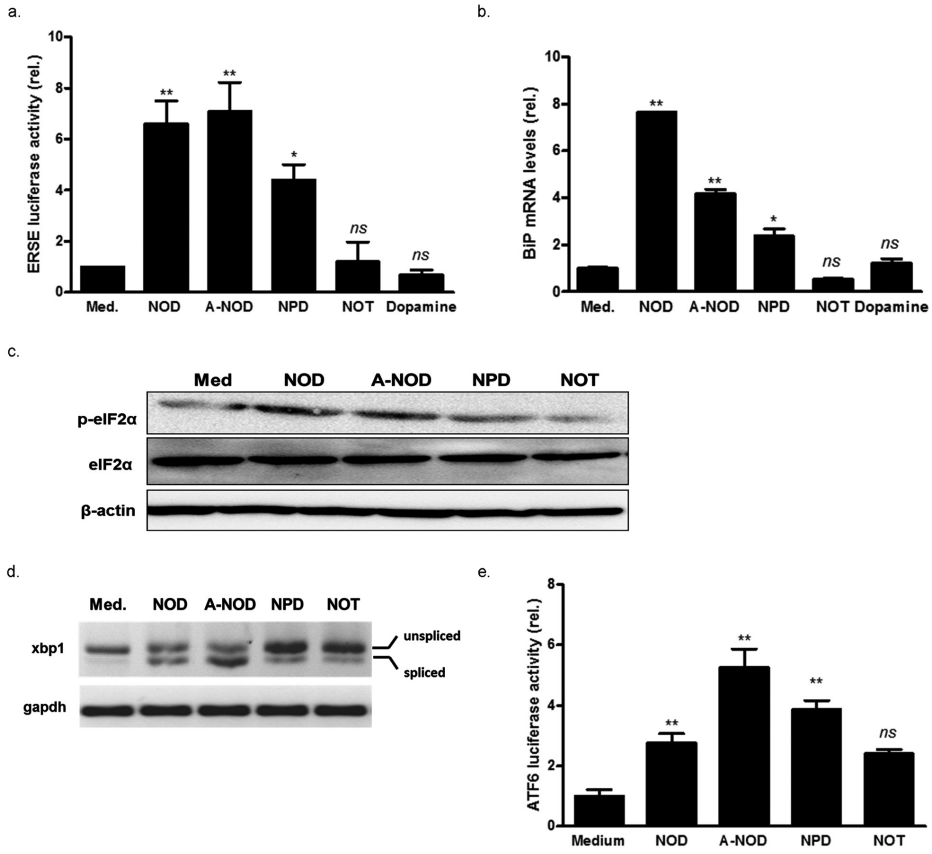

Figure 3. Induction of the UPR by NAD variants.(a) HUVECs were transduced by lentiviral particles containing either an ERSE-luciferase reporter or a luciferase construct under control of a CMV driven promoter as transduction efficiency control. The cells were stimulated for 8 h with 100 μM of different NAD as indicated. Equimolar concentrations of dopamine were also included to assess if dopamine induces the UPR. ERSE dependent luciferase activity was assessed as described in materials and methods and normalized for constitutively expressed luciferase. The results are expressed as normalized ESRE luciferase activity relative to untreated (Med.) cells. Values represent mean±SD from three independent experiments, *$p<0.05$, **$p<0.01$ vs. untreated control, ns: not significant. (b) HUVECs were treated with 100 μM NAD for 8 h. Cells that were not treated (Med.) served as control. Hereafter total RNA was isolated and the expression of BiP and GAPDH were quantitated by qPCR. The results are expressed as BiP mRNA levels, normalized for GAPDH mRNA expression and relative to cells that were not treated (Med), *$p<0.05$, **$p<0.01$ vs. untreated control, ns: not significant. (c) HUVECs were stimulated for 8 h with 100 μM of different NAD, or left untreated (Med). Hereafter protein extracts were made and phosphorylation of eIF2α was assessed by Western blotting. The blots were stripped and re-probed with antibodies directed against total eIF2α and β-actin to test for equal loading. The results of a representative blot are

Using the ERSE-containing luciferase reporter construct, it was shown that only the redox active compounds NOD, A-NOD and to a lesser extent NPiD were able to increase luciferase expression in lentiviral transduced HUVEC, while the redox inactive NOT showed no effect (Figure 3a). In line with these findings, increased BiP mRNA expression and ER-sensor activation (Figure 3b–e) only occurred by the redox active NAD variants. It should be mentioned however that with exception of the ATF6 reporter assay, in all other assays NPiD was consistently weaker compared to NOD and A-NOD. In contrast to the NAD variants, equimolar concentrations of dopamine were not able to activate the UPR (Figure 3a and b).

Since oxidative folding in the ER is catalyzed by protein disulphide isomerase (PDI) we assessed in a test tube assay if PDI activity was impaired by NOD. The known PDI inhibitor bacitracin was included to validate the assay and showed inhibition of 65 and 15 percent at a concentration of 1 and 10 mM respectively (Figure 4a). Although NOD was clearly less effective compared to bacitracin, NOD inhibited PDI in a dose dependent manner with an almost 50 percent inhibition at 10 mM. A-NOD and NPiD did not inhibit PDI activity (Figure 4b).

depicted, a total of 4 independent experiments were performed. (d) HUVECs were stimulated for 8 h with different NAD (100 µM) before total RNA was isolated. Cells that were not treated (Med.) served as control. Spliced and unspliced xbp-1 mRNA were detected by PCR. The spliced and unspliced amplification products differ by 26 bp. (e) Cells were transduced with lentiviral particle containing an ATF-6-driven luciferase reporter or a constitutively expressed luciferase construct. The cells were stimulated for 8 h with different NAD (100 µM). Luciferase activity was assessed as described in materials and methods and normalized for constitutively expressed luciferase activity. The results are expressed as normalized ATF6 luciferase activity relative to untreated (Med.) cells. Values represent mean ± SD from three independent experiments, *$p<0.05$, **$p<0.01$, vs. untreated control, ns: no significant.

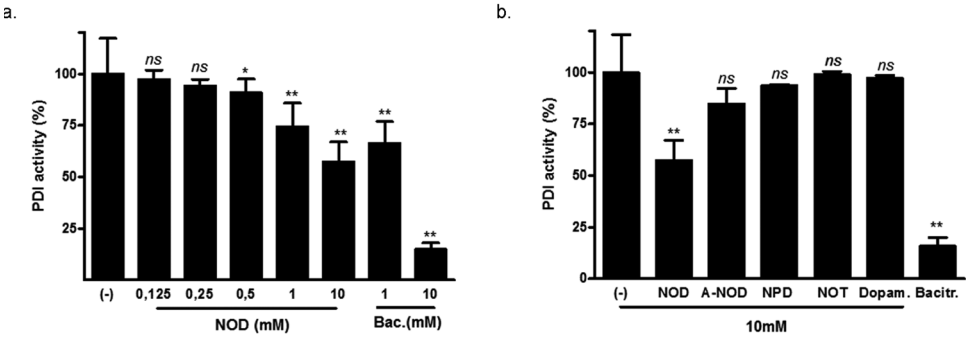

Figure 4. NOD inhibits PDI activity.(a) PDI activity was assessed by monitoring PDI-catalysed reduction of insulin in the presence of Dithiothreitol (DTT) and different concentrations of NOD. Bacitracin in concentrations of 1 and 10 mM was used to validate the assay. (b). Different NAD were tested for inhibition of PDI activity in a similar manner as described in (a). The results from three independent experiments are expressed as mean percent PDI activity ± SD, using PDI activity in the absence of inhibitors (–) as 100 percent, *$p<0.05$, **$p<0.01$ vs. untreated control, ns: no significant.

NOD does not impair cell viability

In keeping with the fact that induction of the UPR may result in apoptosis, we sought to address if NOD treatment affects cell viability. Cell viability was assessed by means of FACS analysis using Annexin V/7-ADD (Figure 5a). While tunicamycin, a known UPR inducer, clearly increased the percentage of 7-AAD single and Annexin V/7-ADD double positive cells, this was not observed for NOD (Figure 5a). Interestingly, when HUVEC were treated with NOD 3 h prior to the addition of tunicamycin, the number of both 7-AAD single and Annexin V/7-AAD double positive cells decreased (Figure 5a). Transient induction of CHOP mRNA was observed for both NOD and tunicamycin, albeit that CHOP mRNA expression was significantly higher for the latter condition (Figure 5b, left panel). No significant difference in CHOP mRNA stability was observed between NOD and tunicamycin treated cells (Figure 5c, middle panel). However, BiP mRNA was more stable in NOD treated cells than tunicamycin-treated cells (Figure 5c, right panel).

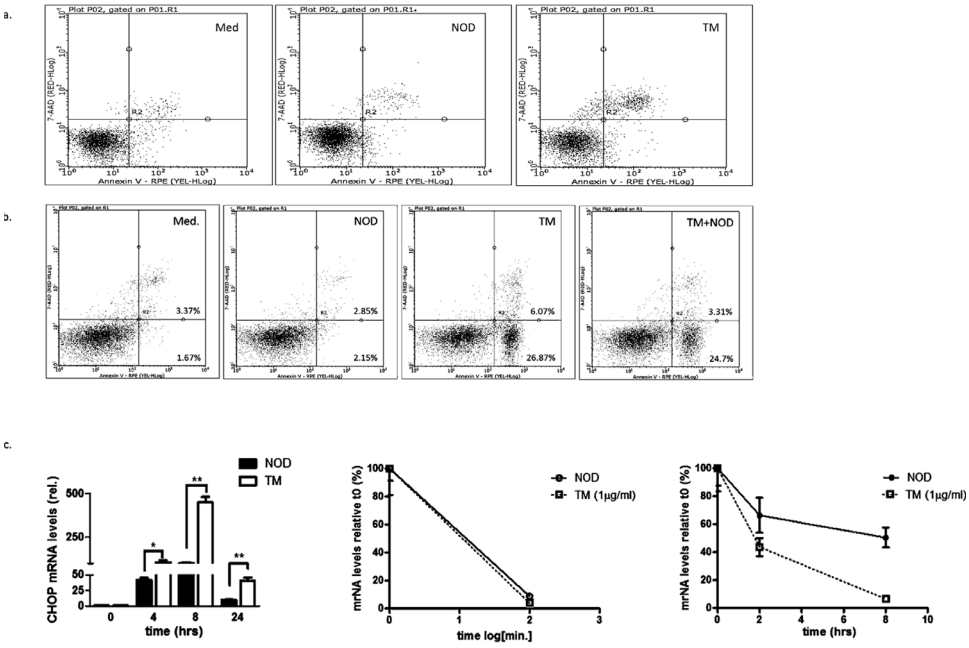

Figure 5. NOD does not impair cell viability.(a) HUVECs were treated for 24 h with NOD (100 µM) or tunicamycin (TM, 1 µg/mL). In addition cells were treated for 3 h with 100 µM of NOD prior to tunicamycin treatment. Cells that were not treated (Med.) served as control. Both floating and adherent cells were harvested, stained for Annexin V and 7-AAD and analysed by flow cytometry. (b) HUVECs were treated with 100 µM NOD or TM (1 µg/mL) for the indicated time periods. Total RNA was isolated and expression of CHOP mRNA was assessed by qPCR and normalized for GAPDH (left panel). Cells were pre-treated either with NOD or with tunicamycin and then chased for 0, 2, 4 and 8 h with AcD 50 ng/mL. Total RNA was isolated and the expression of CHOP (middle panel) and BiP (right panel) mRNA were assessed by qPCR and normalized for GAPDH. The results of three different experiments are expressed as mean mRNA levels ± SD, $^{**}p<0.01$ vs. untreated cells.

Growth arrest, hypometabolism and thermotolerance

In the course of performing this study we consistently observed that the time to confluence was much longer when HUVEC were seeded in culture plates and treated with NOD. Consequently we assessed if NOD affects cell proliferation. As demonstrated in ^{3}[H] thy-

midine incorporation assays, NOD dose dependently inhibited cell proliferation (Figure 6a). NOD treatment changed cell cycle phase distribution, with a relative increase of cells in the S-G2/M phase (Figure 6b), suggesting that cell cycle progression was attenuated at the S-G2/M phase. Importantly, affymetrix analysis also showed a significant decreased mRNA expression for genes involved in S-G2/M progression (table 2), which was confirmed by qPCR (Figure 6c).

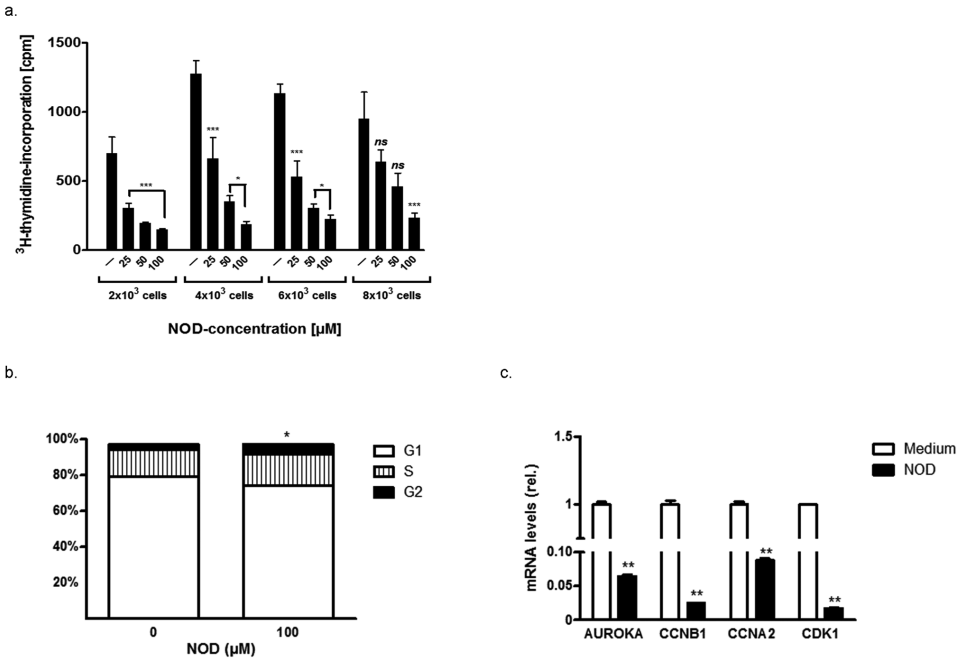

Figure 6. NOD inhibits cell proliferation.(a) HUVECs were seeded in different cell densities in 96 well plates and the next day treated for 48 h with different concentrations of NOD. During the last 16 h the cells were pulsed with 0.2 µCi 3[H] thymidine and subsequently harvested. The results of a representative experiment are depicted and expressed as mean 3H-thymidine incorporation in counts per minute (cpm) ± SD of 6 replicate wells for each condition. A total of 6 experiments were performed with essentially similar results. Significance was defined as *$p<0.05$ and **$p<0.01$ compared to untreated cells, ns: not significant. (b) In separate experiments HUVECs were stimulated with 100 µM of NOD or left untreated. One part of the cells was used for cell cycle analysis, for the other part total RNA was isolated and the expression of AUROKA, CCNB1, CCNA2 and CDK1 was assessed by qPCR (c). A total of three experiments were performed. The results in graph (b) are expressed as mean percentage of cells in G0/1-, S-and G2/M-phase. *$p<0.05$, NOD vs. untreated. The results in graph (c) are expressed as normalized mRNA levels relative to the untreated medium control cells. **$p<0.01$ vs. untreated control.

Table 2. Genes implicated in cell cycle, down-regulated by NOD.

Gene	Fold Change	p-value[a]
CDC20	9.35	2.32
CCNB1	8.48	2.77
CDK1	8.47	2.84
PRC1	8.08	2.30
NUSAP1	7.67	2.75
AURKB	7.26	3.65
NDC80	6.40	3.64
KIF4A	6.27	2.59
CEP55	6.22	2.38
CCNA2	6.15	3.88
CENPE	5.45	2.60
CDKN3	5.31	2.75
SPC25	5.09	2.91
AURKA	4.84	3.14
CDCA8	4.82	9.80

a :p-values for the comparison are given as log10 value. UPR target genes are depicted in bold.

With exception of CHOP, all other UPR target genes tested in this study were up-regulated in a dose dependent manner when HUVEC were treated with low concentrations of NOD (0.1 and 1 µM) form the 2nd passage on until the 6th passage (P2 to P6) (Figure 7a and b). In cells that were treated over this long period of time with NOD, intracellular ATP concentrations were significantly lower as compared to cells from a similar passage without treatment (Figure 7c). The lower intracellular ATP concentration was paralleled by an increased phosphorylation of AMPK (Figure 7d), and was still noted when NOD was removed from the culture 2 or 5 days prior to analysis. In addition to this apparent hypo-metabolic state, cells were also more resistant to cold inflicted injury as determined by LDH release (Figure 7e).

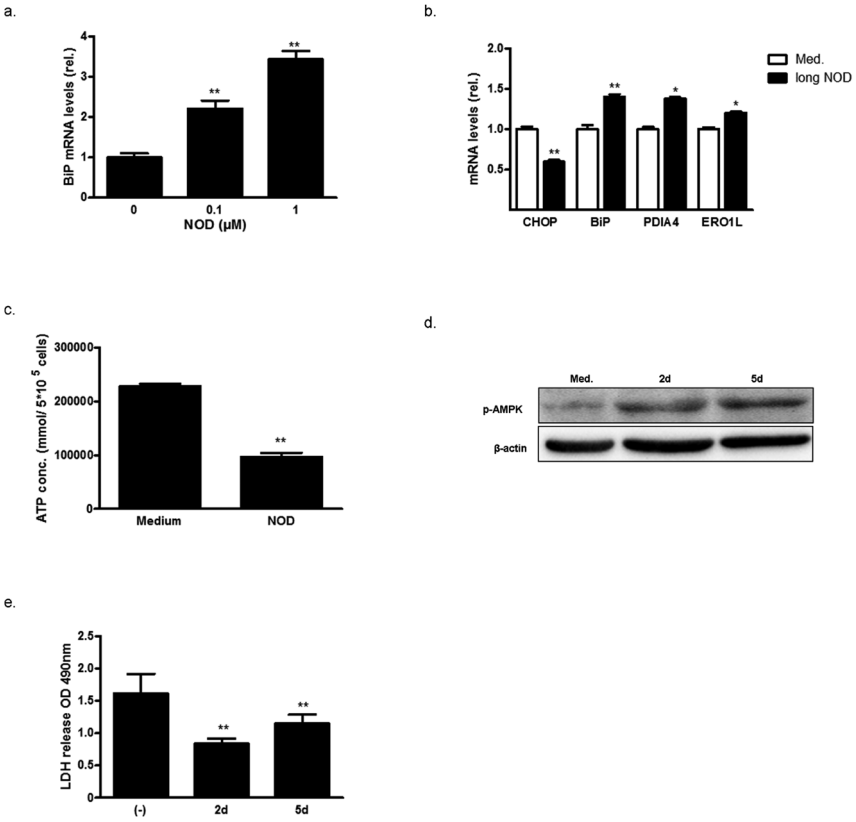

Figure 7. Long-term NOD treatment results in hypometabolism and thermotolerance.Three different primary HUVEC isolations were cultured from P2 until P6 in the absence or presence of the indicated NOD concentrations. (a) BiP mRNA expression for cells cultured in the presence of 0.1 and 1 μM NOD was assessed by qPCR. (b) CHOP, BiP, PDI4, and ERO1L mRNA expression for cells cultured in the presence of 0.1 μM NOD was assessed by qPCR. The results in a and b are expressed as normalized mean mRNA levels relative to untreated controls (0, Med) ± SD of 3 replicates for each condition and for all 3 HUVEC isolations. **p<0.01, *p<0.05 vs. untreated cells. (c) Intracellular ATP concentration was assessed in HUVEC at P6 upon long-term culture in the absence (medium) or presence of NOD (1 μM). The results are expressed as mean ATP concentration (pmol/5 $\times 10^5$ cells) ± SD of 3 replicates for each condition and for all 3 HUVEC isolations. **p<0.01 vs. untreated cells (d,e). In separate experiments NOD (1 μM) containing medium was exchanged for normal cell culture medium at P6 and the cells were cultured for 2 (2d) or 5 (5d) days in the absence of NOD. Cells that were continuously cultured in normal cell culture medium (Med.) were used as control. In (d) protein extracts were made and assessed for phosphorylation of AMPK (p-AMPK) by Western blotting. The blots were stripped and re-probed with antibodies directed against β-actin to test for equal loading. The results of a representative blot are depicted, a total of 3 independent experiments were performed. In (e) the cells were subjected to cold storage (4° C) for 24 h. Hereafter LDH release was assessed in the supernatants. Each condition was tested in triplicate in 2 independent experiments. The results are expressed as mean LDH release (OD490) ± SD, **P<0.01 vs. (Med.) control.

Discussion

In the present study we demonstrate that synthetic NAD transiently activate the UPR. This property seems to be dependent on the redox activity of these compounds. NOD did not affect cell viability, but strongly impaired cell proliferation of HUVEC, most likely by attenuation of cells in the S-G2/M phase. In concordance to this, mRNA expression for a number of genes involved in S-G2/M progression was significantly down-regulated by NOD. Interestingly, long-term NOD treatment resulted in hypometabolism and thermotolerance, as suggested by a decreased intracellular ATP concentration, activation of AMPK and increased resistance to cold inflicted cell injury.

Sensing, responding, and adapting to environmental insults are essential for all living organisms and are originating from evolutionarily conserved unique signal transduction pathways. Being one such a pathway, the role of the UPR is to alleviate ER stress and, paradoxically, to activate apoptosis, depending on the nature and severity of the stressor [29]. NAD are able to activate the UPR mainly due to their redox active catechol structure, albeit that at high NOD concentrations (10 mM) PDI activity was also inhibited in a test tube assay. The latter seems to be a highly unlikely explanation for UPR induction in HUVEC, since low NOD concentrations (25 μM) already induced the UPR. It is therefore more conceivable that oxidation of the catechol containing NAD leads to donation of reduction equivalents, thereby changing an oxidizing ER environment to a more reducing one. This assumption is supported by the finding that for NOT, which contains a low redox active tyramine moiety, UPR induction was not observed. It should also be mentioned that the hydrophobic fatty acid of NAD may facilitate UPR induction by providing an easier access to the ER, in line with the observation that despite its catechol structure dopamine was not able to induce the UPR. We are aware that no definite proof that NOD indeed has access to the ER is provided. However previous published studies in which dopamine uptake was compared to that of NOD [19] revealed that both dopamine and NOD were found in the membrane fraction, which predominantly contains the ER compartment, as well as in the mitochondrial-and cytosolic fraction. Hence, NOD may also impair the redox milieu in other cellular compartments than the ER. It should be emphasized that the ER enriched fraction also contained small amount of mitochondrial proteins, and hence formal proof that NOD has access to the ER compartment is still lacking.

The lower efficacy of NPiD for UPR induction might reflect a more limited access of NPD to the ER as a consequence of the bulky pivanoyl fatty acid. Recently, Achard et al demonstrated that the long-chain saturated palmitate (C16:0) fatty acid activates the UPR [30], questioning as to whether UPR induction as observed in our study could be mediated via intracellular hydrolysis of NAD. This scenario is however unlikely because hydrolysis of NOT would result in the release of octanoic acid (C8:0), yet UPR induction was not observed when equimolar concentrations of NOT were applied to HUVEC. The concentrations of palmitate used by Achard et al were significantly higher compared to concentration of NOD at which UPR induction was already noted (750 vs. 25 μM).

The decision mechanisms for switching the UPR from adaptive response to apoptosis have so far been poorly understood. Cojocari et al [31] recently suggested that the PERK signaling arm is uniquely important for promoting adaptation and survival during hypoxia-induced ER stress. Yet, other reports suggest that UPR mediated cell adaptation is not due to selective UPR sensor activation, but most likely reflects changes in protein composition or mRNA stability of adapted cells [32]. Compared to tunicamycin, NOD mediated induction of both CHOP and BiP mRNA was modest, and may explain why tunicamicin, but not NOD treated HUVEC went into apoptosis. Interestingly, in long-term NOD (1 μM) treated HUVEC CHOP mRNA was down-regulated while that of BiP was persistently up-regulated. This is in line with the observation by Rutkowski et al [32] that over a long time course of low ER stress CHOP up-regulation diminishes, despite persistent up-regulation of the UPR-responsive ER chaperones BiP. It remains to be assessed why prior NOD treatment of HUVEC, abrogates tunicamycin mediated apoptosis, but it may well be a consequence of altered UPR signalling [32–35].

Similar as reported by Rutkowski et al for tunicamycin [32], we also observed that cell growth was retarded when cells were continuously cultured in the presence of low NOD concentrations, as suggested by an increased time to confluence. It has been reported that phenolic compounds significantly affect cell proliferation by arresting cells in the G2/M phase [36–39]. Therefore it is at present unclear if growth inhibition by NOD is causally related to UPR induction or if this is independent of the UPR.

AMP-activated protein kinase (AMPK) is a cellular energy sensor that responds to low endogenous energy by stimulating fatty acid oxidation. It acts as a low-fuel warning system that is activated by depletion of ATP or, alternatively, by increased levels of AMP, to induce an energy-saving state and to prevent lactate accumulation and cell injury [40]. Since long term NOD treatment resulted in decreased intracellular ATP concentrations it is conceivable that this might have triggered the activation of AMPK as observed in our study. More importantly, we also observed that long term NOD treated HUVEC were more resistant to cold inflicted injury. This effect was still apparent when NOD was removed from the culture medium and cells were grown for additional 2 or 5 days. These findings have important implications as pre-conditioning strategies to improve organ functioning after cold storage are primarily focused on influencing cellular metabolism or energy status and reduction of inflammation [41]. Mamady H et al, have suggested that the UPR might be integral to long term survival in a state of cold torpor by coordinating gene expression responses that support the hibernating phenotype [14]. However, it would be prudent to be cautious in concluding that the apparent hypometabolism and thermotolarance mediated by NOD are linked to UPR induction.

We have previously demonstrated that NOD has therapeutic efficacy in ischemia induced acute kidney injury [18]. Induction of the UPR has been suggested to be protective in a variety of ischemia/reperfusion models [42–44]. It therefore remains to be assessed if therapeutic concentrations of NOD are able to activate UPR in vivo and to what extent this contributes to the reno-protective effect of NOD in ischemia induced AKI.

NAD were first described as potent inhibitors of 5-lipoxygenase [45, 46] and through the discovery that NAD are highly expressed in brain tissue, subsequent function have been revealed. Now these conjugates have come to prominence because of their potential roles in the nervous system, vasculature and the immune system and are being explored as potential lead compounds in drug development. The present finding that NAD have the propensity to induce hypometabolism and thremotolerance, irrespective as to whether this is mediated by UPR induction, opens new perspectives in this regard.

References

1. Schroder, M. and R.J. Kaufman, The mammalian unfolded protein response. Annu Rev Biochem, 2005. 74: p. 739–89.
2. Samali, A., et al., Methods for monitoring endoplasmic reticulum stress and the unfolded protein response. Int J Cell Biol, 2010. 2010: p. 830307.
3. Ron, D. and P. Walter, Signal integration in the endoplasmic reticulum unfolded protein response. Nat Rev Mol Cell Biol, 2007. 8(7): p. 519–29.
4. Walter, P. and D. Ron, The unfolded protein response: from stress pathway to homeostatic regulation. Science, 2011. 334(6059): p. 1081–6.
5. Kohno, K., Stress-sensing mechanisms in the unfolded protein response: similarities and differences between yeast and mammals. J Biochem, 2010. 147(1): p. 27–33.
6. Yoshida, H., et al., XBP1 mRNA is induced by ATF6 and spliced by IRE1 in response to ER stress to produce a highly active transcription factor. Cell, 2001. 107(7): p. 881–91.
7. Mori, K., Signalling pathways in the unfolded protein response: development from yeast to mammals. J Biochem, 2009. 146(6): p. 743–50.
8. Acosta-Alvear, D., et al., XBP1 controls diverse cell type-and condition-specific transcriptional regulatory networks. Mol Cell, 2007. 27(1): p. 53–66.
9. Okada, T., et al., Distinct roles of activating transcription factor 6 (ATF6) and double-stranded RNA-activated protein kinase-like endoplasmic reticulum kinase (PERK) in transcription during the mammalian unfolded protein response. Biochem J, 2002. 366(Pt 2): p. 585–94.
10. Harding, H.P., et al., Regulated translation initiation controls stress-induced gene expression in mammalian cells. Mol Cell, 2000. 6(5): p. 1099–108.
11. Harding, H.P., et al., An integrated stress response regulates amino acid metabolism and resistance to oxidative stress. Mol Cell, 2003. 11(3): p. 619–33.
12. Schindler, A.J. and R. Schekman, In vitro reconstitution of ER-stress induced ATF6 transport in COPII vesicles. Proc Natl Acad Sci U S A, 2009. 106(42): p. 17775–80.
13. Wang, S. and R.J. Kaufman, The impact of the unfolded protein response on human disease. J Cell Biol, 2012. 197(7): p. 857–67.
14. Mamady, H. and K.B. Storey, Coping with the stress: expression of ATF4, ATF6, and downstream targets in organs of hibernating ground squirrels. Arch Biochem Biophys, 2008. 477(1): p. 77–85.
15. Suh, D.H., et al., Unfolded protein response to autophagy as a promising druggable target for anticancer therapy. Ann N Y Acad Sci, 2012. 1271: p. 20–32.
16. Connor, M., C.W. Vaughan, and R.J. Vandenberg, N-acyl amino acids and N-acyl neurotransmitter conjugates: neuromodulators and probes for new drug targets. Br J Pharmacol, 2010. 160(8): p. 1857–71.
17. Almasi, R., et al., Actions of 3-methyl-N-oleoyldopamine, 4-methyl-N-oleoyldopamine and N-oleoylethanolamide on the rat TRPV1 receptor in vitro and in vivo. Life Sci, 2008. 82(11–12): p. 644–51.

18. Tsagogiorgas, C., et al., N-octanoyl-dopamine is an agonist at the capsaicin receptor TRPV1 and mitigates ischemia-induced [corrected] acute kidney injury in rat. PLoS One, 2012. 7(8): p. e43525.
19. Losel, R.M., et al., N-octanoyl dopamine, a non-hemodyanic dopamine derivative, for cell protection during hypothermic organ preservation. PLoS One, 2010. 5(3): p. e9713.
20. Vettel, C., et al., Dopamine and lipophilic derivates protect cardiomyocytes against cold preservation injury. J Pharmacol Exp Ther, 2014. 348(1): p. 77–85.
21. Ait-Hsiko, L., et al., N-octanoyl-dopamine is a potent inhibitor of platelet function. Platelets, 2013. 24(6): p. 428–34.
22. Hottenrott, M.C., et al., N-octanoyl dopamine inhibits the expression of a subset of kappaB regulated genes: potential role of p65 Ser276 phosphorylation. PLoS One, 2013. 8(9): p. e73122.
23. Kawabata, T., et al., Iron coordination by catechol derivative antioxidants. Biochem Pharmacol, 1996. 51(11): p. 1569–77.
24. Graf, P.C. and U. Jakob, Redox-regulated molecular chaperones. Cell Mol Life Sci, 2002. 59(10): p. 1624–31.
25. Papp, E., et al., Molecular chaperones, stress proteins and redox homeostasis. Biofactors, 2003. 17(1–4): p. 249–57.
26. Anrather, J., et al., Regulation of NF-kappaB RelA phosphorylation and transcriptional activity by p21(ras) and protein kinase Czeta in primary endothelial cells. J Biol Chem, 1999. 274(19): p. 13594–603.
27. Ni, M. and A.S. Lee, ER chaperones in mammalian development and human diseases. FEBS Lett, 2007. 581(19): p. 3641–51.
28. Takahashi, K., et al., Effects of the ester moiety on stereoselective hydrolysis of several propranolol prodrugs in rat tissues. Biol Pharm Bull, 1995. 18(10): p. 1401–4.
29. Rutkowski, D.T. and R.J. Kaufman, That which does not kill me makes me stronger: adapting to chronic ER stress. Trends Biochem Sci, 2007. 32(10): p. 469–76.
30. Achard, C.S. and D.R. Laybutt, Lipid-induced endoplasmic reticulum stress in liver cells results in two distinct outcomes: adaptation with enhanced insulin signaling or insulin resistance. Endocrinology, 2012. 153(5): p. 2164–77.
31. Cojocari, D., et al., New small molecule inhibitors of UPR activation demonstrate that PERK, but not IRE1alpha signaling is essential for promoting adaptation and survival to hypoxia. Radiother Oncol, 2013. 108(3): p. 541–7.
32. Rutkowski, D.T., et al., Adaptation to ER stress is mediated by differential stabilities of pro-survival and pro-apoptotic mRNAs and proteins. PLoS Biol, 2006. 4(11): p. e374.
33. Rubio, C., et al., Homeostatic adaptation to endoplasmic reticulum stress depends on Ire1 kinase activity. J Cell Biol, 2011. 193(1): p. 171–84.
34. Tsang, K.Y., et al., In vivo cellular adaptation to ER stress: survival strategies with double-edged consequences. J Cell Sci, 2010. 123(Pt 13): p. 2145–54.
35. Scheuner, D., et al., Double-stranded RNA-dependent protein kinase phosphorylation of the alpha-subunit of eukaryotic translation initiation factor 2 mediates apoptosis. J Biol Chem, 2006. 281(30): p. 21458–68.

36. Janicke, B., et al., The antiproliferative effect of dietary fiber phenolic compounds ferulic acid and p-coumaric acid on the cell cycle of Caco-2 cells. Nutr Cancer, 2011. 63(4): p. 611–22.
37. Siveen, K.S. and G. Kuttan, Effect of amentoflavone, a phenolic component from Biophytum sensitivum, on cell cycling and apoptosis of B16F-10 melanoma cells. J Environ Pathol Toxicol Oncol, 2011. 30(4): p. 301–9.
38. Abubakar, M.B., et al., A review of molecular mechanisms of the anti-leukemic effects of phenolic compounds in honey. Int J Mol Sci, 2012. 13(11): p. 15054–73.
39. Tabata, K., et al., Phenolic diterpenes derived from Hyptis incana induce apoptosis and G(2)/M arrest of neuroblastoma cells. Anticancer Res, 2012. 32(11): p. 4781–9.
40. Peralta, C., et al., Adenosine monophosphate-activated protein kinase mediates the protective effects of ischemic preconditioning on hepatic ischemia-reperfusion injury in the rat. Hepatology, 2001. 34(6): p. 1164–73.
41. Bouma, H.R., et al., AMP-activated protein kinase as a target for preconditioning in transplantation medicine. Transplantation, 2010. 90(4): p. 353–8.
42. Cybulsky, A.V., et al., Role of the endoplasmic reticulum unfolded protein response in glomerular epithelial cell injury. J Biol Chem, 2005. 280(26): p. 24396–403.
43. Martindale, J.J., et al., Endoplasmic reticulum stress gene induction and protection from ischemia/reperfusion injury in the hearts of transgenic mice with a tamoxifen-regulated form of ATF6. Circ Res, 2006. 98(9): p. 1186–93.
44. Tadimalla, A., et al., Mesencephalic astrocyte-derived neurotrophic factor is an ischemia-inducible secreted endoplasmic reticulum stress response protein in the heart. Circ Res, 2008. 103(11): p. 1249–58.
45. Bisogno, T., et al., N-acyl-dopamines: novel synthetic CB(1) cannabinoid-receptor ligands and inhibitors of anandamide inactivation with cannabimimetic activity in vitro and in vivo. Biochem J, 2000. 351 Pt 3: p. 817–24.
46. Tseng, C.F., et al., Inhibition of in vitro prostaglandin and leukotriene biosyntheses by cinnamoyl-beta-phenethylamine and N-acyldopamine derivatives. Chem Pharm Bull (Tokyo), 1992. 40(2): p. 396–400.

Summary, Discussion and Future Prespective

Chapter 7

Summary
General discussion
Nederlandse samenvatting

Summary

Organ donor dopamine treatment is associated with improvements of the initial graft function after the kidney transplantation. NOD is a synthetic *N*-acyl dopamine that was developed with the aim to create a hydrophobic dopamine derivative that does not influence systemic blood pressure for use in organ donor. Due to its anti-inflammatory, reno-protective and cytoprotective properties, NOD has become an interesting drug candidate for clinical use in the setting of ischemia-induced acute kidney injury. The main aim of the thesis was to investigate the relevant chemical and biological properties that grant NOD reno-protective effects in this context. We studied NOD's ability to activate TRPV1 and NOD's prominent redox active nature, which may alter the redox milieu within intracellular compartments. The experimental studies described in this thesis were performed firstly, to demonstrate that NOD conveys protection in the setting of ischemia induced AKI via TRPV1 activation, secondly, to delineate the molecular entities within NOD that are required for TRPV1 activation and for its anti-inflammatory property, thirdly to study *in vivo* tissue distribution and the elimination kinetics of NOD and fourthly, to demonstrate that the redox activity of NOD significantly affects the cell behaviour, i.e. NOD induces ER stress and UPR. The potential use of NADs in transplantation medicine is reviewed in **Chapter 2**.

Chapter 3 explored the reno-protective effect of NOD in the setting of warm ischemia-induced AKI. We showed that NOD treatment improves the renal function in warm ischemia-induced AKI, even when treatment is started after the renal ischemia. Improved renal function was not associated with large changes in the renal perfusion. We showed that the reno-protective properties of NOD are mediated via TRPV1. NOD treatment of renal allograft recipient rats did not improve renal function compared to the untreated recipient rats. Since both capsaicin and NOD were able to evoke TRPV1-mediated calcium transients in cold-stored dorsal root ganglions (DRGs), the lack of therapeutic efficacy in the recipient rats could not be explained by the loss of TRPV1 responsiveness.

In **Chapter 4**, we delineated the chemical entities within NOD that mediate TRPV1 activation and that are responsible for the anti-inflammatory effects. For this, we synthesized compounds by modifying NOD at the aromatic-, amide linker-and fatty acid moieties. Calcium microfluorimetry revealed an EC_{50} value for TRPV1 activation by NOD of 12.7μM. Acetylation of the ortho-dihydoxy groups (acetylated (A-) NOD) or shortening of the amide linker (ΔNOD) decreased the efficacy for TRPV1 activation. For ΔNOD, the efficacy further decreased by interchanging the position of the carbonyl and amide groups. The absence of one hydroxyl group at the aromatic ring (*N*-octanoyl tyramine (NOT) or the use of a bulky fatty acid as ester functionality (N-pivaloyl dopamine (NPiD) significantly impaired TRPV1 activation. Docking studies and site-directed mutagenesis revealed similar anchor residues for interactions of capsaicin or NOD with TRPV1. However, mutation of arginine at position 491 (R491) to alanine only affected TRPV1 activation by NOD. With exception of ΔNOD the presence of an intact catechol structure

was mandatory for TNF-α induced the inhibition of VCAM-1 *i.e.* to inhibit inflammation and for the induction of heme oxygenase-1 (HO-1) expression. NPiD and A-NOD both displayed similar anti-inflammatory properties as NOD.

In the **chapter 5**, we developed the radiotracer [^{18}F]F-NOD to assess the *in vivo* elimination kinetics of NOD. We first established that the biological properties of F-NOD and NOD did not differ, i.e. both inhibited TNF-α-induced vascular cell adhesion protein 1 (VCAM-1) expression, both induced the expression and activity HO-1, both protected the endothelial cells against cold-inflicted injury and both activated TRPV1. [^{18}F]F-NOD was efficiently radiolabelled, RCY 45 percent, d. c., and was stable in phosphate buffer and rat plasma (>99 percent after 120 min at 37° C). *In vivo*, [^{18}F]F-NOD was cleared rapidly via the renal and hepatobiliary system.

Because redox conditions differ between intracellular compartments, and NOD participates in redox cycling, we assessed in **chapter 6** if synthetic NADs (including NOD) activate the unfolded protein response (UPR). NOD dose dependently induces the ER stress and UPR. This property seems to depend on the redox activity of these compounds. NOD did not affect cell viability, but strongly impaired cell proliferation of HUVECs, most likely by attenuation of cells in the S-G2/M phase. In concordance with this, expression of several genes involved in S-G2/M progression was significantly downregulated by NOD. Interestingly, long-term NOD treatment resulted in hypo metabolism and thermotolerance, as suggested by a decreased intracellular ATP concentration, activation of AMPK and increased resistance to the cold inflicted cell injury.

General Discussion

N-acyl Dopamines (NADs) are naturally occurring compounds which can be best described as dopamine conjugated to an aliphatic chain at the amine side chain. This makes NADs a class of diverse compounds that vary in length and degree of saturation of the aliphatic chain. *In vivo*, these are most likely formed through the reaction of lipid hydro peroxides with primary amino groups to form *N*-acyl-type (amide linkage) dopamine adducts [1]. Lipid hydro peroxides are a consequence of oxidative stress and can be detected in e.g. brain tissue under a variety of pathological conditions [2, 3]. A number of such dopamine adducts have been found in brain tissue [1, 4, 5] in human plasma [6] and differ in two aspects from NOD, a synthetic NAD, i.e. the length of the aliphatic chain and the degree of saturation.

It should be emphasized that NOD was developed to underpin the relationship between the hydrophobicity and the efficacy of catecholamines to protect tissue from cold inflicted injury. Various *in vitro* and *in vivo* studies revealed the unexpected additional biological properties of NOD. As such NOD not only displayed cytoprotective effects to a wide variety of cultured cells when subjected to cold inflicted injury [7, 8], but also inhibited TNFα-mediated inflammation [9] and T cell proliferation [10] *in vitro*. *In vivo*, NOD treatment after transplantation of organs from the brain dead donor rats, improved allograft function in the renal and cardiac graft recipients [11, 12]. A reno-protective effect of NOD was also observed in the ischemia-induced AKI model [13]. These findings warranted further experimental studies to identify the mechanisms by which NOD conveyed each of these protective effects and to understand how these effects can be explained by NODs structure and *in vivo* bio-distribution.

The studies presented in this thesis have further increased our understanding of the working mechanism of NOD. We identified activation of TRPV1 as a pivotal mechanism in NOD's reno-protection after ischemia-induced AKI. Secondly, the molecular entities within NOD that are required for TRPV1 activation and for its anti-inflammatory property were identified. Thirdly, NOD's *in vivo* tissue distribution and elimination kinetics are described. Finally, it describes that NOD induces ER stress response also known as the unfolded protein response UPR *in vitro* due to its redox active nature figure1.

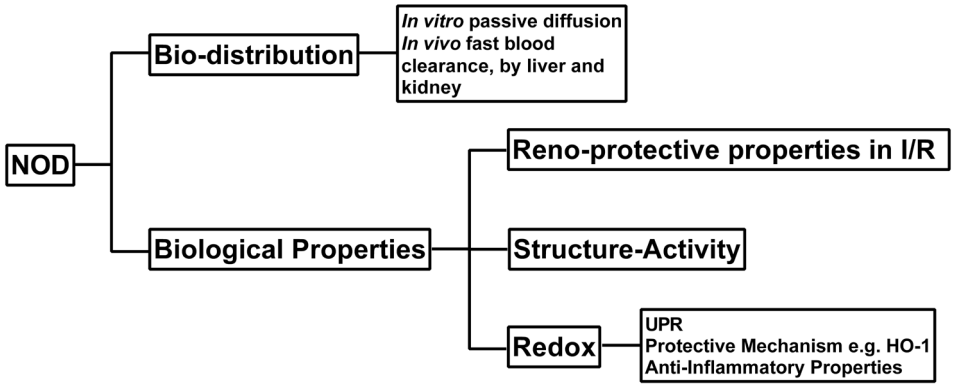

Figure 1. A schematic diagram showing major findings of this thesis.

TRPV1 and inflammation

This thesis provides first report obtained on the bio-distribution of NOD and shows that it has very fast blood clearance i.e within 30 mins by the liver and the kidney. Despite very short lifetime inside the organism (rat) the application of NOD immediately before or after the ischemia induced AKI leads to fast recovery of the renal function. This indicates that NOD delivers its reno-protective effect with short exposure time. Furthermore, *in vitro* cellular uptake studies of NOD shows passive diffusion kinetics for uptake of NOD in the Human Vein Endothelial cells (HUVECs). These findings along with previously conducted the *in vitro* studies suggests that the reno-protective properties of NOD in the context of ischemia induced Acute Kidney Injury could be explained either due to – NOD's ability to activate TRPV1 or NOD's ability to donate reduction equivalence in different cellular compartments to clear ROS regerated during ischemia or both. In this thesis these questions were evaluated *in vivo* in ischemia induced AKI on TRPV1$^{-/-}$ in Sprague Dawley rats. NOD treatment in TRPV1$^{-/-}$ Sprague Dawley rats did not improve the renal function which zeros down the reno-protective effect of NOD in ischemia induced AKI in rats to TRPV1. This establishes firstly, that the reno-protective property of NOD *in vivo* is solely due its ability to activate TRPV1. Secondly, this finding also rules out that the redox active nature of NOD which might help clear the ROS produced during reperfusion plays any protective role *in vivo* in ischemia induced AKI.

TRPV1 activation can elicit protective effects in various organs in the IRI models in terms of restoration of organ function and limiting inflammation [14], [15], [16] [17]. TRPV1 activation in injured tissue causes pain sensation and induces local release of the vasodilators from surrounding neuronal cells causing vasodilation-facilitated perfusion

of blood. The protection might be causally linked to the release of neuropeptides [18]. Although a number of TRPV1 agonists have been tested in ischemia induced AKI models and all have been reported to display therapeutic efficacy [19] [13] in terms of restoration of the kidney function and limiting inflammation (compared to the saline treated control) yet, the course of AKI as such can neither be influenced by TRPV1 inhibition [20] nor with genetic ablation of TRPV1[21]. NOD is a moderately strong TRPV1 agonist. NOD treatment pre [13] or post [21] warm ischaemia improves AKI in a TRPV1 dependent manner. Amongst the endogenous N-acyl dopamines only OLDA has been studied in an *ex vivo* cardiac IRI-model (in mice) and has been described to deliver cardiac protective effect [22]. It is worth to mention here that the endogenous *N*-acyl dopamines NADA and OLDA are not only agonists of TRPV1 but also of Cannabinoid receptor type 1 (CB1) – which evokes an anti-inflammatory effect as described in cerebral ischemia model [23]. Whether or not NOD is an agonist of CB1 is unknown and still needs to be determined. In contrast to NOD, hydrolysis of NADA gives rise to arachidonic acid which may be further converted to TRPV1 activating lipoxygenase products [24–26].

Although inflammation is part of a repair and restoration process that preserves tissue functionality, yet inflammation needs to be controlled and needs to go into resolution to prevent excessive responses that may harm the tissue. NOD treatment in itself or by virtue of TRPV1 activation did not influence gene expression of the inflammatory cytokines in the kidney of rats undergoing ischemia induced AKI, similar to findings of Tsagogiorgas et. al. Even though Tsagogiorgas et. al also describe a damping effect on NF-kB activation in rats treated with NOD when compared to saline treated control rats, it is not conclusive due to small sample size (n=4) and the heterogeneous effect of NFκB activation in the saline treated control group. TRPV1$^{-/-}$Sprague Dawley rats irrespective of their treatment (NaCl or NOD) displayed less infiltration of ED1^{+}macrophages in kidneys of rats undergoing AKI when compared with WT Sprague Dawley rats.

In certain organ system like heart TRPV1 activation yields anti-inflammatory effects and helps restore the organ function. Genetic ablation of TRPV1 impairs post-ischemic recovery in the isolated perfused heart, exacerbates inflammation, and affects cardiac remodelling after myocardial infarction (MI) in mice [15]. Furthermore, TRPV1 gene deletion results in excessive inflammation, disproportional left ventricular remodelling, and deteriorated cardiac function after MI, indicating that TRPV1 may prevent the infarct expansion and cardiac injury by inhibiting inflammation and abnormal tissue remodelling [27]. It seems that the beneficial cardiovascular effects of the TRPV1 agonists may be caused by an ischemic preconditioning phenomenon, release of neurotransmitters, and inhibition of platelet aggregation [28]. Contrary to the beneficial effect of TRPV1 activation in the heart, in eye TRPV1 activation elicits a neurogenic inflammation in the surrounding area aimed to repair injury following a damaging infectious or non-infectious insult. TRPV1 activation in non-neuronal cells of the eye may lead to phosphorylation of a variety of downstream kinases and transcription factors, e.g. transforming growth factor β-activated kinase 1 (TAK1), c-jun N-terminal protein kinase 1 (JNK1), nuclear factor (NF)-κB. These further contribute to a pro-inflammatory milieu through

the upregulation of transcription of chemoattractant-encoding genes [29]. However, uncontrolled TRPV1 leads to dysregulated and prolonged responses causing opacification of cornea and a decline in visual acuity instead of restoration of corneal transparency. TRPV1$^{-/-}$ mice regained corneal transparency following an alkali burn, while in wild type (WT) littermates the corneas remained inflamed and scarred [30]. Administration of the systemic TRPV1 antagonists also resulted in restoration of corneal transparency like observed with TRPV1$^{-/-}$ mice. This indicates that limited activation or absence of TRPV1 is essential in proper wound healing i.e. resolution of inflammation and suppression of fibrotic processes. In fact, it has been shown that activation of Cannabinoid receptor type 1 (CB1) which is also expressed on trigeminal neurons innervating the cornea desensitizes TRPV1 in a calcineurin dependent manner [31–33].

From these findings it can be inferred that controlled or limited TRPV1 activation has an adaptive benefit and - despite being inflammatory - is pro healing. Thus, localisation of TRPV1, the extent of activation and the co-expression of other receptors are important factors in determining the fate of TRPV1 activation, whether it will lead to an uncontrolled or controlled inflammatory process i.e. the microenvironment dictates the final inflammatory status.

Oxidative stress and ROS signalling

In vitro, NOD down-regulates inflammatory mediators by impairing NFκB activation, it strongly inhibits platelet function [5, 6] and can transiently inhibit T cell proliferation [7]. NOT, a NOD variant lacking redox-active catechol moiety is unable to yield any of these effects, suggesting these effects of NOD are attributed to NOD's redox active nature. These *in vitro* finding are substantiated *in vivo* in Brain-dead model of the kidney and the heart transplant where NOD treatment of the brain dead donors (rats) yielded better graft function and reduced acute rejection in the renal allograft recipients compared to the untreated rats as well as diminished expression of the pro-inflammatory cell adhesion molecules like (ICAM-1) and vascular cell adhesion molecule 1 (VCAM-1) in the kidney and the heart [11]. These anti-inflammatory effects yielded by NOD in the brain-dead transplantation model can be explained due to anti-oxidative properties of the catechol structure present in NOD and due to semblance between *in vitro* and *in vivo* experiments. However, NOD treatment failed to display the anti-inflammatory effects *in vivo* in ischemia induced AKI model in Fisher and TRPV1$^{-/-}$Sprague Dawley rats, and in the renal allograft recipients [21]. These findings raise the question why under certain conditions NOD can deliver anti-oxidative property *in vivo* and why under certain conditions NOD treatment yields no effect. Before investigating all these properties *in vivo* it is of prime importance to understand what anti-oxidant properties are displayed by NOD *in vitro* and what cellular pathways are affected by NOD's redox active nature and what structural entity of NOD is responsible for its anti-oxidative property.

2e-oxidation and Unfolded Protein Response

NOD is a redox active molecule with hydrophobic character which passively diffuses into cell and different cellular compartments and interferes with the redox equilibrium of the respective cellular compartment. This is supported by the fact that NOD induced Unfolded Protein Response (UPR) in a dose-dependent fashion while NOT, which is structurally similar to NOD except that it contains a low redox active tyramine moiety did not induce UPR [34]. The catechol moiety present in the NADs might participate in $2e^-$ oxidation reactions, in which the catechol structure is oxidized to quinones by donation of two protons $2H^+$ and two electrons ($2e^-$) to the oxidizing agent. These quinones in turn are easily reduced back to catechols, a process referred as $2e^-$ redox cycling Figure 2.

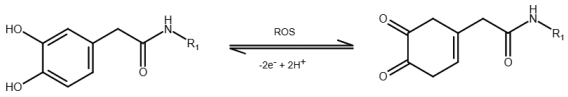

Figure 2. A schematic showing catechol moiety in NAD undergoing $2e^-$ redox cycling.

In the mitochondria and the endoplasmic reticulum (ER) $2e^-$ redox cycling is of pivotal importance for functioning of the respiratory chain and for the oxidative protein folding i.e. formation of disulphide bonds between cysteine residues in proteins to provide the protein right confirmation. NOD interferes with the $2e^-$ redox cycling thereby shifts an oxidizing ER environment to a more reducing. This disrupts efficiency of the protein folding. It has been shown in-test tube assay that NOD interferes with the activity of protein disulphide isomerase (PDI) which catalyses protein folding. Accumulation of the misfolded proteins within ER lead to "ER stress" [35] which subsequently induce a signal transduction pathway called the UPR to restore cell homeostasis. First adaptive responses are invoked like the upregulation of molecular chaperones and protein-processing enzymes to increase the folding and handling efficiency, translational attenuation to reduce the ER workload and prevent further accumulation of the unfolded proteins, and an increase in the ER-associated protein degradation (ERAD) and autophagy. If despite activation of these components clearance of unwanted proteins fails to restore protein-folding homeostasis, UPR progresses into the "terminal UPR" that ultimately promotes apoptosis. NOD induced UPR dose dependently and activated all the proximal UPR sensor as PERK, IRE1 and ATF6. NOD seems to induce an adaptive UPR response as it did not induced apoptosis but induced growth arrest. Whether NOD induced ER stress results in autophagy or induces adaptive UPR *in vivo* needs to be evaluated.

A wide range of cellular disturbances such as nutrient deprivation, hypoxia, loss of calcium homeostasis and change in redox imbalances which happen during Ischemia Reperfusion Injury (IRI) can also induce UPR. IRI has been shown to induce ER stress in renal tubule epithelial cells. Indeed after cardiac arrest-induced IRI in mice,

an increase in phosphorylation of PERK, a proximal UPR sensor, in tubular epithelial cells is reported [36]. Furthermore, ER chaperone BiP/Grp78 which is fundamental for the activation of the three main sensors of UPR, was activated in mice following 35 min of bilateral renal ischemia and reperfusion [37]. Likewise chemical inducer of UPR, BIX is shown to selectively induce ATF6 pathway (one of the three main proximal UPR sensors) and ameliorate renal IRI *in vivo* [38, 39].

Although ER stress and consequently UPR to a limited extent is described yielding protective effect in IRI, yet the mechanism underlying ER stress in AKI remains poorly understood. Several have demonstrated role of autophagy in ER stress-related protective effects in renal IRI. For instance, Chandrika et al. showed that tunicamycin (ER stress inducer) induced UPR and autophagy in renal tubular cells *in vitro* and in kidneys in mice. They also reported inhibition of autophagy increased tubular cell death *in vitro* and worsened ischemia induced AKI in mice, indicating a protective role of autophagy [40]. Study conducted by Ling and colleagues further demonstrated that the exogenous H_2S alleviated renal IRI by up-regulating ER stress-induced autophagy in rats [41].

Although a number of studies state a protective role of UPR/ER stress in renal IRI yet there is also evidence that UPR/ER stress in renal IRI might be detrimental. Intermedin (IMD), a protein which belongs to calcitonin/calcitonin gene-related peptide family and is potent systemic and pulmonary vasodilator. Intermedin supresses BiP, an important ER stress sensor, CHOP (which is induced by ER stress and it mediates apoptosis) , and caspase-12. Overexpression of Intermedin in rats IRI model significantly reduced apoptosis in renal epithelial cells and improved renal function after IRI in rats, suggesting a pathological role of ER stress in renal IRI [42]. Exact cause of the discrepancy between this study and the study mentioned in previous paragraph remains unclear. However, it is important to acknowledge that the mechanism underlying ER stress in AKI remains poorly understood. Based on the limited information perhaps it can be surmised that an initial adaptive UPR post IRI tends to restore homeostasis and repair by stopping translation of new proteins and getting rid of the non-functional protein, rescuing cells by digesting the damaged parts/compartments of the cells by means autophagy. When these adaptive responses are insufficient UPR progress into terminal phase which leads to pathophysiological developments.

Oxidation-reduction reactions exist in all cells and are essential to maintain cell homeostasis and signalling, including energy metabolism, gene expression, cell cycle regulation, immune response, cell growth, and cell apoptosis [43]. In addition to UPR, cell cycle progression is also regulated by the cellular redox environment as it changes toward a more oxidizing environment as G1 cells move through the cell cycle [44, 45]). As cellular uptake of NOD shifts the redox milieu to a more reducing milieu, also explains the G1 arrest of activated T cells [10] and endothelial cells in the presence of NOD. Growth arrest might suggest that the cell choose to go into senescence instead of apoptosis, however this still needs to be evaluated. It also remains to be determined if NOD treated cells exhibit growth arrest which is temporary and can be reversed by removal of NOD or it promotes the cells to enter senescence.

The influence of NADs on the respiratory chain, another cellular process which are redox sensitive, is still elusive and warrants further studies as an energy shift from mitochondrial oxidative phosphorylation to glycolysis dramatically affects cell metabolism and its consequences [46]. Apart from inhibition of cell cycle progression NADs may act immunosuppressive on lymphocytes as has been shown for NADA [47] and NOD [10]. Inhibition of redox-dependent transcription factors like NF-κB, NFAT, and AP-1, is most likely underlying the immunosuppressive effect of NADs.

Keap1-Nrf2-ARE pathway

This pathway acts as an early warning and attack system to ROS induces adaptive response during oxidative stress. Under normal physiological conditions Keap1 is associated with Nrf2 which leads to ubiquitination and subsequent degradation of Nrf2 [48]. Under oxidative stress increased level of intracellular ROS promotes the dissociation of Nrf2 and Keap1. Dissociated Nrf2 trans locates to nucleus and translates detoxification enzymes such as HO-1 and MnSOD [48]. NOD is also able to induce Nrf-2 in vitro and consequently increases expression of HO-1 in HUVECs. NOD's ability to activate HO-1 is solely dependent on an intact catechol structure as NOT, NOD structural variant with tyramine entity is not able to induce HO-1. NADA is also able to induce HO-1 in vitro. Several studies have demonstrated that HO-1 expression yields cytoprotective effects [49] in AKI. Whether or not NOD is able to induce Nrf-2 and HO-1 in vivo and exhibit cytoprotective still needs to be determined. It has been reported that the presence of these compounds scavenge ROS and enhance or stimulate adaptive anti-oxidant pathways during or immediately after ischemia facilitates reduction/neutralization of the ROS and thereby reducing the injury to the tissue. Despite the fact that NOD is also able to scavenge ROS by virtue of its catechol structure *in vitro*. Absence of beneficial effects with NOD administration in TRPV1$^{-/-}$Sprague Dawley AKI hints NOD mediated Keap1-Nrf2-ARE might not play any protective role in vivo.

Compounds which can neutralize ROS and activate the Keap1-Nrf2-ARE pathway have been already proven beneficial to treat IRI of kidneys e.g. Curcumin [50, 51] and Resveratrol [52]. Curcumin is produced by turmeric, a member of the ginger family, and it induces the expression of cytoprotective proteins regulated by NRF2 such as superoxide dismutase, catalase, glutathione reductase, glutathione peroxidase, HO-1 [50]. Similarly, Resveratrol, a polyphenolic compound found in grapes, berries, red wines, and peanut skins is reported to ameliorate ischemia-induced AKI by upregulating Nrf2 expression, downregulating the TLR4-induced NF-κB signalling pathway [53]. All these compounds scavenge ROS and enhance or stimulate adaptive anti-oxidant pathways.

Future perspectives

The journey of the development and characterization of NOD has brought us to new avenues where three interesting aspects have emerged, and should be considered for the future research work – firstly, the potential of using endogenous NADs as drug candidates should be explored, secondly, the potential of NOD as a drug should be further evaluated, and thirdly, the knowledge acquired during through the development of NOD, can be deployed to develop an improved version of a bi-functional synthetic NAD, where the role of the fatty acid tail is not restricted to facilitate membrane crossing. I will describe each of these in the following paragraphs.

There is nothing better than to use endogenous compounds as drugs to promote healing, or limit damage. NADs display renoprotective effects in IRI. They are agonist at TRPV1 and Cannabinoid receptors and exhibit anti-inflammatory effects dependent and independent of these receptors. These properties make these endogenous interesting drug candidates to be used for situation where ischemia is anticipated e.g. surgical procedures where IRI injury is anticipated. However, there are several questions which need to be addressed in order to increase the merit of these compounds as drugs candidates such as information regarding toxicity of NADA and OLDA. Further studies are required to investigate the metabolism of NADA by other enzymes in additional cellular locations including COX and LOX, which will help determine which enzymatic mechanism for degradation of NADA predominates *in vivo*. NADA has a long hydrocarbon chain which is necessary for TRPV1 activation and makes NADA it hydrophobic. This poses a challenge on the development of drug formulation. Another small point to consider is that NADA is not stable at the room temperature thus definitive drug formulation with NADA will further add to costs during drug development, production and storage.

In terms of emerging drug candidate NOD is only a little bit better characterized than NADA, as reno-protective effects displayed by NOD can be narrowed down to the ability of NOD to activate TRPV1. Furthermore, this thesis gives first insights in the biodistribution of NOD. Despite these information NOD is still far away from being implemented in the clinical settings. Toxicological studies and detailed pharmacodynamics and pharmacokinetics still needs to be performed for NOD. As in the case of NADA, metabolites as well as precursors yield biological properties, it is of importance to evaluate the biological properties of NOD's metabolites. The effects of NOD so far have been only studied in the endothelial cells [21] and T cells [10, 21], it is of utmost importance that *in vitro* studies with different cells from kidney should be also be done. In particular endothelial cells from glomeruli as macro-vascular and micro-vascular endothelial cells exhibit different responses. Since NOD is mostly applied systematically, it is necessary to evaluate if NOD can cross blood-brain barrier and if it can its interaction with neuronal cells should be established. In this context it is also important to evaluate the cytotoxic properties of NOD with respect to the other cells which are sensitive to oxidative stress. Although the anti-inflammatory properties of NOD are attributed to the ability of NOD to scavenge ROS and on its redox active nature [9]. Effect of NOD on potential ROS sources

such as xanthine oxidase, NADPH oxidase (Nox), mitochondria, and uncoupled nitric oxide which are major contributors to reperfusion-induced oxidative stress and cause reperfusion-induced organ dysfunction and tissue damage [55] still needs to be determined. Although, NOD is a promising drug candidate yet there are several known several unknowns which need to be determined before considering it for clinical application.

Finally, dopamine conjugation with octanoic acid to develop a more hemodynamic neutral dopamine bring us to an interesting point where development of dopamine conjugate of fatty acids which possess anti-inflammatory properties is interesting. This can lead to development of bi-functional drugs which might be able to address IRI not just by TRPV1 activation or by virtue of redox-active catechol structure but also by anti-inflammatory characteristics of the fatty acid used. Especially, dopamine conjugate with PUFAs like DHA and EPA and derivatives of these fatty acids which are processed into anti-inflammatory compounds called Resolvins [56] might hold a promise for IRI injuries. Resolvins have been reported as natural anti-inflammatory response of the body limiting inflammation via monocyte/macrophage uptake of debris, apoptotic PMNs, and killing/clearing microbes [57]. Although these resolvins are not redox active but they exhibit anti-inflammatory properties which might yield synergistic effect to catechol entity. Several of the Resolvins have been described to exhibit beneficial effect in IRI such as RvD1 alleviates Ischemia Reperfusion injury in the lung [58]; in liver [59] and rvd2 is beneficial in cerebral ischemia. Since DHA and EPA are majorly found in brain it is important to evaluate the toxic effect of these compounds on neuronal cells as well. Liu et. al suggest that dopamine adducts derived from brain polyunsaturated fatty acids might be involved in pathogenesis in Parkinson disease [1]. Before development of such compound structure-activity-relationship of the resolvins should be carefully performed.

References

1. Liu, X., et al., Formation of dopamine adducts derived from brain polyunsaturated fatty acids: mechanism for Parkinson disease. J Biol Chem, 2008. 283(50): p. 34887–95.
2. Dexter, D.T., et al., Increased levels of lipid hydroperoxides in the parkinsonian substantia nigra: an HPLC and ESR study. Mov Disord, 1994. 9(1): p. 92–7.
3. Liu, X., N. Yamada, and T. Osawa, Amide-type adduct of dopamine-plausible cause of Parkinson diseases. Subcell Biochem, 2014. 77: p. 49–60.
4. Huang, S.M., et al., An endogenous capsaicin-like substance with high potency at recombinant and native vanilloid VR1 receptors. Proc Natl Acad Sci U S A, 2002. 99(12): p. 8400–5.
5. Chu, C.J., et al., N-oleoyldopamine, a novel endogenous capsaicin-like lipid that produces hyperalgesia. J Biol Chem, 2003. 278(16): p. 13633–9.
6. Hauer, D., et al., Plasma concentrations of endocannabinoids and related primary fatty acid amides in patients with post-traumatic stress disorder. PLoS One, 2013. 8(5): p. e62741.
7. Vettel, C., et al., Dopamine and lipophilic derivates protect cardiomyocytes against cold preservation injury. J Pharmacol Exp Ther, 2014. 348(1): p. 77–85.
8. Losel, R.M., et al., N-octanoyl dopamine, a non-hemodyanic dopamine derivative, for cell protection during hypothermic organ preservation. PLoS One, 2010. 5(3): p. e9713.
9. Hottenrott, M.C., et al., N-octanoyl dopamine inhibits the expression of a subset of kappaB regulated genes: potential role of p65 Ser276 phosphorylation. PLoS One, 2013. 8(9): p. e73122.
10. Wedel, J., et al., N-Octanoyl dopamine transiently inhibits T cell proliferation via G1 cell-cycle arrest and inhibition of redox-dependent transcription factors. J Leukoc Biol, 2014. 96(3): p. 453–62.
11. Spindler, R.S., et al., N-Octanoyl Dopamine for Donor Treatment in a Brain-death Model of Kidney and Heart Transplantation. Transplantation, 2015. 99(5): p. 935–41.
12. Li, S., et al., Donor preconditioning after the onset of brain death with dopamine derivate n-octanoyl dopamine improves early posttransplant graft function in the rat. Am J Transplant, 2017.
13. Tsagogiorgas, C., et al., N-octanoyl-dopamine is an agonist at the capsaicin receptor TRPV1 and mitigates ischemia-induced [corrected] acute kidney injury in rat. PLoS One, 2012. 7(8): p. e43525.
14. Pegorini, S., et al., Capsaicin exhibits neuroprotective effects in a model of transient global cerebral ischemia in Mongolian gerbils. Br J Pharmacol, 2005. 144(5): p. 727–35.
15. Wang, L. and D.H. Wang, TRPV1 gene knockout impairs postischemic recovery in isolated perfused heart in mice. Circulation, 2005. 112(23): p. 3617–23.
16. Harada, N., et al., Ischemia/reperfusion-induced increase in the hepatic level of prostacyclin is mainly mediated by activation of capsaicin-sensitive sensory neurons in rats. J Lab Clin Med, 2002. 139(4): p. 218–26.
17. Wang, M., et al., TRPV1 agonist capsaicin attenuates lung ischemia-reperfusion injury in rabbits. J Surg Res, 2012. 173(1): p. 153–60.

18. Zhong, B. and D.H. Wang, TRPV1 gene knockout impairs preconditioning protection against myocardial injury in isolated perfused hearts in mice. Am J Physiol Heart Circ Physiol, 2007. 293(3): p. H1791–8.
19. Ueda, K., et al., Preventive effect of TRPV1 agonists capsaicin and resiniferatoxin on ischemia/reperfusion-induced renal injury in rats. J Cardiovasc Pharmacol, 2008. 51(5): p. 513–20.
20. Chen, L., et al., Role of TRPV1 channels in ischemia/reperfusion-induced acute kidney injury. PLoS One, 2014. 9(10): p. e109842.
21. Klotz, S., et al., N-octanoyl dopamine treatment exerts renoprotective properties in acute kidney injury but not in renal allograft recipients. Nephrol Dial Transplant, 2016. 31(4): p. 564–73.
22. Zhong, B. and D.H. Wang, N-oleoyldopamine, a novel endogenous capsaicin-like lipid, protects the heart against ischemia-reperfusion injury via activation of TRPV1. Am J Physiol Heart Circ Physiol, 2008. 295(2): p. H728–35.
23. Zhuang, Q., et al., Stimulated CB1 Cannabinoid Receptor Inducing Ischemic Tolerance and Protecting Neuron from Cerebral Ischemia. Cent Nerv Syst Agents Med Chem, 2017. 17(2): p. 141–150.
24. Rimmerman, N., et al., Microsomal omega-hydroxylated metabolites of N-arachidonoyl dopamine are active at recombinant human TRPV1 receptors. Prostaglandins Other Lipid Mediat, 2009. 88(1–2): p. 10–7.
25. Caterina, M.J., et al., The capsaicin receptor: a heat-activated ion channel in the pain pathway. Nature, 1997. 389(6653): p. 816–24.
26. van der Stelt, M., et al., Neuroprotection by Delta9-tetrahydrocannabinol, the main active compound in marijuana, against ouabain-induced in vivo excitotoxicity. J Neurosci, 2001. 21(17): p. 6475–9.
27. Huang, W., et al., Transient receptor potential vanilloid gene deletion exacerbates inflammation and atypical cardiac remodeling after myocardial infarction. Hypertension, 2009. 53(2): p. 243–50.
28. Adams, M.J., K.D. Ahuja, and D.P. Geraghty, Effect of capsaicin and dihydrocapsaicin on in vitro blood coagulation and platelet aggregation. Thromb Res, 2009. 124(6): p. 721–3.
29. Pan, Z., et al., TRPV1 activation is required for hypertonicity-stimulated inflammatory cytokine release in human corneal epithelial cells. Invest Ophthalmol Vis Sci, 2011. 52(1): p. 485–93.
30. Okada, Y., et al., TRPV1 involvement in inflammatory tissue fibrosis in mice. Am J Pathol, 2011. 178(6): p. 2654–64.
31. Yang, Y., et al., Cannabinoid receptor 1 suppresses transient receptor potential vanilloid 1-induced inflammatory responses to corneal injury. Cell Signal, 2013. 25(2): p. 501–11.
32. Nagarkatti, P., et al., Cannabinoids as novel anti-inflammatory drugs. Future Med Chem, 2009. 1(7): p. 1333–49.
33. Patwardhan, A.M., et al., The cannabinoid WIN 55,212–2 inhibits transient receptor potential vanilloid 1 (TRPV1) and evokes peripheral antihyperalgesia via calcineurin. Proc Natl Acad Sci U S A, 2006. 103(30): p. 11393–8.

34. Stamellou, E., et al., N-octanoyl dopamine treatment of endothelial cells induces the unfolded protein response and results in hypometabolism and tolerance to hypothermia. PLoS One, 2014. 9(6): p. e99298.
35. Walter, P. and D. Ron, The unfolded protein response: from stress pathway to homeostatic regulation. Science, 2011. 334(6059): p. 1081–6.
36. Montie, H.L., et al., Renal ischemia and reperfusion activates the eIF 2 alpha kinase PERK. Biochim Biophys Acta, 2005. 1741(3): p. 314–24.
37. Noh, M.R., et al., C/EBP homologous protein (CHOP) gene deficiency attenuates renal ischemia/reperfusion injury in mice. Biochim Biophys Acta, 2015. 1852(9): p. 1895–901.
38. Gao, X., et al., The nephroprotective effect of tauroursodeoxycholic acid on ischaemia/reperfusion-induced acute kidney injury by inhibiting endoplasmic reticulum stress. Basic Clin Pharmacol Toxicol, 2012. 111(1): p. 14–23.
39. Prachasilchai, W., et al., The protective effect of a newly developed molecular chaperone-inducer against mouse ischemic acute kidney injury. J Pharmacol Sci, 2009. 109(2): p. 311–4.
40. Chandrika, B.B., et al., Endoplasmic Reticulum Stress-Induced Autophagy Provides Cytoprotection from Chemical Hypoxia and Oxidant Injury and Ameliorates Renal Ischemia-Reperfusion Injury. PLoS One, 2015. 10(10): p. e0140025.
41. Ling, Q., et al., Roles of the Exogenous H2S-Mediated SR-A Signaling Pathway in Renal Ischemia/ Reperfusion Injury in Regulating Endoplasmic Reticulum Stress-Induced Autophagy in a Rat Model. Cell Physiol Biochem, 2017. 41(6): p. 2461–2474.
42. Wang, Y., et al., Intermedin protects against renal ischemia-reperfusion injury by inhibiting endoplasmic reticulum stress. BMC Nephrol, 2015. 16: p. 169.
43. Sarsour, E.H., et al., Redox control of the cell cycle in health and disease. Antioxid Redox Signal, 2009. 11(12): p. 2985–3011.
44. Goswami, P.C., et al., Cell cycle-coupled variation in topoisomerase IIalpha mRNA is regulated by the 3'-untranslated region. Possible role of redox-sensitive protein binding in mRNA accumulation. J Biol Chem, 2000. 275(49): p. 38384–92.
45. Conour, J.E., W.V. Graham, and H.R. Gaskins, A combined in vitro/bioinformatic investigation of redox regulatory mechanisms governing cell cycle progression. Physiol Genomics, 2004. 18(2): p. 196–205.
46. Burns, J.S. and G. Manda, Metabolic Pathways of the Warburg Effect in Health and Disease: Perspectives of Choice, Chain or Chance. Int J Mol Sci, 2017. 18(12).
47. Sancho, R., et al., Immunosuppressive activity of endovanilloids: N-arachidonoyl-dopamine inhibits activation of the NF-kappa B, NFAT, and activator protein 1 signaling pathways. J Immunol, 2004. 172(4): p. 2341–51.
48. Villeneuve, N.F., A. Lau, and D.D. Zhang, Regulation of the Nrf2-Keap1 antioxidant response by the ubiquitin proteasome system: an insight into cullin-ring ubiquitin ligases. Antioxid Redox Signal, 2010. 13(11): p. 1699–712.
49. Bolisetty, S., A. Zarjou, and A. Agarwal, Heme Oxygenase 1 as a Therapeutic Target in Acute Kidney Injury. Am J Kidney Dis, 2017. 69(4): p. 531–545.
50. Trujillo, J., et al., Renoprotective effect of the antioxidant curcumin: Recent findings. Redox Biol, 2013. 1: p. 448–56.

51. Bayrak, O., et al., Curcumin protects against ischemia/reperfusion injury in rat kidneys. World J Urol, 2008. 26(3): p. 285–91.
52. Buys-Goncalves, G.F., et al., Antioxidants as Renoprotective Agents for Ischemia during Partial Nephrectomy. Biomed Res Int, 2019. 2019: p. 8575398.
53. Li, J., et al., Resveratrol Alleviates Inflammatory Responses and Oxidative Stress in Rat Kidney Ischemia-Reperfusion Injury and H2O2-Induced NRK-52E Cells via the Nrf2/TLR4/NF-kappaB Pathway. Cell Physiol Biochem, 2018. 45(4): p. 1677–1689.
54. Novosadova, E.V., et al., Neuroprotective Properties of Endocannabinoids N-Arachidonoyl Dopamine and N-Docosahexaenoyl Dopamine Examined in Neuronal Precursors Derived from Human Pluripotent Stem Cells. Biochemistry (Mosc), 2017. 82(11): p. 1367–1372.
55. Granger, D.N. and P.R. Kvietys, Reperfusion injury and reactive oxygen species: The evolution of a concept. Redox Biol, 2015. 6: p. 524–551.
56. Duvall, M.G. and B.D. Levy, DHA-and EPA-derived resolvins, protectins, and maresins in airway inflammation. Eur J Pharmacol, 2016. 785: p. 144–155.
57. Serhan, C.N. and B.D. Levy, Resolvins in inflammation: emergence of the pro-resolving superfamily of mediators. J Clin Invest, 2018. 128(7): p. 2657–2669.
58. Zhao, Q., et al., Resolvin D1 Alleviates the Lung Ischemia Reperfusion Injury via Complement, Immunoglobulin, TLR4, and Inflammatory Factors in Rats. Inflammation, 2016. 39(4): p. 1319–33.
59. Kang, J.W., et al., Resolvin D1 activates the sphingosine-1-phosphate signaling pathway in murine livers with ischemia/reperfusion injury. Biochem Biophys Res Commun, 2019. 514(4): p. 1058–1065.

Nederlandse samenvatting

De behandeling van orgaandonoren met dopamine gaat gepaard met een significante verbetering van de initiële transplantaat functie bij ontvangers van een nier of hart transplantaat. NOD is een synthetische N-acyl dopamine ontwikkeld voor gebruik bij orgaandonoren met als doel een hydrofoob dopamine derivaat te creëren dat geen invloed heeft op de systemische bloeddruk. Door zijn ontstekingsremmende, nier beschermende en cel protectieve eigenschappen is NOD een interessante kandidaat voor klinisch gebruik in settings van ischemie geinduceerde acute nierbeschadiging. Het belangrijkste doel van dit proefschrift was het onderzoeken van relevante chemische en biologische eigenschappen die NOD zijn nier beschermende effecten verlenen. We bestudeerden het vermogen van NOD om TRPV1 te activeren en het prominente redox-actieve karakter, dat het redoxmilieu binnen de intracellulaire compartimenten kan veranderen.

De experimentele studies beschreven in dit proefschrift werden uitgevoerd, ten eerste om aan te tonen dat NOD bescherming biedt in een model van ischemie-geïnduceerde acute nier schade, ookwel aute kidney injury (AKI) genoemd, via TRPV1 activering. Ten tweede om de moleculaire entiteiten binnen NOD af te bakenen die nodig zijn voor TRPV1 activering en voor zijn ontstekingsremmende eigenschappen. Ten derde om de invivo weefseldistributie en eliminatiekinetiek van NOD te bestuderen en ten vierde om aan te tonen dat de redoxactiviteit van NOD het celgedrag significant beïnvloedt, d.w.z. dat NOD ER stress en UPR induceert. Het potentiële de potentiële mogelijkheden voor het gebruik van NAD's in de transplatatiegeneeskunde wordt besproken in **hoofdstuk 2.**

In **hoofdstuk 3** wordt het nier beschermende effect van NOD in een setting van warme ischemie-geinduceerde AKI onderzocht. We hebben aangetoond dat de behandeling met NOD de nierfunctie bij warme ischemie-geïnduceerde AKI verbetert, zelfs wanneer de behandeling na het optreden van de nier ischemie wordt gestart. Een verbeterde nierfunctie ging niet gepaard met grote veranderingen in de nierperfusie. Wij hebben aangetoond dat de nier beschermende eigenschappen van NOD via TRPV1 plaatsvindt. NOD behandeling van ontvanger ratten na niertransplantatie leidt niet tot een verbetering van de nierfunctie in vergelijking met onbehandelde ontvanger ratten. Het gebrek aan een therapeutisch effect van NOD bij ontvanger ratten kon niet worden verklaard door het verlies van TRPV1 – functionaliteit.

In **hoofdstuk 4** hebben we de chemische entiteiten binnen NOD onderzocht die TRPV1 activeren en verantwoordlijk zijn voor de ontstekingsremmende effecten. Door het veranderen van de aromatische-, amide-linker-en vetzuurgroepen van NOD hebben we nieuwe verbindingen gesynthetiseerd. Met behulp van calcium microfluorimetrie hebben we een EC50 waarde van 12,7µM voor TRPV1 activering door NOD gemeten. Acetylering van de orthodihydoxygroepen (geacetyleerd (A-) NOD) of verkorting van de amide-linker (ΔNOD) verminderde de effectiviteit voor TRPV1 activering. Een verdere afname van het effect van ΔNOD werd gevonden de positie van de carbonyl-en amidegroepen te verwisselen. De afwezigheid van één hydroxylgroep aan de aromatische ring (N-octanoyl tyramine (NOT)) of het gebruik van een vertakte vetzuur als esterfunctie

(N-pivaloyl dopamine (NPiD)) resulteerde in een significante afname van de TRPV1-activatie. Docking studies en site-directed mutagenese hebben soortgelijke ankerresiduen voor interacties van capsaïcine of NOD met TRPV1 aan het licht gebracht. Echter,een mutatie van arginine naar alanine op positie 491 (R491) had alleen invloed op TRPV1 activering door NOD maar niet door capsaïcine. Met uitzondering van ΔNOD is de aanwezigheid van een intacte catecholstructuur een voorwaarde voor TNF-α induceerde remming van VCAM-1 en voor de inductie van heem oxygenase-1 (HO-1) expressie. NPiD en A-NOD vertonen beide ontstekingsremmende eigenschappen vergelijkbaar met NOD.

In **hoofdstuk 5** hebben we de radiotracer [18F] F-NOD ontwikkeld om de in vivo eliminatiekinetiek van NOD te bestuderen. Eerst hebben we aangetoond dat de biologische eigenschappen van F-NOD en NOD niet van elkaar verschillen, d.w.z. beide remmen de TNF-α-geïnduceerde VCAM-1 expressie, beide induceren de expressie van HO-1, beide beschermen de endotheelcellen tegen koud-geinduceerde schade en beide activeren TRPV1. [18F]F-NOD kan efficiënt radioactief gelabeld en is stabiel inratten plasma en fosfaatbuffer. In vivo wordt [18F]F-NOD snel via het nier-en hepatobiliaire systeem geelimineerd.

Omdat redoxcondities tussen intracellulaire compartimenten verschillen, en NOD zeer éénvoudig in een greduceerde als ook in een geoxideerde vorm over kan gaan, bekeken we in **hoofdstuk 6** of synthetische N-acetyl dopamines (NAD's), ER stress bewerkstelligt met als consequentie dat de zogenaamde unfolded protein response (UPR) geinduceerd wordt. Deze eigenschap van NAD's lijkt afhankelijk te zijn van de redox-activiteit van deze verbindingen. In niet toxische concentratries remt NOD de celproliferatie van HUVEC's sterk, zeer waarschijnlijk door een vertraging in cell cyclus progressie zodat de cellen in de S-G2/M-fase va de cell cyclus blijven. In overeenstemming hiermee werd gevonden dat de expressie van verschillende genen, betrokken bij de S-G2/M-progressie, door NOD aanzienlijk verlaagd worden. Interessant is dat behandeling met NOD op lange termijn resulteerde in hypo-metabolisme en thermotolerantie, zoals gesuggereerd wordt door een verminderde intracellulaire ATP-concentratie, activering van AMPK en een verhoogde weerstand tegen de kou toegebrachte celbeschadiging.

Appendix

Acknowlegements

At times our own light goes out and is rekindled by a spark from another person. Each of us has cause to think with deep gratitude of those who have lighted the flame within us—Albert Schweitzer.

I take this moment to thank everyone who has helped me endure this journey and help me realise this dream.

First and foremost a special thanks and appreciation goes to my enthusiastic supervisor, Prof. Dr. Benito Yard. My PhD has been an amazing experience and I thank Benito wholeheartedly, not only for his tremendous academic support, but also for giving me so many wonderful opportunities like interaction with university of Groningen and participation in transplantation Summer School Groningen. I am thankful to him for his patience, dedication and ingenious teaching techniques.

I am thankful to Prof. Dr. Mathias Hafner, for his valuable advices during my doctoral thesis endeavour for past four and half years. His observation and comments helped me moved ahead in investigational path in depth. I am thankful to him for introducing me to many new and productive collaboration opportunities. I deeply appreciate your help with travel and living cost for attending San Francisco WTC: I am thankful to Albert und Anneliese Konanz-Stiftung, from Hochschule Mannheim for providing me scholarship.

I humbly thank Marco. C. Harmsen for accepting me as his PhD student and for providing me this opportunity. For kindess, patience ,constant encouragement and support that I have received from him. I am very thankful to his constant input with writing of the thesis and optimism with which he always bolstered my confidence. I also highly thankful for several inspirational discussions.

I am grateful to Prof. Dr. med. Hans-Peter Hammes for providing me opportunity to be part of the GRK880/3–4, Vascular Medicine Graduate School and for organizing various interesting scientific lectures and the financial support during initial phase of my PhD studies.

I thank Prof. Dr. med. Bernhard Krämer, Director of Nephrology, for providing me a chance to be part of Nephrology Department.

Thanks to Prof. Dr. med. Rolf-Detlef Treede for collaboration and for providing access to the calcium imaging facility. I am thankful to Dr. Wolfgang Greffrath and Dr. Uta Binzen for support and trust they have showed in me and for wonderful learning experience. I am thankful to Mrs. Handan Morez and Mrs. Ulrike Horst for introducing me to calcium imaging technique which proved to be a great research tool in the study.

I am grateful to Dr. Marc Pretze and Dr. Ralf Losel, who have helped me transform basic ideas and mere chemical structures from Chemdraw screens into reality by synthesis. I also thank Dr. Marc Pretze for numerous useful discussions which provided breakthrough in understanding of NADs behaviour. I am highly grateful to Marc for helping in the tumultuous times and standing by me not only as a supporting collab-

orator but also providing insight in chemical experimental work. I am thankful to Dr. Bastian Theisinger and Novaliq GmbH for support with production of NOD and other *N*-Acyl dopamine derivatives.

I thank Dr. Sarah Klotz for helping with the animal experiments, for collaboration and profound scientific discussions.

I would like to express my sincere thanks to Dr. Julio Caballero for generously sharing his time and expert knowledge on molecular docking. With his help TRPV1-NADs molecular model was established and which proved to be great leap in helping me understand the interaction of TRPV1 and NADs and wet lab data.

I am grateful to Dr. Christin Saur from Department of Pathology, University Hospital Mannheim Medical faculty Mannheim, University of Heidelberg for his help with the sequencing of the mutants, which saved not only saved funds but also time.

I would like to thank present and past members of the Prof. Yard's working group, Mrs. Annette Breedijk, Mrs. Katharina Prem, Mrs. Renate Stein, Mrs. Silke Deiters, and Dr. Sarah Klotz for technical support, friendly conversation and for proving a very friendly and independent working environment. I thank Dr. Shiqi Zhang, Dr. Eleni Stamellou and Dr. Johannes Wedel for useful discussion and collaborations. I thank Danfeng Zhang, Yinchung Li, Angelica Rodrigues, Björn Hofmann, Diego Pastene, Sara Medina Balbuena, Lovis Kling, Jana Braun, and Thomas Albrecht for the friendly and organised working environment.

My special thanks goes to Hilda van den Bos, Kathrin Hammon, Pietro Marcato, Igor Dolgowjasow, Jonas Heckeli and Isabel Ann Wedenig. Teaching is a part of learning and the privilege to supervise them during their interships, Bachelor or Master thesis in the lab has been an enriching learning experience.

My heartily thanks go to Annette Breedijk, Sarah Klotz and Marianne Heitzmann for the delightful and amicable conversation in the office. I found many insights and new ways of thinking. In lows, I found my high, and in high I still could survive, for you were there and I am thankful to thy.

My sincere thanks go to the neighbouring lab and their members who have rendered their help several occasions. I am thankful to Ms. Jutta Schulte, Dr. Sonia Velasquez, Ms. Miriam Bierbaum, and Ms. Nadine Dietrich for lending a helping hand.

I am also grateful to Ms. Ariane Tomsche from HS Mannheim for her support every now and then with techniques, troubleshooting and help with bureaucracy.

I also want to thank my fellow scientist friends from India Dr. Nagesh Shanbhag, Dr. Siladitta Biswas, Dr. Anupriya Chatterjee for their company and constructive discussions which have brought me forward many times and help me clear views on many topics.

My heartfelt thanks go to Dr. Linda Hartmann, Dr. Paulina Nunez, Dr. Kristina Mauer, Dr. Daniela Rosenberg, Dr. Juan Juan Zhang, Dr. Sabrina Voss, Dr. Jagriti Srivastava, and Ms. Handan Morez for their camaraderie and company, making the non-scientific part of my thesis colourful. I am also thankful to Mrs. Jenni Maier and Mr. Oliver Kresten for the friendship and affection they have provided. My sincere thanks go to

Dr. Martin Dittmer, who has been one of my best friends and helped me out with many things. I thank you for the care and positive mind-set that you have lent in several of occasions.

A note of thanks also goes to Prof. Dr. Kunal Mukhopadhyay from the Department of Bioengineering Birla institute of Technology, Mesra Ranchi and Prof. Dr. H. Devaraj from the Department of Zoology, University of Madras who have helped me with my first steps in research.

Finally, I thank my parents who have always been inspiration and great support throughout my life. I thank you for your patience and optimism in all of my adventures. Your words always made it bright in darkest of the night and I could keep my equipoise in many tempestuous situations. I am also grateful to my two lovely siblings; Chetna and Utkarsh, who have been my best friends and are sunshine in my life, supporting me through ups and downs.

I am very thankful to Ram, who I met towards the completion of my work, who cheered me up and supported me in all possible ways to make me reach the end line. He anchored me to hope when I saw none.

Prama Pallavi

Abbreviations

Abbreviation	Full Form
($[Ca^{++}]^i$)	Cytoplasmic calcium
[18F]	Fluorine-18 radioisotope
° C	Degree centigrade
µ	Micro
3-MT	3-methoxytyramine
A	Alanine
ADP	Adenosine diphosphate
AKI	Acute kidney injury
Allo	Allogeneic
AMP	Adenosine monophosphate
AMPK	5' AMP-activated protein kinase
A-NOD	Acteylated NOD
AP-1	Activator protein 1
ARE	Antioxidant response element
ASL	Arterial spin labelling
ATF6	Activating transcription factor 6
ATP	Adenosine triphosphate
BBr_3	Boron tribromide
BD	Braindead
Bq	Becquerel, unit of radioactivity
BSA	Bovine serum albumin
C/EBP	C/EBP homologous protein
Ca^{+2}	Calcium ion
CaCl2	Calcium chloride
cAMP	Cyclic AMP
CAP	Capsaicin
CAP-OH	(E)-N-(3,4-dihydroxybenzyl)-8-methylnon-6-enamide
CB1	Cannabinoid receptor type 1
CB2	Cannabinoid receptor type 2
cDNA	Complementary DNA
CGRP	Calcitonin gene-related peptide
CH2Cl2	Dichloromethane
Ci	Curie, non-SI unit of radioactivity
CMV	Cytomegalovirus
COMT	Catechol O-methyl transferase COMT

Abbreviation	Full Form
COX-2	Cyclooxygenase-2
COX-2	Cyclooxygenase-2
CPZ	Capsazepine
d.c.	Decay counted
DA	Dopamine
DGF	Delayed graft function
DHA	Docosahexaenoic acid
DMF	Dimethylformamide
DMSO	Dimethyl sulfoxide
DRG	Dorsal root ganglion
DTT	Dithiothreitol
e^-	Eletron
EC_{50}	Effective concentration 50
ED1	Ectodysplasin A
EDTA	Ethylenediaminetetraacetic acid
EPA	Eicosapentaenoic acid
ER	Endoplasmic reticulum
ERSE	Acting ER-stress response element
Et_2O	Petroleum ether
F	Phenylalanine
FAIR	Flow-sensitive alternating inversion recovery
FBS	Fetal bovin Serum
FCS	Fetal calf Serum
FDA	Food and Drug Administration
F-NOD	2-fluoro-N-octanoyl dopamine
g	Gram
GAPDH	Glyceraldehyde 3-phosphate dehydrogenase
H^+	Proton
H_2O	Water
H_2O_2	Hydrogen peroxide
H_2S	Hydrogen sulphide
HEK293	Human Embroynic Kidney cells 293
HEPES	4-(2-hydroxyethyl)-1-piperazineethanesulfonic acid)
HO-1	Heme oxygenase-1
HPLC	High performance liquid chromatography
hr	Hour
HRP	Horseradish peroxidase

Abbreviation	Full Form
HUVECs	Human umbilical vein endothelial cells
Hz	Hertz
I	Isoleucine
I/R-injury	Ischemia reperfusion injury
ICAM1	Intercellular adhesion molecule 1)
IL-6	Interleukin 6
IPC	Ischemic preconditioning
IRE1	Inositol requiring kinase
JNK1	C-jun N-terminal protein kinase 1 (JNK1)
k	Kilo
K^+	Potassium ion
K_2CO_3	Potassium carbonate
KCl	Potassium chloride
l	Liter
L	Leucine
LDH	Lactate dehydrogenase
$LiAlH_4$	Lithium aluminium hydride
LOX	Lysyl oxidase)
LT	Leukotrienes
M	Molar
M	Methionine
m	Mili
MALDI-TOF	Matrix-assisted laser desorption/ionization-time of flight
MAPK	Mitogen-activated protein kinase
MeCN	Acetonitrile
$MgCl_2$	Magnesium chloride
$MgSO_4$	Magnesium sulfate
min	Minute
mm	Milimeter
MOI	Multiplicity of infection
MRI	Magnetic resonance imaging
mRNA	Messenger RNA
n	Nano
N	Asparagine
Na^+	Sodium ion
NAANs	N-acyl conjugates of amino acids and neurotransmitters
NaCl	Sodium chloride

Abbreviation	Full Form
NADA	N-arachidonoyl dopamine
NADH	Nicotinamide adenine dinucleotide
NADPH	Reduced form of NADP
NADs	N-acyl dopamines
$NaHCO_3$	Sodium bicarbonate
NFAT	Nuclear Factor of Activated T-cells
NF-κB	Nuclear factor κb
nm	Nanometer
NMR	Nuclear magnetic resonance
NO	Nitrogen oxide
NOD	N-octanoyl dopamine
NOT	N-octanoyl tyramine
NPiD	N-pivaloyl dopamine
Nrf-2	Nuclear factor erythroid 2-related factor 2
OLDA	N-oleoyl dopamine
PBS	Phosphate-buffered saline
PDI	Protein disulfide isomerase
PERK	(PKR)-like ER kinase
PET	Positron-emission tomography
PG	Prostaglandins
PMNs	Polymorphonuclear leukocyte
PPAR	Peroxisome proliferator-activated receptors
ppm	Parts per million
PVDF	Polyvinylidene fluoride
QPCR	Quantitative polymerase chain reaction
R	Arginine
RCY	(Radiochemical yield
RNA	Ribonucleic acid
ROI	Regions of interest
RT PCR	Reverse transcription polymerase chain reaction
rTRPV1	Rat TRPV1
S	Serine
s	Seconds
SAM	S-adenosyl-l-methionine
SD	Standard deviation
sd	Sprague Dawley rat
SEM	Standard error of mean

Abbreviation	Full Form
SP	Substance P
SUVbw	Standardized uptake value based on body weight
Syn	Syngeneic
T	Threonine
TAK1	Transforming growth factor β-activated kinase 1
TBS	Tris-buffered saline
TFA	Trifluoroacetic acid
THF	Tetrahydrofuran
TI	Inversion time
TLC	Thin-layer chromatography
TNF	Tumor necrosis factor
TRPV1	Transient receptor potential channel of the vanilloid receptor subfamily, subtype 1
Tx	Transplantation
UPR	Unfolded protein response
UV	Ultraviolet
VCAM1	Vascular cell adhesion protein 1
VDW	Van der Waals force
WT	Wild type
Xbp1	X-box-binding protein 1
Y	Tyrosine
ΔNOD	Delta NOD
ΔNODR	Delta NOD reverse
DNA	Deoxyribonucleic acid

Author affiliations

Anna-Isabelle Kälsch[1]
Benito. A. Yard[1]
Bernhard K. Krämer [1]
Björn B. Hofmann [1]
Björn Wängler[2]
Carmen Wängler[3]
Charalambos Tsagogiorgas[4]
Eleni Stamellou[1]
Fabian Zimmer [6]
Frank G. Zöllner [6]
Handan Morez[7]
Jakob Walter[8]
Johannes Wedel[1]
Julio Caballero[9]
Marc Pretze[2]
Mareike Roscher[2]
Martin.C. Harmsen[10]
Mathias Hafner[11]
Rolf-Detlef Treede[7]
Sarah Klotz [1]
Simone Hoeger[1]
Uta Binzen[7]
Wolfgang Greffrath[7]
Yingchun Li [1]

1: V Department of Medicine, University Hospital Mannheim, Medical Faculty Mannheim, Heidelberg University
2: Molecular Imaging and Radiochemistry, Department of Clinical Radiology and Nuclear Medicine, Medical Faculty Mannheim, Heidelberg University, Mannheim, Germany
3: Biomedical Chemistry, Department of Clinical Radiology and Nuclear Medicine, Medical Faculty Mannheim of Heidelberg University
4: Department of Anaesthesiology and Intensive Care Medicine, University Hospital Mannheim, Mannheim, Germany
5: Experimental Dermatology, Medical Faculty Mannheim, Heidelberg University, Mannheim, Germany.
6: Computer Assisted Clinical Medicine, Medical Faculty Mannheim, Heidelberg University, Mannheim, Germany
7: Division of Neurophysiology, Centre of Biomedicine and Medical Technology Mannheim (CBTM), Medical Faculty Mannheim, Heidelberg university, Mannheim, Germany
8: Bayer Healthcare Pharma AG, Berlin, Germany
9: Center for Bioinformatics and Molecular Simulations, Faculty of Engineering in Bioinformatics, Universidad de Talca, Talca, Chile
10: University of Groningen, University Medical Centre Groningen, Department of Pathology and Medical Biology, Groningen, The Netherlands
11: Institute for Molecular and Cellular Biology, Mannheim University of Applied Sciences, Mannheim, Germany